

SPRINGER BRIEFS IN
APPLIED SCIENCES AND TECHNOLOGY

M. Khalid Jawed · Alyssa Novelia
Oliver M. O'Reilly

A Primer on the Kinematics of Discrete Elastic Rods



Springer

SpringerBriefs in Applied Sciences and Technology

Thermal Engineering and Applied Science

Series editor

Francis A. Kulacki, Minneapolis, MN, USA

SpringerBriefs present concise summaries of cutting-edge research and practical applications across a wide spectrum of fields. Featuring compact volumes of 50–125 pages, the series covers a range of content from professional to academic.

Typical publications can be:

- A timely report of state-of-the art methods
- An introduction to or a manual for the application of mathematical or computer techniques
- A bridge between new research results, as published in journal articles
- A snapshot of a hot or emerging topic
- An in-depth case study
- A presentation of core concepts that students must understand in order to make independent contributions

SpringerBriefs are characterized by fast, global electronic dissemination, standard publishing contracts, standardized manuscript preparation and formatting guidelines, and expedited production schedules.

On the one hand, **SpringerBriefs in Applied Sciences and Technology** are devoted to the publication of fundamentals and applications within the different classical engineering disciplines as well as in interdisciplinary fields that recently emerged between these areas. On the other hand, as the boundary separating fundamental research and applied technology is more and more dissolving, this series is particularly open to trans-disciplinary topics between fundamental science and engineering.

Indexed by EI-Compendex and Springerlink.

More information about this series at <http://www.springer.com/series/8884>

M. Khalid Jawed • Alyssa Novelia
Oliver M. O'Reilly

A Primer on the Kinematics of Discrete Elastic Rods

M. Khalid Jawed
Department of Mechanical
and Aerospace Engineering
University of California, Los Angeles
Los Angeles, CA, USA

Alyssa Novelia
Department of Mechanical Engineering
University of California, Berkeley
Berkeley, CA, USA

Oliver M. O'Reilly
Department of Mechanical Engineering
University of California, Berkeley
Berkeley, CA, USA

ISSN 2191-530X ISSN 2191-5318 (electronic)
SpringerBriefs in Applied Sciences and Technology
ISSN 2193-2530 ISSN 2193-2549 (electronic)
Thermal Engineering and Applied Science
ISBN 978-3-319-76964-6 ISBN 978-3-319-76965-3 (eBook)
<https://doi.org/10.1007/978-3-319-76965-3>

Library of Congress Control Number: 2018935262

© The Author(s) 2018

This work is subject to copyright. All rights are reserved by the Publisher, whether the whole or part of the material is concerned, specifically the rights of translation, reprinting, reuse of illustrations, recitation, broadcasting, reproduction on microfilms or in any other physical way, and transmission or information storage and retrieval, electronic adaptation, computer software, or by similar or dissimilar methodology now known or hereafter developed.

The use of general descriptive names, registered names, trademarks, service marks, etc. in this publication does not imply, even in the absence of a specific statement, that such names are exempt from the relevant protective laws and regulations and therefore free for general use.

The publisher, the authors and the editors are safe to assume that the advice and information in this book are believed to be true and accurate at the date of publication. Neither the publisher nor the authors or the editors give a warranty, express or implied, with respect to the material contained herein or for any errors or omissions that may have been made. The publisher remains neutral with regard to jurisdictional claims in published maps and institutional affiliations.

Printed on acid-free paper

This Springer imprint is published by the registered company Springer International Publishing AG part of Springer Nature.

The registered company address is: Gewerbestrasse 11, 6330 Cham, Switzerland

To my sister Farha Jawed (MKJ)

*To my parents Tjong Frendy Sugito and Tati
Malina (AN)*

To my wife Christina (OMO'R)

Preface

In the late 2000s, a novel formulation of Kirchhoff's celebrated rod theory was published by Bergou et al. [4]. In this formulation, an elastic rod is discretized into a series of segments (or edges) connecting vertices (or nodes). The edges are free to stretch and rotate relative to their adjacent neighbors. The relative rotations of the cross sections of the rod are modeled with the help of a pair of material vectors that are associated with each edge. The original formulation has been extended in a variety of directions including an extension to viscous threads and sound generation. The discrete elastic rod formulation is computationally cheap and, as a result, is used in computer graphics to render images of hairs and trees and is the technical underpinning behind the *Bristle Brush* feature in Adobe Illustrator and Adobe Photoshop.

Bergou et al.'s discrete elastic rod (DER) formulation uses ideas from the nascent field of discrete differential geometry and concepts such as holonomy from classic differential geometry. As a result, understanding the DER formulation (even for students who have exceptional backgrounds in continuum mechanics) can be challenging. Indeed, initially we were unable to rederive many of the key results in the papers by Bergou et al. [3, 4] and the related works by Audoly et al. [2] and Kaldor et al. [29]. The remarkable simulations in these four papers provided sufficient motivation for us to eventually prove the main results contained in [2–4, 29].

The present Brief is a result of our efforts to understand the DER formulation and we hope that it provides an accessible introduction to this remarkable formulation. We assume that the reader has a background in continuum mechanics at the level of Chadwick [8] or Gurtin [20]. The Brief starts with a pair of motivational examples. We then proceed to give a rapid summary of Kirchhoff's rod theory before discussing a discretized space curve and three frames that can be associated with it. Next, derivations of gradients and variations for various kinematical quantities that have appeared in the literature are discussed. One unusual feature of the DER formulation is the use of holonomy to help determine the twist of the rod. We devote an entire chapter to discussing results from differential geometry of spherical triangles and spherical quadrilaterals that are used to determine the twist of the rod.

The final chapter synthesizes the kinematical results and shows how they are used to formulate a set of ordinary differential equations for the position vectors of the nodes of the rod and the twisting of the edges. To help the reader, we present several examples of classic problems in the theory of rods that are solved using the discrete elastic rod formulation.

The C++ source code for the discrete elastic rod formulation discussed in this Brief can be found at

http://www.cs.columbia.edu/cg/elastic_coiling/

Source code for the input files used for the examples discussed in the Brief can be accessed at

<http://dynamics.berkeley.edu/>

We received a total of \$500 from Springer-Nature for publishing this Brief. These funds have been donated to an organization that supports LGBTQ people who are held in immigrant detention in the United States: *Mariposas Sin Fronteras*.

Los Angeles, CA, USA
Berkeley, CA, USA
Berkeley, CA, USA

M. Khalid Jawed
Alyssa Novelia
Oliver M. O'Reilly

Acknowledgments

The discrete elastic rod formulation discussed in these pages was first brought to the attention of Oliver O'Reilly by Arun Srinivasa (Texas A&M University) during the Annual Meeting of the Society of Engineering Science at the University of Maryland in the fall of 2016. The formulation's capability of modeling knotted structures and potential application to simulating soft robot locomotion were the primary reasons that O'Reilly and Alyssa Novelia then began studying the papers by Bergou et al. [3, 4]. They had the good fortune at the time to be collaborating with Carmel Majidi's group at Carnegie Mellon University on soft robots. The third author, M. Khalid Jawed, was a postdoctoral researcher with Majidi's group whose Ph.D. thesis [25] at the MIT used Bergou et al.'s discrete elastic rod formulation to solve a variety of problems. Thus, by a series of fortunate coincidences and the support of colleagues, work on this Brief commenced. Our initial goal was to write a set of notes explaining all of the technical details in Bergou et al. [3, 4] but as the notes expanded substantially beyond our original expectations, we realized they would make a Brief that researchers on Bergou et al.'s discrete elastic rod formulation might hopefully find useful.

Part of the reason the notes expanded beyond our original horizon lay in our difficulty comprehending the holonomy results (7.1) and (7.2). These results play a central role in computing the torsional strain in the discrete elastic rod formulations presented in the papers [3, 4] and discussed in this Brief. We would not be able to explain the holonomy results were it not for the exceptionally helpful comments [65] and feedback provided by Etienne Vouga (University of Texas at Austin). Khalid Jawed is also grateful to Fang Da (Columbia University), Eitan Grinspun (Columbia University), Jungseock Joo (UCLA), Noor Khouri (MIT), and Pedro Reis (EPFL) who were involved in the adaptation, implementation, and experimental validation of the discrete elastic rod formulation with application to engineering problems.

As mentioned earlier, our primary motivation to study the discrete elastic rod formulation came from a desire to simulate the locomotion of soft robots. This research on soft robots is supported by grant number W911NF-16-1-0242 from the U.S. Army Research Organization administered by Dr. Samuel C. Stanton. Alyssa

Novelia is also grateful for the support of a Zee Fellowship from the Department of Mechanical Engineering at the University of California at Berkeley.

It has been a pleasure working with Michael Luby at Springer US on this Brief, and we are delighted that he chose to publish our work. We are also grateful that digital copies of this work will be freely available to students and faculty from the publisher's website.

It is impossible to remove all grammatical and typographical errors in a manuscript of the present size. We thank Evan Hemingway (University of California, Berkeley) for his careful proofreading and comments on an earlier draft of this Brief. The responsibility for all remaining errors, typographical and technical, rests on our shoulders and we would be most grateful if you could bring them to our attention.

Los Angeles, CA, USA
Berkeley, CA, USA
Berkeley, CA, USA

M. Khalid Jawed
Alyssa Novelia
Oliver M. O'Reilly

Contents

| | | |
|----------|--|-----------|
| 1 | Introduction | 1 |
| 1.1 | Opening Remarks..... | 1 |
| 1.2 | A Cantilevered Rod | 2 |
| 1.2.1 | Euler's Theory of the Elastica | 3 |
| 1.2.2 | Discrete Elastic Rod | 4 |
| 1.3 | Bending a Rod into a Helical Form | 4 |
| 1.3.1 | Kirchhoff's Rod Theory..... | 4 |
| 1.3.2 | Discrete Elastic Rod | 6 |
| 1.4 | Summary of Terminology | 7 |
| 1.5 | Background on Vector and Tensor Notations | 7 |
| 2 | Kirchhoff's Theory of an Elastic Rod | 11 |
| 2.1 | Introduction | 11 |
| 2.2 | The Frenet, Bishop, and Director Framings of the Material Curve | 12 |
| 2.3 | Angular Velocity and Darboux Vectors..... | 14 |
| 2.3.1 | An Identity Pertaining to Twist | 17 |
| 2.3.2 | An Identity for a Relative Angular Velocity | 18 |
| 2.4 | A Helical Space Curve | 19 |
| 2.4.1 | Computing a Bishop Frame for a Helical Space Curve | 21 |
| 2.5 | Governing Equations for the Kirchhoff Rod | 22 |
| 3 | The Discretized Curve: Vertices, Edges, and Curvature | 25 |
| 3.1 | Introduction | 25 |
| 3.2 | A Turning Angle and Curvatures | 26 |
| 3.3 | An Orthogonal Triad at a Vertex | 28 |
| 3.4 | The Discretized Helical Space Curve | 29 |
| 3.5 | Closing Remarks..... | 32 |

| | |
|--|----|
| 4 Bishop Frames and Reference Frames Along the Discretized Curve | 33 |
| 4.1 Introduction | 33 |
| 4.2 Space-Parallel and Time-Parallel Transport Operators | 33 |
| 4.2.1 The Operator $P_{t^{k-1}}^t$ and Its Associated Darboux Vector $\kappa_k \mathbf{b}_k$ | 34 |
| 4.2.2 The Operator $\bar{P}^k(t, \Delta t)$ and Its Associated Angular Velocity Vector $P \bar{\omega}^k(t)$ | 35 |
| 4.3 Bishop Frames and Reference Frames | 38 |
| 4.3.1 The Discretized Circular Space Curve | 40 |
| 4.4 An Additional Representation for the Operator $P_{t^{k-1}}^t$ | 41 |
| 4.5 Computation of Reference Twist in a Simple Rod | 42 |
| 5 Material Frames and Measures of Twists | 47 |
| 5.1 Introduction | 47 |
| 5.2 The Material Triad | 48 |
| 5.2.1 The Operators $M_{t^{k-1}}^t$ and $\bar{M}^k(t, \Delta t)$ | 49 |
| 5.3 Bending Strains and Curvatures | 50 |
| 5.4 Discrete Integrated Twist | 51 |
| 5.5 Decompositions of the Rotation $M_{t^{k-1}}^t$ | 52 |
| 5.6 Discrete Integrated Twist and Induced Reference Twist | 52 |
| 5.7 Representations for the Operator $\bar{M}^k(t, \Delta t)$ and the Vector $\bar{\omega}^k(t)$ | 55 |
| 5.8 Velocity Vectors of the Material Vectors \mathbf{m}_1^k and \mathbf{m}_2^k | 56 |
| 5.9 Uncoiling of a Twisted Rod | 56 |
| 6 Variations, Gradients, and Hessians | 59 |
| 6.1 Introduction | 59 |
| 6.2 Notation for Gradients and Hessians | 60 |
| 6.3 Variations of the Tangent Vectors | 60 |
| 6.4 Variation of the Turning Angle Between Two Edge Vectors | 61 |
| 6.5 Variation of the Vector $(\kappa \mathbf{b})_k$ | 62 |
| 6.6 Variation of the Material Vectors \mathbf{m}_1^k and \mathbf{m}_2^k | 64 |
| 6.7 Variations and Gradients of the Curvatures κ_{k_1} and κ_{k_2} | 65 |
| 6.8 Gradients and Time Derivative of the Reference Twist m_{ref}^k | 67 |
| 6.9 Preliminary Results for Computing Hessians | 69 |
| 6.10 Hessians of the Reference Twist m_{ref}^k | 70 |
| 6.11 Hessians of the Curvatures κ_{k_1} and κ_{k_2} | 71 |
| 6.12 Closing Remarks | 73 |
| 7 Spherical Excess and Reference Twist | 75 |
| 7.1 Introduction | 75 |
| 7.2 Background from Spherical Geometry | 77 |
| 7.2.1 An Expression for the Variation in the Spherical Excess | 79 |

| | | |
|-------|---|-----|
| 7.3 | Spherical Excess and an Angle of Rotation for a Compound Rotation | 81 |
| 7.3.1 | A Composition of Parallel Transports | 81 |
| 7.3.2 | Computing the Angle $f^k(\epsilon)$ | 84 |
| 7.4 | The Angle $f^k(\epsilon)$ and the Reference Twist $m_{\text{ref}}^k(\epsilon) - m_{\text{ref}}^k(0)$ | 85 |
| 7.4.1 | A Related Result Featuring the Bishop Frame Vectors | 87 |
| 7.5 | Variations of the Twist m_k and Reference Twist δm_{ref}^k | 88 |
| 7.5.1 | Variation of an Angle of Twist ψ_k | 89 |
| 7.6 | A Rod with Three Vertices | 89 |
| 7.6.1 | Spherical Excess and Reference Twist | 90 |
| 7.6.2 | Variation of the Spherical Excess..... | 92 |
| 8 | Equations of Motion and Energetic Considerations | 93 |
| 8.1 | Introduction | 93 |
| 8.2 | Kinetic Energies, Momenta, and Inertias | 94 |
| 8.2.1 | Masses and Inertias..... | 94 |
| 8.2.2 | Linear Momentum, Angular Momentum, and Kinetic Energy | 97 |
| 8.3 | Elastic Energies | 98 |
| 8.4 | Forces, Moments, and Gradients of Elastic Energies | 99 |
| 8.5 | Hessians of the Elastic Energies | 101 |
| 8.5.1 | Validating the Expressions for the Hessians | 105 |
| 8.6 | Viscous Dissipation | 106 |
| 8.7 | Composing the Generalized Force Vector \mathbf{F}_{int} | 107 |
| 8.8 | Composing the Generalized Force Vector \mathbf{F}_{ext} from Applied Forces and Applied Moments | 107 |
| 8.8.1 | Prescribing Terminal Moments: An Example..... | 108 |
| 8.9 | Work-Energy Theorem | 109 |
| 8.10 | Displacement Boundary Conditions | 110 |
| 8.11 | A Vibrating Sagged Cable..... | 110 |
| 8.12 | Closing Remarks..... | 111 |
| | References | 113 |
| | Index | 117 |

Chapter 1

Introduction



“So we beat on, boats against the current, borne back ceaselessly into the past.”

F. Scott Fitzgerald The Great Gatsby.

1.1 Opening Remarks

A formulation of an elastic rod theory which exploits recent developments in discrete differential geometry was developed by Bergou et al. [3, 4]. In their formulation, the rod is modeled as a collection of points (vertices or nodes) connected by stretchable edges. Associated with each edge are a pair of directors (or material vectors) and either a Bishop frame or a reference frame. Later works by Jawed et al. [26, 27] found excellent agreement between the numerical results produced by the formulation and experiments on slender rod-like bodies. The formulation is a novel, computationally efficient, discretized version of the celebrated Kirchhoff rod theory. In a historical context, the formulation is arguably among the most significant additions to the literature since the numerical formulation of Kirchhoff's rod theory by Simo and Vu-Quoc [60] in 1988 and the introduction of Cosserat rod theories to the computer graphics community by Pai [52] in 2002. While Bergou et al.'s formulation has been extended to a shearable rod theory by Linn and Dreßler [38], viscous threads in Bergou et al. [3], and sound generation by Schweickart et al. [57], we confine our attention in this Brief to the version of the theory that approximates a Kirchhoff rod.

Our purpose is to present a comprehensive description of the discrete elastic rod formulation, or DER as it is sometimes known. To motivate our work, we discuss two classic examples from applications of rod theory in this chapter. The pair of examples discussed in this chapter use results from a C++ implementation of the discrete elastic rod formulation. This implementation is discussed in further detail in Jawed et al. [26] and source files for these two examples and others that are presented in this Brief can be accessed at

<http://dynamics.berkeley.edu/>

The first example is a heavy cantilevered rod, while the second example is a rod bent into a helical shape by the application of applied terminal moments. The reader who is familiar with Kirchhoff's rod theory and Euler's theory of the elastica will hopefully find that these examples illuminate some of the novel features of the discrete elastic rod formulation.

The material in this short text covers a range of topics, such as parallel propagation and holonomy from differential geometry, notions on curvature from the nascent field of discrete differential geometry, and Kirchhoff's theory of rods from continuum mechanics. In the interests of conciseness, we refer the reader to the wide range of excellent textbooks on elementary differential geometry (e.g., [23, 53]) and the classic texts by Antman [1] and Love [40] on rod theories for relevant background. Some readers may also find the recent textbook [51] on modeling using rod theories to be helpful. We have assembled most of the necessary background on discrete differential geometry in Chap. 3, however our discussion may be too brief for some readers. For additional detailed expositions on this rapidly developing field, we refer the reader to the lecture notes by Bobenko [6] and Hoffmann [24], and Kirsch's thesis [32].

We are not in a position to survey the extensive literature on finite element formulations of rod theories or to provide a detailed discussion of the place occupied by the discrete elastic rod formulation in the pantheon of numerical formulations of rod theories. To these ends, we refer the interested reader to the recent comprehensive review by Meier et al. [43], a paper on discrete elastic rods by Jung et al. [28], and the introductory sections of [2–4, 29]. As can be seen from a casual reading of the papers [4, 38, 39, 41, 61], the numerical formulations of Kirchhoff's rod theory are capable of modeling complex knots and tangled structures and finds application in a wide range of areas including computer graphics and manufacturing technologies. However, much research remains to be performed in this area to capture the dynamics of knotted structures such as the failure of the shoelace knot discussed in [10].

1.2 A Cantilevered Rod

To illustrate the discrete elastic rod formalism, we consider the problem of a uniform inextensible rod of length ℓ which is cantilevered at one end and free of external loadings at the other end (cf. Fig. 1.1). A vertical gravitational force $-\rho_0 A g \mathbf{E}_2$ is assumed to act at each point of the centerline of the rod. Here, ρ_0 is the mass density per unit volume of the material that the rod is composed of and A is the cross-sectional area of the rod.

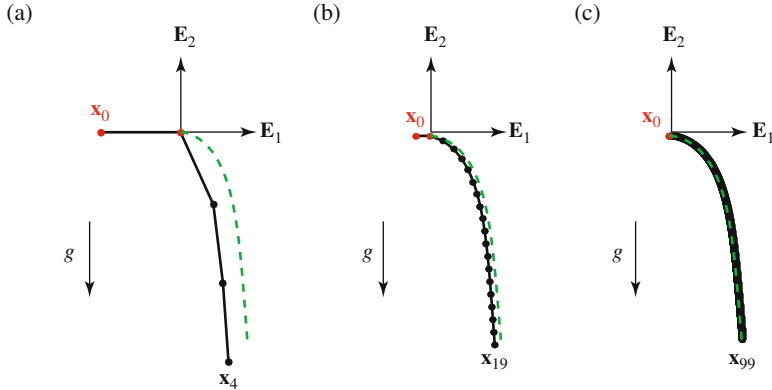


Fig. 1.1 Predictions for the deformed shape of the centerline of a cantilevered rod using Euler's classic theory of the elastica (shown as a dashed green line) and the discrete elastic rod formulation (shown as a solid black line connecting vertices): (a) Four edges and five vertices: $\mathbf{x}_0, \dots, \mathbf{x}_4$; (b) Nineteen edges and twenty vertices: $\mathbf{x}_0, \dots, \mathbf{x}_{19}$; and (c) 100 vertices and 99 edges: $\mathbf{x}_0, \dots, \mathbf{x}_{99}$. The first edge in these models are assumed fixed: \mathbf{x}_0 and \mathbf{x}_1 are constant

1.2.1 Euler's Theory of the Elastica

The simplest model for such a rod is Euler's theory of the elastica [11, 40]. This classic theory, which dates to 1744, assumes that the bending moment in the rod is linearly proportional to the curvature of the centerline of the rod, that the deformation of the rod is planar, and that cross-sections that were normal to the centerline in an undeformed configuration remain normal to the centerline as the rod is deformed. For the static problem at hand, it is straightforward to formulate the governing differential equation for the angle θ subtended by the tangent vector to the rod with the horizontal. This second-order differential equation is supplemented by a pair of differential equations for the position vector $\mathbf{r} = x\mathbf{E}_1 + y\mathbf{E}_2$ of the centerline¹:

$$\begin{aligned} \frac{\partial}{\partial s} \left(EI \frac{\partial \theta}{\partial s} \right) + \rho_0 A g (\ell - s) \cos(\theta) &= 0, \\ \frac{\partial x}{\partial s} = \cos(\theta), \quad \frac{\partial y}{\partial s} = \sin(\theta). \end{aligned} \quad (1.1)$$

Here, EI is the flexural rigidity of the rod and s is the arclength parameter. The differential equations are supplemented by the boundary conditions

¹In the interest of brevity, the reader is referred to [51, Chap. 4] for a discussion on the formulation of this boundary-value problem using Euler's theory of the elastica.

$$\theta(s=0) = 0, \quad \frac{\partial\theta}{\partial s}(s=\ell) = 0, \quad x(s=0) = 0, \quad y(s=0) = 0. \quad (1.2)$$

As shown in Fig. 1.1, Eqs. (1.1) and (1.2) are solved numerically to determine the deformed centerline of the rod.

1.2.2 Discrete Elastic Rod

The cantilevered rod can also be modeled using Bergou et al.'s [3, 4] theory of a discrete elastic rod. In this formulation, the centerline rod is subdivided into a series of $n - 1$ connected segments (edges). The points where the edges meet are known as vertices. The parameters, EI , ρ_0 , and segment lengths ℓ_k for this rod are specified along with boundary conditions and initial conditions. For the example considered here, we assume that the rod has a circular cross-section of radius r_0 and unstretched length ℓ with the following parameter values:

$$\ell = 0.2 \text{ m}, \quad \ell_k = \frac{0.2}{n-1} \text{ m}, \quad r_0 = 1 \text{ mm}, \quad E = 1 \text{ MPa}. \quad (1.3)$$

The mass density per unit volume in the reference state of the slender three-dimensional body that the rod is modeling is $\rho_0 = 1000 \text{ kg/m}^3$. The shape of the centerline after the transients have decayed sufficiently is shown in Fig. 1.1. As can be seen from this figure, as n increases, the solution provided by the discrete elastic rod formulation converges to the deformed centerline predicted by Euler's theory of the elastica.

1.3 Bending a Rod into a Helical Form

The next problem we consider is also classic and involves bending a rod of length ℓ through the application of equal and opposite terminal moments \mathbf{M}_0 and \mathbf{M}_ℓ . We assume that the rod is isotropic with a flexural rigidity EI and a torsional rigidity \mathcal{D} . In its undeformed state, the centerline of the rod is assumed to be straight and the rod is assumed to be free of twist. This problem is discussed in [51, Sect. 5.14] and, in the interest of brevity, we refer the reader to this text for additional details.

1.3.1 Kirchhoff's Rod Theory

The classic model for this problem dates to Kirchhoff in 1858. In his theory [31], the centerline of the rod is not restricted to be planar and the cross-sections of the rod are free to twist about the centerline. The cross-sections are assumed to remain

normal to the centerline and their orientation can be described using a rotation tensor \mathbf{R}_D . A solution to the boundary-value problem in this theory provides the position vector $\mathbf{r} = \mathbf{r}(s, t)$ of points on the centerline as well as $\mathbf{R}_D = \mathbf{R}_D(s, t)$. Here, s denotes the arc length parameter of the inextensible centerline and t denotes time.

The deformation of the rod is given by the bending strains v_1 and v_2 and the torsional strain v_3 . These three strains are the components of the axial vector $\text{ax}(\mathbf{R}_D^T \frac{\partial \mathbf{R}_D}{\partial s})$. The moment \mathbf{M} in the rod is given by the expression

$$\mathbf{M}(s) = EI(v_1(s)\mathbf{d}_1(s) + v_2(s)\mathbf{d}_2(s)) + \mathcal{D}v_3(s)\mathbf{d}_3(s). \quad (1.4)$$

Here, \mathbf{d}_i are directors (which we will discuss further in Chap. 2). The terminal moments are $\mathbf{M}_0 = -\mathbf{M}(0)$ and $\mathbf{M}_\ell = \mathbf{M}(\ell)$ where $\mathbf{M}_\ell = -\mathbf{M}_0$.

It can be shown that the moment \mathbf{M} and force \mathbf{n} are constant throughout the rod. In addition, analytical expressions can be found for the strains:

$$\begin{bmatrix} v_1(s) \\ v_2(s) \end{bmatrix} = \begin{bmatrix} \cos(\delta s) & \sin(\delta s) \\ -\sin(\delta s) & \cos(\delta s) \end{bmatrix} \begin{bmatrix} v_1(0) \\ v_2(0) \end{bmatrix}, \quad (1.5)$$

where

$$v_3(s) = v_3(0), \quad \delta = \left(1 - \frac{\mathcal{D}}{EI}\right) v_3(0). \quad (1.6)$$

That is, the torsional strain in the rod is constant. Additionally, the curvature κ and torsion τ of the centerline of the rod are constant:

$$\kappa = \sqrt{v_1^2(s) + v_2^2(s)} = \sqrt{v_1^2(0) + v_2^2(0)}, \quad \tau = \left(\frac{\mathcal{D}}{EI}\right) v_3(0). \quad (1.7)$$

Finally, the twist angle ϕ of the rod can be found by integrating

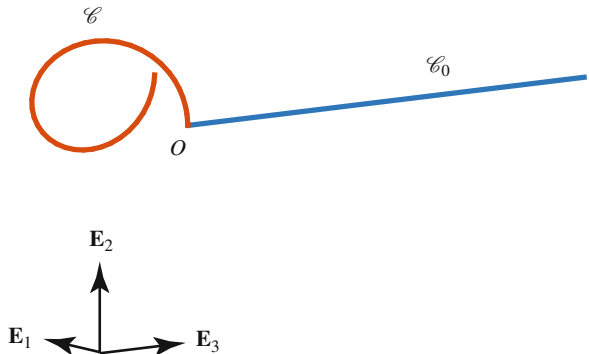
$$\frac{\partial \phi}{\partial s} = \delta. \quad (1.8)$$

We refer the reader to [51, Sect. 5.14] for details on the computation of $v_i(s)$, τ , κ , and $\frac{\partial \phi}{\partial s}$. As discussed in classic texts on differential geometry (see, e.g., Kreyszig [34]), the only curve which has a constant curvature and constant non-zero torsion is a circular helix and so we conclude that the centerline of the rod is a helical space curve and the rod has a constant twist $\frac{\partial \phi}{\partial s}$.

The example shown in Fig. 1.2 pertains to a rod with a circular cross-section of radius r_0 and unstretched length ℓ with the following parameter values:

$$\ell = 0.2 \text{ m}, \quad r_0 = 0.79 \text{ mm}, \quad EI = 3.97687 \times 10^{-7} \text{ Nm}^2, \quad \mathcal{D} = \frac{2}{3}EI, \quad (1.9)$$

Fig. 1.2 Predicted deformed shape of the centerline of a rod using Kirchhoff's rod theory. The centerline \mathcal{C} has a constant curvature and torsion [cf. Eq. (1.11)]. For completeness, the reference configuration \mathcal{C}_0 of the centerline is also shown. The parameter values for this rod are presented in Eq. (1.9) and the terminal moments can be inferred from Eq. (1.10)



and terminal moment

$$\mathbf{M}_0 = 20EI(\mathbf{E}_1 + \mathbf{E}_2) - 20\mathcal{D}\mathbf{E}_3. \quad (1.10)$$

In its undeformed state, the mass density per unit volume of the slender three-dimensional body that the rod is modeling is $\rho_0 = 1000 \text{ kg/m}^3$. Solving the resulting boundary-value problem produces a rod with a constant twist and a centerline in the shape of a helical space curve with

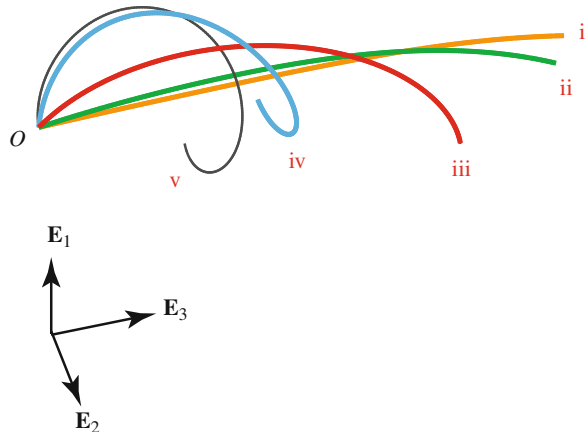
$$\kappa = 28.2843 \text{ m}^{-1}, \quad \tau = 13.3333 \text{ m}^{-1}. \quad (1.11)$$

1.3.2 Discrete Elastic Rod

The solution to the rod that is bent under the action of terminal moments is shown in Fig. 1.3. The discrete elastic rod formulation solves an initial-value problem where the rod is initially straight and evolves in time to its bent final configuration. For the solution shown in Fig. 1.3, the rod is discretized using 99 edges and has $n = 100$ vertices (or nodes): $\mathbf{x}_0, \dots, \mathbf{x}_{n-1}$. The edges of the rod are $\mathbf{e}^0, \dots, \mathbf{e}^{n-2}$. Each of the terminal moments are accommodated using a pair of couples which we discuss in further detail in Sect. 8.8.1.

A small viscous damping is present in the formulation so that dynamical effects dissipate and a static equilibrium configuration is attained. The shape of the final deformed configuration of the rod is identical to that predicted by Kirchhoff's rod theory. Further details on the dissipation can be found in Sect. 8.6.

Fig. 1.3 Predicted deformed shape of the centerline of a rod using the discrete elastic rod formulation: i: $t = 1$ s; ii: $t = 2$ s; iii: $t = 5$ s; iv: $t = 10$ s; and v: $t = 20$ s. For this simulation, $n = 100$ and the remaining rod parameter values are presented in Eq. (1.9)



1.4 Summary of Terminology

While the formulation of a discrete elastic rod discussed in this text features terminology that is adapted from theories of rods, a wide range of new quantities are introduced. For the reader's convenience, the most significant of these kinematical quantities are summarized in Tables 1.1 and 1.2.

1.5 Background on Vector and Tensor Notations

We assume that the reader has background in vector and tensor calculus at the level discussed in continuum mechanics textbooks such as Chadwick [8] and Gurtin [20]. With the notable exception of the parallel transport operators $\bar{P}^k(t, \Delta t) \equiv P_{t^k(t)}^{t^k(t+\Delta t)}$ and $P_{t^k-1}^{t^k}$ and their respective material vector rotations $\bar{M}^k(t, \Delta t) \equiv M_{t^k(t)}^{t^k(t+\Delta t)}$ and $M_{t^k-1}^{t^k}$, vectors and tensors are denoted by bold-faced letters (e.g., \mathbf{R}, \mathbf{x}_k) and arrays are denoted using a sans-serif font (e.g., \mathbf{F}_{ext}). We define $\{\mathbf{E}_1, \mathbf{E}_2, \mathbf{E}_3\}$ to be a fixed right-handed Cartesian basis for \mathbb{E}^3 and introduce several other bases throughout this book. In contrast to many works on continuum mechanics, lower-case Roman indices in this text will range from 0 to $n - 1$ or 0 to $n - 2$.

The tensor product of any pair \mathbf{a} and \mathbf{b} of vectors is defined as

$$(\mathbf{a} \otimes \mathbf{b}) \mathbf{c} = (\mathbf{b} \cdot \mathbf{c}) \mathbf{a}, \quad (1.12)$$

Table 1.1 A partial summary of the notation and terminology for kinematical quantities associated with discrete elastic rods

| Notation | Terminology |
|---|--|
| φ_k | Turning angle at the k th vertex |
| \mathbf{x}_k | Position vector of the k th vertex (or node) |
| ℓ_k | Length of the Voronoi domain at a vertex (or node) |
| \mathbf{e}^k | Edge vector to the k th edge |
| \mathbf{t}^k | Unit tangent vector to the k th edge |
| $\Delta \mathbf{t}_k = \mathbf{t}^k - \mathbf{t}^{k-1}$ | Difference in the tangent vectors at the k th vertex |
| \mathbf{t}_{γ_k} | Discrete vertex tangent on the k th edge |
| \mathbf{b}_k | Discrete binormal vector |
| κ_i | Discrete integrated curvature at the k th vertex |
| $\hat{\kappa}_i$ | Discrete pointwise curvature at the k th vertex |
| $(\kappa \mathbf{b})_i = \kappa_i \mathbf{b}_i$ | Discrete integrated curvature vector at the i th vertex |
| $\{\mathbf{t}^k, \mathbf{u}^k, \mathbf{v}^k = \mathbf{t}^k \times \mathbf{u}^k\}$ | Bishop frame on the k th edge |
| $\{\mathbf{t}^k, \mathbf{m}_1^k, \mathbf{m}_2^k = \mathbf{t}^k \times \mathbf{m}_1^k\}$ | Director (or material) frame on the k th edge |
| $\{\mathbf{t}^k, \mathbf{a}_1^k, \mathbf{a}_2^k = \mathbf{t}^k \times \mathbf{a}_1^k\}$ | Reference frame on the k th edge |
| $P_{\mathbf{t}^{k-1}}^{\mathbf{t}^k} = \mathbf{R}(\varphi_k, \mathbf{b}_k)$ | Space-parallel transport operator at the k th vertex |
| $\bar{P}^k(t, \Delta t) \equiv P_{\mathbf{t}^k(t)}^{\mathbf{t}^k(t+\Delta t)} = \mathbf{R}(\alpha^k(t, \Delta t), \mathbf{h}^k(t, \Delta t))$ | Time-parallel transport operator on the k th edge |
| $M_{\mathbf{t}^{k-1}}^{\mathbf{t}^k}$ | Relative rotation tensor for the material vectors on the k th edge |
| $\bar{M}^k(t, \Delta t) \equiv M_{\mathbf{t}^k(t)}^{\mathbf{t}^k(t+\Delta t)}$ | Relative rotation tensor for the material vectors on the k th edge |

Table 1.2 Summary of the measures associated with the i th vertex and the k th edge of a discrete elastic rod and the angles used to define these measures

| Notation | Terminology |
|--|--|
| $\kappa_i = \tan\left(\frac{\varphi_i}{2}\right)$ | Discrete integrated curvature at the i th vertex |
| ϑ^k | Rotation angle between \mathbf{m}_1^k and \mathbf{u}^k along the k th edge |
| m_{ref}^{k+1} | Referential twist associated with the $(k+1)$ th edge |
| $\chi^k(t + \Delta t)$ | Angle between $\mathbf{u}^k(t + \Delta t)$ and $\bar{P}^k(t, \Delta t) \mathbf{u}^k(t)$ along the k th edge at time $t + \Delta t$ |
| γ^k | Turning angle between \mathbf{a}_1^k and \mathbf{m}_1^k along the k th edge |
| β^k | Turning angle between \mathbf{u}^k and \mathbf{a}_1^k along the k th edge |
| $m_k = \vartheta^k - \vartheta^{k-1} = \gamma^k - \gamma^{k-1} + m_{\text{ref}}^k$ | Discrete integrated twist along the k th edge |
| $\kappa_{i_1} = \frac{1}{2} \left(\mathbf{m}_2^{i-1} + \mathbf{m}_2^i \right) \cdot (\kappa \mathbf{b})_i$ | Vertex-based material curvature at the i th vertex |
| $\kappa_{i_2} = -\frac{1}{2} \left(\mathbf{m}_1^{i-1} + \mathbf{m}_1^i \right) \cdot (\kappa \mathbf{b})_i$ | Vertex-based material curvature at the i th vertex |

for any vector \mathbf{c} . The transpose \mathbf{A}^T of a second-order tensor \mathbf{A} satisfies the identity

$$(\mathbf{A}^T \mathbf{a}) \cdot \mathbf{b} = (\mathbf{Ab}) \cdot \mathbf{a}, \quad (1.13)$$

for any two vectors \mathbf{a} and \mathbf{b} . Thus, $(\mathbf{c} \otimes \mathbf{d})^T = \mathbf{d} \otimes \mathbf{c}$.

Given any tensor \mathbf{A} , the symmetric part and skew-symmetric parts of the tensor can be computed using the following operators:

$$\text{sym}(\mathbf{A}) = \frac{1}{2}(\mathbf{A} + \mathbf{A}^T), \quad \text{skw}(\mathbf{A}) = \frac{1}{2}(\mathbf{A} - \mathbf{A}^T). \quad (1.14)$$

If \mathbf{B} is a skew-symmetric tensor, $\mathbf{B} = -\mathbf{B}^T$, then $\text{sym}(\mathbf{B}) = \mathbf{0}$ and $\text{skw}(\mathbf{B}) = \mathbf{B}$.

A skew-symmetric tensor $\mathbf{C} = -\mathbf{C}^T$ has an associated axial vector $\text{ax}(\mathbf{C})$:

$$\text{ax}(\mathbf{C}) \times \mathbf{b} = \mathbf{Cb} \text{ for any vector } \mathbf{b} \text{ where } \mathbf{C} = -\mathbf{C}^T. \quad (1.15)$$

For instance, the axial vector associated with $\mathbf{C} = \mathbf{E}_2 \otimes \mathbf{E}_1 - \mathbf{E}_1 \otimes \mathbf{E}_2$ is \mathbf{E}_3 . Equivalently, a skew-symmetric tensor can be defined for a vector \mathbf{c} :

$$\text{skewt}(\mathbf{c}) \mathbf{b} = \mathbf{c} \times \mathbf{b} \text{ for any vector } \mathbf{b}. \quad (1.16)$$

The correspondence between a skew-symmetric tensor and a vector is used to compute the angular velocity and Darboux vectors associated with the partial derivatives of rotation tensors.

A very useful representation for a tensor \mathbf{A} can be found by considering the action of this operator on an orthonormal basis. We denote the orthonormal basis by $\{\mathbf{f}_1, \mathbf{f}_2, \mathbf{f}_3\}$ and compute

$$\mathbf{g}_1 = \mathbf{Af}_1, \quad \mathbf{g}_2 = \mathbf{Af}_2, \quad \mathbf{g}_3 = \mathbf{Af}_3. \quad (1.17)$$

Then, it can be shown that

$$\mathbf{A} = \mathbf{g}_1 \otimes \mathbf{f}_1 + \mathbf{g}_2 \otimes \mathbf{f}_2 + \mathbf{g}_3 \otimes \mathbf{f}_3. \quad (1.18)$$

This representation is appealed to repeatedly in Chaps. 4 and 5 to compute representations for $P_{\mathbf{t}^{k-1}}^{\mathbf{t}^k}$, $\bar{P}^k(t, \Delta t)$, $M_{\mathbf{t}^{k-1}}^{\mathbf{t}^k}$, and $\bar{M}^k(t, \Delta t)$.

Chapter 2

Kirchhoff's Theory of an Elastic Rod



2.1 Introduction

Rod theories are theories of deformable media that are used to model long slender bodies. There are numerous theories including Euler's planar theory of the elastica [40], Antman's Cosserat rod theory [1], and Green and Naghdi's Cosserat rod theories [18, 19]. Of particular interest in this book is a nonlinear theory of a deformable elastic rod that dates to Kirchhoff [31] in 1859. As discussed in [1, 40], his formulation has been generalized and improved and our developments below take advantage of these works.

From the simplest such theory to the most elaborate, a primary feature of rod theories is the identification of a material curve in the slender body. The material curve is often chosen to be the centerline of the body but it can also be chosen as a material curve on the lateral surface of the body. One also identifies two configurations of the slender body: the reference configuration \mathcal{K}_0 and the present configuration \mathcal{K} . The material curve \mathcal{L} in these configurations occupies the respective space curves \mathcal{C}_0 and \mathcal{C} . The position vector of a point on the material curve in the present configuration at time t is defined by the position vector

$$\mathbf{r}(s, t) = x(s, t)\mathbf{E}_1 + y(s, t)\mathbf{E}_2 + z(s, t)\mathbf{E}_3, \quad (2.1)$$

where s is the arclength parameter for \mathcal{C} . The unit tangent vector to \mathcal{C} is denoted by $\mathbf{e}_t = \frac{\partial \mathbf{r}}{\partial s}$. The curve traced by the image of \mathbf{e}_t on the unit sphere is known as the tangent indicatrix c_t . We shall assume that the centerline is inextensible.

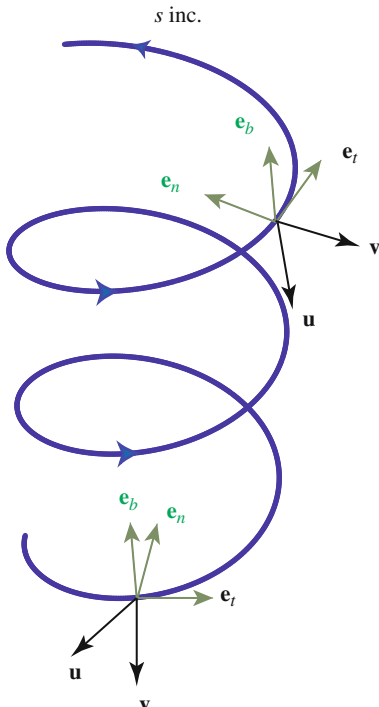
While the material curve \mathcal{L} is intended to capture the deformation of the centerline, the behavior of the cross-sections of the rod is equally important. To capture their deformation using a rod theory, two linearly independent vectors, \mathbf{d}_1 and \mathbf{d}_2 , which are often known as directors, are associated with each point of the material curve \mathcal{L} . For many rod theories, including Kirchhoff's rod theory, the

directors in the reference configuration are chosen to be normal to the centerline and they are assumed to remain perpendicular to the centerline: $\mathbf{d}_1 \cdot \mathbf{e}_t = 0$ and $\mathbf{d}_2 \cdot \mathbf{e}_t = 0$. In such theories, the cross-sections are also assumed to retain their dimensions and so \mathbf{d}_1 and \mathbf{d}_2 are chosen to be unit vectors that remain orthogonal: $\mathbf{d}_1 \cdot \mathbf{d}_2 = 0$. The motion of the rod is defined by the pair $(\mathbf{r}, \mathbf{R}_D)$ where $\mathbf{R}_D(s, t)$ is the rotation tensor associated with the directors.

2.2 The Frenet, Bishop, and Director Framings of the Material Curve

The director triad $\{\mathbf{e}_t, \mathbf{d}_1, \mathbf{d}_2\}$ at each point s of a space curve \mathcal{C} . An infinite number of other framings are possible and the two most popular are the Frenet triad $\{\mathbf{e}_t, \mathbf{e}_n, \mathbf{e}_b\}$ and the Bishop triad $\{\mathbf{e}_t, \mathbf{u}, \mathbf{v}\}$ (cf. Figs. 2.1 and 2.2). The latter framing was developed by Bishop [5] in 1975 and was subsequently employed in the context of elastic rods by Langer and Singer [36] in 1996. Unlike the Frenet triad, the Bishop triad is uniquely defined even at inflection points on the curve where the curvature vanishes and is parallel

Fig. 2.1 A right-handed helix showing the Frenet triad $\{\mathbf{e}_t, \mathbf{e}_n, \mathbf{e}_b\}$ and a Bishop triad $\{\mathbf{e}_t, \mathbf{u}, \mathbf{v}\}$ at two points along its length



propagated (or transported) along \mathcal{C} .¹ The singular feature of the Frenet triad motivated Bishop's work on alternative framings. It is interesting to note that while the Frenet framing can be traced to Serret [58] and Frenet [13] in the 1850s and the director framing dates to the Cosserat brothers in 1907 [9], the introduction of the Bishop frame in 1975 is remarkably recent. Inspired by Langer and Singer [36], the Bishop frame is starting to be used by the mechanics community (see, for instance, [51, 67] and references therein). As a consequence of the parallel propagation, the Bishop triad is said to be free of twist. Thus, the rate of change with respect to s of the angle of rotation of the director \mathbf{d}_1 relative to \mathbf{u} (or, equivalently, the director \mathbf{d}_2 relative to \mathbf{v}) is used as a measure of the torsional strain of the rod.

The Bishop, Frenet, and director triads along with the associated space curve \mathcal{C} constitute examples of adapted frames. The adjective adapted refers to the fact that one of the vectors in each of these triads is the unit tangent vector to \mathcal{C} . To help illuminate the previous developments, examples of the Frenet and Bishop triads for a helical space curve will be presented in Sect. 2.4.

Given a frame, we can define a rotation tensor which captures the motion of the frame from a fixed reference configuration to the current (or present) configuration. Thus, a rotation tensor $\mathbf{R}_B = \mathbf{R}_B(s, t)$ can be associated with the Bishop frame. This tensor is a function of time t and also the placement s along the material curve. Referring the reader to Figs. 2.2 and 2.3, the rotation tensors \mathbf{R}_{SF} and \mathbf{R}_D associated with the Frenet and director triads differ from \mathbf{R}_B by rotations about $\mathbf{e}_t = \mathbf{d}_3$:

$$\mathbf{R}_D = \mathbf{R}(\phi, \mathbf{e}_t) \mathbf{R}_{SF} = \mathbf{R}(\phi + \varphi, \mathbf{e}_t) \mathbf{R}_B, \quad (2.2)$$

where the angle φ is defined by the relation

$$\tau = \frac{\partial \varphi}{\partial s}, \quad (2.3)$$

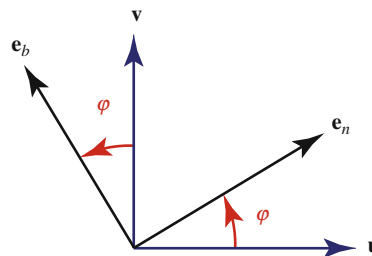
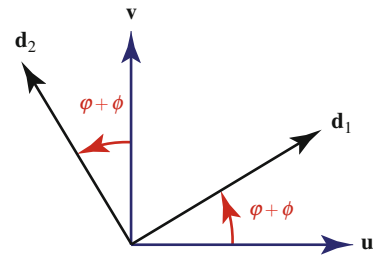


Fig. 2.2 The Bishop frame vectors \mathbf{u} and \mathbf{v} at a point on a space curve lie in the plane to the space curve formed by the normal \mathbf{e}_n and binormal \mathbf{e}_b vectors. The pairs of vectors $(\mathbf{e}_n, \mathbf{e}_b)$ and (\mathbf{u}, \mathbf{v}) are related by an angle φ where $\frac{\partial \varphi}{\partial s} = \tau$ with τ denoting the (geometric) torsion of the space curve

¹At an inflection point, the curvature κ of the space curve vanishes and the derivative of \mathbf{e}_t cannot be used to uniquely define the normal vector \mathbf{e}_n to the space curve.

Fig. 2.3 The directors \mathbf{d}_1 and \mathbf{d}_2 at a point on a space curve lie in the plane to the space curve formed by the Bishop frame vectors \mathbf{u} and \mathbf{v} . These pairs of vectors are related by an angle $\varphi + \phi$ where $\frac{\partial \phi}{\partial s} + \frac{\partial \varphi}{\partial s} = v_3$



and $\mathbf{R}(\theta, \mathbf{r})$ denotes a counterclockwise rotation through an angle θ about a unit vector \mathbf{r} :

$$\mathbf{R}(\theta, \mathbf{r}) = \cos(\theta) (\mathbf{I} - \mathbf{r} \otimes \mathbf{r}) + \sin(\theta) \text{skewt}(\mathbf{r}) + \mathbf{r} \otimes \mathbf{r}. \quad (2.4)$$

The operator $\text{skewt}(\mathbf{r})$ defines a skew-symmetric tensor (cf. Sect. 1.5) and τ denotes the (geometric) torsion of the space curve.

We can choose the reference configuration for \mathcal{L} such that

$$\mathbf{e}_t = \mathbf{R}_B \mathbf{E}_3, \quad \mathbf{u} = \mathbf{R}_B \mathbf{E}_1, \quad \mathbf{v} = \mathbf{R}_B \mathbf{E}_2, \quad (2.5)$$

where $\{\mathbf{E}_1, \mathbf{E}_2, \mathbf{E}_3\}$ is a fixed right-handed Cartesian basis for \mathbb{E}^3 . With this choice of reference, the rotation tensors have the following representations:

$$\begin{aligned} \mathbf{R}_B &= \mathbf{e}_t \otimes \mathbf{E}_3 + \mathbf{u} \otimes \mathbf{E}_1 + \mathbf{v} \otimes \mathbf{E}_2, \\ \mathbf{R}_{SF} &= \mathbf{e}_t \otimes \mathbf{E}_3 + \mathbf{e}_n \otimes \mathbf{E}_1 + \mathbf{e}_b \otimes \mathbf{E}_2, \\ \mathbf{R}_D &= \mathbf{e}_t \otimes \mathbf{E}_3 + \mathbf{d}_1 \otimes \mathbf{E}_1 + \mathbf{d}_2 \otimes \mathbf{E}_2. \end{aligned} \quad (2.6)$$

Representations of this type can be established for any rotation tensor and will be particularly useful in Chaps. 4, 5, and 7.

2.3 Angular Velocity and Darboux Vectors

Given an orthonormal triad $\{\mathbf{f}_1(s, t), \mathbf{f}_2(s, t), \mathbf{f}_3(s, t)\}$ and an associated rotation tensor $\mathbf{F}(s, t)$, we can define a pair of axial vectors:

$$\boldsymbol{\omega} = \text{ax}(\dot{\mathbf{F}}\mathbf{F}^T), \quad \mathbf{v} = \text{ax}(\mathbf{F}'\mathbf{F}^T). \quad (2.7)$$

Here, the \cdot denotes the partial derivative with respect to t and the prime denotes the partial derivative with respect to s . The vector \mathbf{v} is often referred to as a Darboux vector while $\boldsymbol{\omega}$ is known as an angular velocity vector. We identify the unit tangent vector $\mathbf{e}_t = \mathbf{f}_3$. Thus, the frame is adapted (to the curve \mathcal{C}).

Consider a rotation tensor $\mathbf{R} = \mathbf{R}(\theta, \mathbf{r})$ where the angle θ and axis of rotation depend on a parameter u : $\theta = \theta(u)$ and $\mathbf{r} = \mathbf{r}(u)$. It can be shown that the axial vector associated with the change in \mathbf{R} has a classic representation²:

$$\boldsymbol{\omega}_u = \text{ax} \left(\frac{\partial \mathbf{R}}{\partial u} \mathbf{R}^T \right) = \frac{\partial \theta}{\partial u} \mathbf{r} + \sin(\theta) \frac{\partial \mathbf{r}}{\partial u} + (1 - \cos(\theta)) \mathbf{r} \times \frac{\partial \mathbf{r}}{\partial u}. \quad (2.8)$$

In many instances, \mathbf{R} is decomposed into a series of rotations:

$$\mathbf{R} = \mathbf{R}_2(\theta_2, \mathbf{r}_2) \mathbf{R}_1(\theta_1, \mathbf{r}_1), \quad (2.9)$$

where \mathbf{r}_2 depends on \mathbf{R}_1 . For such rotations, we can use the notion of a relative angular velocity vector to show that³

$$\boldsymbol{\omega}_u = \frac{\partial \theta_2}{\partial u} \mathbf{r}_2 + \frac{\partial \theta_1}{\partial u} \mathbf{r}_1 + \sin(\theta_1) \frac{\partial \mathbf{r}_1}{\partial u} + (1 - \cos(\theta_1)) \mathbf{r}_1 \times \frac{\partial \mathbf{r}_1}{\partial u}. \quad (2.10)$$

Here, $\frac{\partial \theta_2}{\partial u} \mathbf{r}_2$ can be interpreted as the angular rate of \mathbf{R}_2 relative to \mathbf{R}_1 . Prominent instances of relative rotations in this Brief include the twisting of a rod [cf. Eq. (2.20)] and the determination of the angular velocity associated with the rotation of the material frame vectors [cf. Eq. (5.25)].

By examining the identities $\dot{\mathbf{f}}_3 = \boldsymbol{\omega} \times \mathbf{f}_3$ and $\mathbf{f}'_3 = \mathbf{v} \times \mathbf{f}_3$, one finds that the axial vectors also have the following representations⁴:

$$\boldsymbol{\omega} = \sum_{i=1}^3 \omega_i \mathbf{f}_i = \mathbf{f}_3 \times \dot{\mathbf{f}}_3 + \omega_3 \mathbf{f}_3, \quad \mathbf{v} = \sum_{i=1}^3 v_i \mathbf{f}_i = \mathbf{f}_3 \times \mathbf{f}'_3 + v_3 \mathbf{f}_3. \quad (2.11)$$

After manipulating the mixed derivative $\dot{\mathbf{F}}'$, we find that \mathbf{v} and $\boldsymbol{\omega}$ satisfy the compatibility condition [2, 17]

$$\dot{\mathbf{v}} = \boldsymbol{\omega}' + \boldsymbol{\omega} \times \mathbf{v}. \quad (2.12)$$

As emphasized in [3, 4] and illuminated by Eq. (2.11), the components of \mathbf{v} and $\boldsymbol{\omega}$ orthogonal to the vector \mathbf{f}_3 are specified completely by \mathbf{f}_3 and its partial derivatives.

Returning to the rotation tensor \mathbf{R}_B associated with the Bishop frame, this tensor has a pair of axial vectors:

²For details on this calculation, see the authoritative review by Shuster [59].

³The relative angular velocity vector of interest is discussed in Casey and Lam [7]. The textbook [50] presents several examples highlighting Casey and Lam's relative angular velocity vector. Among the examples considered are the rotation sequence used in Euler angle parameterizations of rotations.

⁴The kinematic quantity $\tau = \mathbf{v}_D \cdot \mathbf{d}_3$ where $\mathbf{d}_3 = \mathbf{e}_t$ is referred to as the kinematic twist in [2], but this terminology can be confusing to those familiar with angle of twist ϕ . Here, $\mathbf{v}_D = \text{ax}(\mathbf{R}'_D \mathbf{R}_D^T)$.

$$\mathbf{v}_B = \text{ax} \left(\mathbf{R}'_B \mathbf{R}_B^T \right), \quad \boldsymbol{\omega}_B = \text{ax} \left(\dot{\mathbf{R}}_B \mathbf{R}_B^T \right). \quad (2.13)$$

The axial vectors have the representations

$$\begin{aligned} \boldsymbol{\omega}_B &= \omega_{B_3} \mathbf{e}_t + \omega_{B_1} \mathbf{u} + \omega_{B_2} \mathbf{v}, \\ \mathbf{v}_B &= v_{B_3} \mathbf{e}_t + \kappa_1 \mathbf{u} + \kappa_2 \mathbf{v}. \end{aligned} \quad (2.14)$$

The Bishop frame is chosen so that $v_{B_3} = 0$ and is sometimes referred to as a twist-free frame for this reason. For this pair of axial vectors, it can be shown that $\dot{\mathbf{v}}_B = \boldsymbol{\omega}'_B$. In addition, we note that

$$\begin{aligned} \dot{\mathbf{e}}_t &= \boldsymbol{\omega}_B \times \mathbf{e}_t, & \dot{\mathbf{u}} &= \boldsymbol{\omega}_B \times \mathbf{u}, & \dot{\mathbf{v}} &= \boldsymbol{\omega}_B \times \mathbf{v}, \\ \mathbf{e}'_t &= \mathbf{v}_B \times \mathbf{e}_t, & \mathbf{u}' &= \mathbf{v}_B \times \mathbf{u}, & \mathbf{v}' &= \mathbf{v}_B \times \mathbf{v}. \end{aligned} \quad (2.15)$$

Related results hold for other framings of the curve.

Recall that the rotation tensors \mathbf{R}_{SF} for the Frenet triad and \mathbf{R}_D for the director triad provide linear mappings:

$$\begin{aligned} \mathbf{e}_t &= \mathbf{R}_{SF} \mathbf{E}_3, & \mathbf{e}_n &= \mathbf{R}_{SF} \mathbf{E}_1, & \mathbf{e}_b &= \mathbf{R}_{SF} \mathbf{E}_2, \\ \mathbf{d}_1 &= \mathbf{R}_D \mathbf{E}_1, & \mathbf{d}_2 &= \mathbf{R}_D \mathbf{E}_2, & \mathbf{d}_3 &= \mathbf{R}_D \mathbf{E}_3. \end{aligned} \quad (2.16)$$

Here, for notational convenience, $\mathbf{d}_3 = \mathbf{e}_t$. The Darboux vector associated with the Frenet triad has the representation

$$\mathbf{v}_{SF} = \kappa \mathbf{e}_b + \tau \mathbf{e}_t, \quad (2.17)$$

where we recall that τ is the geometric torsion and κ is the curvature. It is useful to observe that

$$\kappa \mathbf{e}_b = \mathbf{e}_t \times \mathbf{e}'_t, \quad \tau = \frac{1}{\| \mathbf{e}_t \times \mathbf{e}'_t \|^2} (\mathbf{e}_t \times \mathbf{e}'_t) \cdot \mathbf{e}''_t. \quad (2.18)$$

Thus, $\kappa \mathbf{e}_b$ is completely defined by \mathbf{e}_t and its spatial derivative. It is important to emphasize that the Darboux vector associated with the Bishop frame is torsionless:

$$\mathbf{v}_B = \kappa \mathbf{e}_b = \kappa_1 \mathbf{u} + \kappa_2 \mathbf{v}. \quad (2.19)$$

Whence, the Bishop triad is said to be parallel transported along the space curve. This transport is best visualized by considering the tangent indicatrix c_t of the space curve on the unit sphere. The corresponding images of the vectors \mathbf{u} and \mathbf{v} will be

tangent to the sphere and are parallel transported along c_t .⁵ Examples of parallel propagation (or transport) are shown in Fig. 2.7 for the cases where the space curve \mathcal{C} is a circle and a circular helix.⁶

The Darboux vector and its counterpart for the director triad are related by an angle of twist ϕ (cf. Love [40, Chap. 18] or [51, Chap. 5]):

$$\begin{aligned}\mathbf{v}_D &= \sum_{i=1}^3 v_i \mathbf{d}_i = \text{ax}(\mathbf{R}'_D \mathbf{R}_D^T) \\ &= \mathbf{v}_{SF} + \frac{\partial \phi}{\partial s} \mathbf{e}_t \\ &= \mathbf{v}_B + \left(\tau + \frac{\partial \phi}{\partial s} \right) \mathbf{e}_t.\end{aligned}\quad (2.20)$$

The components v_i of \mathbf{v}_D are the strains for an elastic rod: v_1 and v_2 are associated with bending and v_3 is associated with torsion and is referred to as the twist in Love [40, Article 252]. Observe that the torsional strain $v_3 = \tau + \frac{\partial \phi}{\partial s}$. Only in certain limited situations is the torsional strain equal to the geometric torsion.

It is misleading to consider the angle $\phi + \varphi$ shown in Fig. 2.3 as an angle of torsional rotation of the rod. The reason for this is that the Bishop triad vectors are not material. Indeed, using the integral of \mathbf{v} to determine a relative rotation has long been known to be misleading in the related field of rigid body dynamics.⁷ However, in the discrete elastic rods formulation discussed in Bergou et al. [4], the difference in the value of the angle $\phi + \varphi$ between two successive edges is correctly employed as a means to approximate torsional strain v_3 .

2.3.1 An Identity Pertaining to Twist

Given a pair of axial vectors \mathbf{v} and $\boldsymbol{\omega}$ associated with the spatial and temporal derivatives of a rotation tensor, we now show that the derivatives of ω_3 and v_3 are related: Based on results for the twist of a space curve, it can be proven that

$$\omega'_3 = \dot{v}_3 - \mathbf{v} \cdot \dot{\mathbf{f}}_3, \quad \dot{v}_3 = \omega'_3 - \boldsymbol{\omega} \cdot \mathbf{f}'_3. \quad (2.21)$$

These relations are often used with $\mathbf{f}_3 = \mathbf{e}_t$.

⁵The reader seeking additional background on parallel transport is referred to the textbooks by Henderson [23, Chap. 5] and Pressley [53, Chap. 7].

⁶Additional illuminating examples of Bishop frames and comparisons with the Frenet frame can be found in Hanson and Ma [21].

⁷See Goodman and Robinson [15] and Eq. (7.3) on Page 76.

To prove Eq. (2.21)₁, we parallel the arguments in [32] and note that $\dot{\mathbf{f}}_1 = \boldsymbol{\omega} \times \mathbf{f}_1 = \omega_3 \mathbf{f}_2 - \omega_2 \mathbf{f}_1$, thus

$$\begin{aligned}
\omega'_3 &= ((\boldsymbol{\omega} \times \mathbf{f}_1) \cdot \mathbf{f}_2)' \\
&= \dot{\mathbf{f}}'_1 \cdot \mathbf{f}_2 + \dot{\mathbf{f}}_1 \cdot \mathbf{f}'_2 \\
&= \frac{d}{dt} (\mathbf{v} \times \mathbf{f}_1) \cdot \mathbf{f}_2 + (\boldsymbol{\omega} \times \mathbf{f}_1) \cdot (\mathbf{v} \times \mathbf{f}_2) \\
&= \frac{d}{dt} (\nu_3 \mathbf{f}_2 - \nu_2 \mathbf{f}_3) \cdot \mathbf{f}_2 + (\boldsymbol{\omega} \times \mathbf{f}_1) \cdot \nu_1 \mathbf{f}_3 \\
&= \dot{\nu}_3 + \nu_2 (-\boldsymbol{\omega} \times \mathbf{f}_3) \cdot \mathbf{f}_2 - (\boldsymbol{\omega} \times \mathbf{f}_3) \cdot \nu_1 \mathbf{f}_1 \\
&= \dot{\nu}_3 - (\nu_1 \mathbf{f}_1 + \nu_2 \mathbf{f}_2) \cdot (\boldsymbol{\omega} \times \mathbf{f}_3) \\
&= \dot{\nu}_3 - \mathbf{v} \cdot \dot{\mathbf{f}}_3.
\end{aligned} \tag{2.22}$$

Thus, Eq. (2.21)₁ is established. Its companion result Eq. (2.21)₂ can be proven in a similar manner.

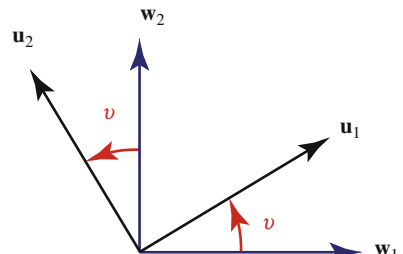
2.3.2 An Identity for a Relative Angular Velocity

A result that will prove useful in the sequel features a pair of frames $\{\mathbf{u}_1, \mathbf{u}_2, \mathbf{u}_3\}$ and $\{\mathbf{w}_1, \mathbf{w}_2, \mathbf{w}_3\}$ where $\mathbf{w}_i = \mathbf{R}(\nu, \mathbf{u}_3) \mathbf{u}_i$ (cf. Fig. 2.4). That is, \mathbf{w}_i are related to \mathbf{u}_i by a rotation through an angle ν about \mathbf{u}_3 . The angular velocities for the two frames satisfy the relations:

$$\dot{\mathbf{u}}_k = \boldsymbol{\omega}_1 \times \mathbf{u}_k, \quad \dot{\mathbf{w}}_k = \boldsymbol{\omega}_2 \times \mathbf{w}_k, \quad \boldsymbol{\omega}_2 = \boldsymbol{\omega}_1 + \dot{\nu} \mathbf{u}_3. \tag{2.23}$$

While the identity (2.23)₃ may be considered as obvious, it is non-trivial to establish. In our experience, the easiest method to establish Eq. (2.23)₃ is to use the relative angular velocity vector discussed in Casey and Lam [7].

Fig. 2.4 A pair of orthonormal vectors \mathbf{u}_1 and \mathbf{u}_2 and their rotated counterparts \mathbf{w}_1 and \mathbf{w}_2 . The vector $\mathbf{w}_3 = \mathbf{u}_3 = \mathbf{u}_1 \times \mathbf{u}_2$ is not shown



It can be verified that

$$(1 + \cos(\nu)) (\mathbf{w}_2 - \mathbf{u}_2) = \sin(\nu) (\mathbf{w}_1 + \mathbf{u}_1). \quad (2.24)$$

Assuming that ν and the vectors are functions of time t , the identity (2.24) can be manipulated to show that

$$(\dot{\mathbf{w}}_2 - \dot{\mathbf{u}}_2) = \frac{d}{dt} \left(\frac{\sin(\nu)}{1 + \cos(\nu)} \right) (\mathbf{w}_1 + \mathbf{u}_1) + \frac{\sin(\nu)}{1 + \cos(\nu)} (\dot{\mathbf{w}}_1 + \dot{\mathbf{u}}_1) \quad (2.25)$$

and, consequently,

$$(\dot{\mathbf{w}}_2 - \dot{\mathbf{u}}_2) \cdot \mathbf{u}_3 = \frac{\sin(\nu)}{1 + \cos(\nu)} \mathbf{u}_3 \cdot (\dot{\mathbf{w}}_1 + \dot{\mathbf{u}}_1). \quad (2.26)$$

Substituting for $\dot{\mathbf{w}}_2$ and $\dot{\mathbf{u}}_2$ using Eq. (2.23) and manipulating the triple product, we find that

$$\omega_2 \cdot \mathbf{w}_1 - \omega_1 \cdot \mathbf{u}_1 = \left(\frac{2 \sin(\nu)}{1 + \cos(\nu)} \mathbf{u}_3 \right) \cdot \frac{1}{2} (\dot{\mathbf{w}}_1 + \dot{\mathbf{u}}_1). \quad (2.27)$$

This identity, which we credit to Kirsch [32, Theorem 4.60], is closely related to an identity (7.48) that will feature in Chap. 7 where \mathbf{u}_1 and \mathbf{w}_1 are identified as tangent vectors and \mathbf{u}_3 is identified as a binormal vector:

$$\begin{aligned} \mathbf{u}_1 &\rightarrow \mathbf{t}^{k-1}, & \mathbf{w}_1 &\rightarrow \mathbf{t}^k, & \mathbf{u}_3 &\rightarrow \mathbf{b}_k, \\ \nu &\rightarrow m_{\text{ref}}^k, & \frac{2 \sin(\nu)}{1 + \cos(\nu)} \mathbf{u}_3 &\rightarrow \kappa_k \mathbf{b}_k. \end{aligned} \quad (2.28)$$

These vectors and angles pertain to a discretized space curve and will be defined in Chaps. 3, 4, and 5.

2.4 A Helical Space Curve

Partially because of its familiar presence in classic solutions of rod theory, we consider the example of helical space curve (cf. Fig. 2.1). A parametric representation of this curve using a polar angle θ is

$$\mathbf{r} = R \mathbf{e}_r + \alpha R \theta \mathbf{E}_3, \quad (2.29)$$

where R and α are constants, and the unit vector \mathbf{e}_r and its companion \mathbf{e}_θ are defined as follows:

$$\mathbf{e}_r = \cos(\theta) \mathbf{E}_1 + \sin(\theta) \mathbf{E}_2, \quad \mathbf{e}_\theta = \cos(\theta) \mathbf{E}_2 - \sin(\theta) \mathbf{E}_1. \quad (2.30)$$

For the helical space curve, it is straightforward to show that the arc-length parameter s is related to θ by the relation

$$\frac{\partial s}{\partial \theta} = R\sqrt{1 + \alpha^2}, \quad (2.31)$$

where we choose s to increase with increasing θ . In the sequel, we choose

$$\theta_0 = 0, \quad s_0 = R\sqrt{1 + \alpha^2}\theta_0 = 0. \quad (2.32)$$

The Frenet triad for the space curve is

$$\mathbf{e}_t = \frac{1}{\sqrt{1 + \alpha^2}} (\mathbf{e}_\theta + \alpha \mathbf{E}_3), \quad \mathbf{e}_n = -\mathbf{e}_r, \quad \mathbf{e}_b = \frac{1}{\sqrt{1 + \alpha^2}} (-\alpha \mathbf{e}_\theta + \mathbf{E}_3). \quad (2.33)$$

To show how the rotation \mathbf{R}_{SF} can be described, we note that we can express the relations (2.33) using the product of two rotations:

$$\begin{bmatrix} \mathbf{e}_n \\ \mathbf{e}_b \\ \mathbf{e}_t \end{bmatrix} = \begin{bmatrix} 1 & 0 & 0 \\ 0 & \frac{1}{\sqrt{1+\alpha^2}} & \frac{\alpha}{\sqrt{1+\alpha^2}} \\ 0 & -\frac{\alpha}{\sqrt{1+\alpha^2}} & \frac{1}{\sqrt{1+\alpha^2}} \end{bmatrix} \begin{bmatrix} \cos(\theta + \pi) & \sin(\theta + \pi) & 0 \\ -\sin(\theta + \pi) & \cos(\theta + \pi) & 0 \\ 0 & 0 & 1 \end{bmatrix} \begin{bmatrix} \mathbf{E}_1 \\ \mathbf{E}_2 \\ \mathbf{E}_3 \end{bmatrix}. \quad (2.34)$$

That is, \mathbf{R}_{SF} is a compound rotation: a rotation about $\theta + \pi$ about \mathbf{E}_3 followed by a rotation through an angle corresponding to the pitch angle γ of the helix about \mathbf{e}_n :

$$\cos(\gamma) = \frac{1}{\sqrt{1 + \alpha^2}}, \quad \sin(\gamma) = \frac{\alpha}{\sqrt{1 + \alpha^2}}. \quad (2.35)$$

This space curve is unusual in that it has a constant curvature and torsion,

$$\kappa = \frac{1}{R(1 + \alpha^2)}, \quad \tau = \alpha\kappa, \quad (2.36)$$

and a constant Darboux vector:

$$\begin{aligned} \mathbf{v}_{SF} &= \kappa \mathbf{e}_b + \tau \mathbf{e}_t \\ &= \frac{1}{R\sqrt{1 + \alpha^2}} \mathbf{E}_3. \end{aligned} \quad (2.37)$$

By way of contrast $\mathbf{v}_B = \kappa \mathbf{e}_b$ for this space curve is only a constant when $\alpha = 0$ (i.e., the helical space curve is a circular arc).

2.4.1 Computing a Bishop Frame for a Helical Space Curve

A Bishop frame for the helix can be computed. We choose

$$\begin{aligned}\mathbf{u} (s_0 = 0) &= \mathbf{e}_n (\theta_0 = 0) = -\mathbf{E}_1, \\ \mathbf{v} (s_0 = 0) &= \mathbf{e}_b (\theta_0 = 0) = \frac{1}{\sqrt{1 + \alpha^2}} (-\alpha \mathbf{E}_2 + \mathbf{E}_3).\end{aligned}\quad (2.38)$$

Because $\mathbf{v}_{SF} - \mathbf{v}_B = \tau \mathbf{e}_t$ and τ is constant, it is straightforward to show that

$$\begin{bmatrix} \mathbf{u}(s) \\ \mathbf{v}(s) \end{bmatrix} = \begin{bmatrix} \cos(\varphi) & -\sin(\varphi) \\ \sin(\varphi) & \cos(\varphi) \end{bmatrix} \begin{bmatrix} \mathbf{e}_n(s) \\ \mathbf{e}_b(s) \end{bmatrix}, \quad (2.39)$$

where the twisting angle φ is (cf. Fig. 2.2)

$$\varphi = \tau s = \frac{\alpha \theta}{\sqrt{1 + \alpha^2}}. \quad (2.40)$$

For a right-handed helix, $\alpha > 0$ and the Bishop frame rotates clockwise relative to the Frenet frame as s increases. It should also be noted that the Bishop frame depends on the choice of the initial conditions $\mathbf{u}(s_0 = 0)$ and $\mathbf{v}(s_0 = 0)$. If $\alpha = 0$ and the space curve is a circle, then, for the choice (2.38), the Bishop frame will coincide with the Frenet frame: $\mathbf{u} = -\mathbf{e}_r$ and $\mathbf{v} = \mathbf{E}_3$ (cf. Fig. 2.5). More generally, the Bishop frame vectors \mathbf{u} and \mathbf{v} for a circular arc can be chosen such that $\mathbf{u} = \cos(\varphi_0)(-\mathbf{e}_r) - \sin(\varphi_0)\mathbf{E}_3$ and $\mathbf{v} = \cos(\varphi_0)\mathbf{E}_3 + \sin(\varphi_0)(-\mathbf{e}_r)$ where the constant angle φ_0 is usually set to 0.

It is instructive to construct the tangent indicatrix for the helix. This is the path c_t traced out by the unit tangent vector on the unit sphere. We also map the Frenet

Fig. 2.5 A circle of radius R showing the tangent and normal vectors. In this figure, the arc-length parameter s is assumed to increase as the circle is traversed in the counterclockwise direction

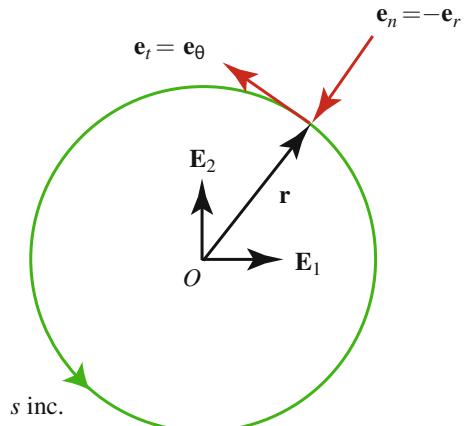


Fig. 2.6 The tangent indicatrix c_t of a circle. The images of the Bishop frame vectors \mathbf{u} and \mathbf{v} are also shown. As the vectors \mathbf{u} and \mathbf{v} are parallel propagated along c_t , they retain a constant orientation relative to \mathbf{e}_n and \mathbf{e}_b

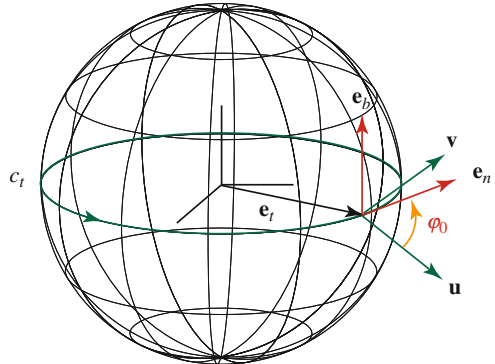
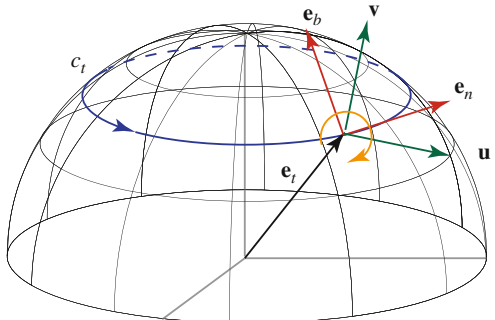


Fig. 2.7 The tangent indicatrix c_t of a helix. As the Bishop frame vectors \mathbf{u} and \mathbf{v} are parallel propagated along c_t , they rotate relative to \mathbf{e}_n and \mathbf{e}_b for the circular helix. This is in contrast to the case where the space curve is a circle. The tangent indicatrix for a circle is a great circle and \mathbf{u} and \mathbf{v} retain a constant orientation to \mathbf{e}_n and \mathbf{e}_b



triad and Bishop triad to the unit sphere. The mappings of the vectors \mathbf{u} , \mathbf{v} , \mathbf{e}_n , and \mathbf{e}_b lie in the tangent space to the sphere. For ease of exposition, we do not distinguish these vectors and their images under the mapping in our forthcoming discussion. It is straightforward to see that the unit tangent vector to c_t is parallel to the unit normal vector \mathbf{e}_n . Two cases are of particular interest: a circle and a circular helix. As shown in Fig. 2.6 for the circle, the tangent indicatrix is a great circle (i.e., a geodesic on the unit sphere). For this curve, the angle φ between the Bishop vectors \mathbf{u} and \mathbf{v} and \mathbf{e}_n and \mathbf{e}_b remains constant: $\varphi = \varphi_0$. On the other hand, for a circular helix, the tangent indicatrix is a circle of radius $\frac{1}{\sqrt{1+\alpha^2}}$ and geodesic curvature $\kappa_g = \frac{\tau}{\kappa} = \alpha$. For the case illustrated in Fig. 2.7, the helix is assumed to be right-handed and the Bishop vectors \mathbf{u} and \mathbf{v} rotate clockwise relative to \mathbf{e}_n and \mathbf{e}_b [cf. Eq. (2.39)].

2.5 Governing Equations for the Kirchhoff Rod

The equations governing the Kirchhoff rod provide a set of partial differential equations for $\mathbf{r}(s, t)$ and $\mathbf{R}_D(s, t)$. These equations are discussed in textbooks such as [1, 40, 51] and in hundreds of papers in the literature. It suffices to outline the simplest form of the governing equations for the present purposes. We assume that

the Kirchhoff rod is being used to model a homogeneous three-dimensional slender body. The body has a constant mass density per unit volume ρ_0 in its reference configuration. The centerline of the rod is chosen to be the centerline of the slender body and the directors are chosen to be parallel to the principal axes of the cross-sections of the slender body. Taking the integral of ρ_0 over a cross-section of the slender body provides the mass density (per unit length) $\hat{\rho}_0$ of the rod. The moments of area of the cross-sections are denoted by I_1 and I_2 .

The external applied forces and moments acting on the slender body are approximated by the applied force $\hat{\rho}_0\mathbf{f}$ and applied moment \mathbf{m}_a acting on the rod. Correspondences between $\hat{\rho}_0\mathbf{f}$ and \mathbf{m}_a and applied loadings on the slender body can be found in [1, 40, 51]. These texts also discuss the wide range of applications of Kirchhoff's rod theory and the classic solutions for which it is celebrated. The contact force in the rod is denoted by \mathbf{n} and the contact moment is denoted by \mathbf{m} . The governing equations can be expressed in the following form:

$$\begin{aligned}\mathbf{n}' + \hat{\rho}_0\mathbf{f} &= \hat{\rho}_0\ddot{\mathbf{r}}, \\ \mathbf{m}' + \mathbf{r}' \times \mathbf{n} + \mathbf{m}_a &= \mathbf{d}_1 \times (\rho_0 I_2 \ddot{\mathbf{d}}_1) + \mathbf{d}_2 \times (\rho_0 I_1 \ddot{\mathbf{d}}_2).\end{aligned}\quad (2.41)$$

The first of these equations can be considered as a force balance and the second as a moment balance. The partial differential equations are supplemented by constitutive relations for the moment \mathbf{m} . The classic constitutive relations are

$$\mathbf{m} = EI_1 v_1 \mathbf{d}_1 + EI_2 v_2 \mathbf{d}_2 + \mathcal{D}v_3 \mathbf{d}_3. \quad (2.42)$$

Here, $\mathbf{d}_3 = \mathbf{e}_t$, EI_1 and EI_2 are flexural stiffness, \mathcal{D} is a torsional stiffness, and E is Young's modulus. The constitutive relations for \mathbf{m} are easily modified if the rod has an intrinsic curvature or intrinsic twist (see [16, 51] for applications where such modifications are necessary). Unlike \mathbf{m} , the three components of $\mathbf{n} = \sum_{i=1}^3 n_i \mathbf{d}_i$ are constraint responses and must be solved as part of the solution to the boundary-value problem.

In the discrete elastic rod formulation, the partial differential equations are discretized by first approximating the centerline with a discrete set of points (vertices or nodes) that are connected by extensible segments (or edges). A concomitant pair of material vectors (or directors) are associated with each edge. At a discrete instant of time, force and moment balances that are inspired by (2.41) are solved and then a time-stepping scheme is used to compute the time evolution of the discrete elastic rod. In the discrete elastic rod formulation, the rod is also assumed to be extensible. The relaxation of the inextensibility constraint on the Kirchhoff rod theory discussed in this chapter is easily achieved and is left to the reader as an exercise.

Chapter 3

The Discretized Curve: Vertices, Edges, and Curvature



3.1 Introduction

In the discrete elastic rod formulation of Kirchhoff's rod theory, the material curve \mathcal{L} is discretized into a set of $n - 1$ segments (cf. Fig. 3.1). The edges of the segments are defined by a pair of vertices. We use the widely adopted notational convention that quantities associated with a vertex are labelled with a subscript and those associated with an edge are labelled with a superscript (cf. [2, 3, 32]). The amount of new terminology introduced in this chapter can be intimidating and we encourage the reader to have copies of Tables 1.1 and 1.2 from Chap. 1 in hand.

As shown in Fig. 3.1, the curve of interest is discretized into n vertices

$$\mathbf{x}_0, \quad \mathbf{x}_1, \quad \dots, \quad \mathbf{x}_{n-1}. \quad (3.1)$$

Edges (or bond vectors) and tangents can be defined using this collection of points:

$$\mathbf{e}^0 = \mathbf{x}_1 - \mathbf{x}_0, \quad \mathbf{e}^1 = \mathbf{x}_2 - \mathbf{x}_1, \quad \dots, \quad \mathbf{e}^{n-2} = \mathbf{x}_{n-1} - \mathbf{x}_{n-2}. \quad (3.2)$$

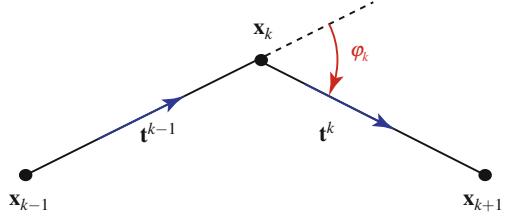
The associated unit tangent vectors are

$$\mathbf{t}^0 = \frac{\mathbf{e}^0}{\|\mathbf{e}^0\|}, \quad \mathbf{t}^1 = \frac{\mathbf{e}^1}{\|\mathbf{e}^1\|}, \quad \dots, \quad \mathbf{t}^{n-2} = \frac{\mathbf{e}^{n-2}}{\|\mathbf{e}^{n-2}\|}. \quad (3.3)$$

The arc-length parameters at the vertices are

$$s_0 = 0, \quad s_1 = \|\mathbf{e}^0\| + s_0, \quad s_2 = \|\mathbf{e}^1\| + s_1, \quad \dots, \\ s_j = \|\mathbf{e}^{j-1}\| + s_{j-1}, \quad \dots, \quad s_{n-1} = \|\mathbf{e}^{n-2}\| - s_{n-2}. \quad (3.4)$$

Fig. 3.1 Three vertices \mathbf{x}_{k-1} , \mathbf{x}_k , and \mathbf{x}_{k+1} , and the unit vectors associated with the edges



The length ℓ_k of the Voronoi region (or cell) associated with a vertex \mathbf{x}_k is

$$\begin{aligned}\ell_0 &= \frac{1}{2} \|\mathbf{e}^0\|, \\ \ell_k &= \frac{1}{2} (\|\mathbf{e}^{k-1}\| + \|\mathbf{e}^k\|), \quad (k = 1, \dots, n-2), \\ \ell_{n-1} &= \frac{1}{2} \|\mathbf{e}^{n-2}\|. \end{aligned}\tag{3.5}$$

This length scale is used to define the curvature and elastic energies.

3.2 A Turning Angle and Curvatures

One also defines the angle φ_k between the edges of the discretized curve at \mathbf{x}_k :

$$\varphi_k = \arccos(\mathbf{t}^{k-1} \cdot \mathbf{t}^k).\tag{3.6}$$

That is,

$$\cos(\varphi_k) = \mathbf{t}^{k-1} \cdot \mathbf{t}^k, \quad |\sin(\varphi_k)| = \|\mathbf{t}^{k-1} \times \mathbf{t}^k\|.\tag{3.7}$$

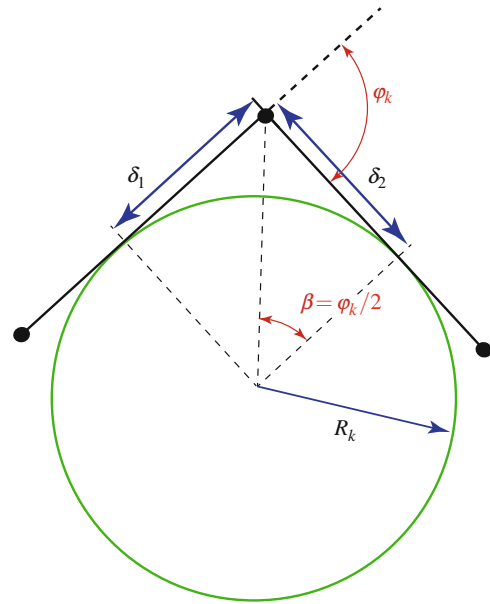
The angle φ_k , which is known as the turning angle, can be used to define a discrete pointwise curvature $\hat{\kappa}_k$ at \mathbf{x}_k :

$$\frac{1}{R_k} = \hat{\kappa}_k = \frac{2}{\ell_k} \tan\left(\frac{\varphi_k}{2}\right) = \frac{2 \sin(\varphi_k)}{\ell_k(1 + \cos(\varphi_k))},\tag{3.8}$$

where ℓ_i is the length of the Voronoi domain of the vertex at \mathbf{x}_i . As shown in Fig. 3.2, the curvature $\hat{\kappa}_k$ is the inverse of the radius R_k of the osculating circle to the edges emanating from a vertex \mathbf{x}_k .

As lucidly discussed in [6, p. 15], the definition (3.8) of the discrete curvature follows from the continuous case by considering curvature as a measure of the change in arc-length of a plane curve when it is moved along the normal direction.

Fig. 3.2 The osculating circle of radius R_k is constructed by projecting perpendicular lines from the edges with $\delta_1 = \delta_2 = \frac{\ell_k}{2}$. Elementary geometry is all that is needed to show that $R_k = \frac{\ell_k}{2} \cot\left(\frac{\varphi_k}{2}\right)$



For instance, if an arc of radial extent $1/R$ of a circle of radius R is deformed into an arc of a circle of radius $R + \epsilon$, then the arc length will have changed by an amount ϵ/R . Thus, κ can be considered as the rate of change of the arc length with respect to ϵ . For discretized curves, the only change in arc length is achieved at a vertex \mathbf{x}_k and the change in length is directly related to the angle φ_k subtended by \mathbf{t}^{k-1} and \mathbf{t}^k .

The discrete integrated curvature κ_i is related to the discrete pointwise curvature $\hat{\kappa}_i$ using the length ℓ_i :

$$\begin{aligned}\kappa_i &= \hat{\kappa}_i \ell_i \\ &= \frac{2 \sin(\varphi_i)}{1 + \cos(\varphi_i)} \\ &= 2 \tan\left(\frac{\varphi_i}{2}\right).\end{aligned}\tag{3.9}$$

Furthermore, the discrete binormal vector to the curve at the i th vertex can be defined as

$$\mathbf{b}_i = \frac{\mathbf{t}^{i-1} \times \mathbf{t}^i}{\|\mathbf{t}^{i-1} \times \mathbf{t}^i\|} = \frac{\mathbf{t}^{i-1} \times \mathbf{t}^i}{\sqrt{1 - (\mathbf{t}^{i-1} \cdot \mathbf{t}^i)^2}}.\tag{3.10}$$

Combining the expression for κ_i with the expression for \mathbf{b}_i , we find the pair of commonly used expressions for the discrete integrated curvature vector $(\kappa \mathbf{b})_i$ at the vertex \mathbf{x}_i :

$$(\kappa \mathbf{b})_i = \kappa_i \mathbf{b}_i = \frac{2\mathbf{t}^{i-1} \times \mathbf{t}^i}{1 + \mathbf{t}^{i-1} \cdot \mathbf{t}^i} = \frac{2\mathbf{e}^{i-1} \times \mathbf{e}^i}{\|\mathbf{e}^{i-1}\| \|\mathbf{e}^i\| + \mathbf{e}^{i-1} \cdot \mathbf{e}^i}. \quad (3.11)$$

Although this vector has parallels to the component $\kappa \mathbf{e}_b$ of the Darboux vector, it is important to note that it is dimensionless unlike $\kappa \mathbf{e}_b$ which has the dimensions of $1/L$. In addition, as the discretization of a curve becomes finer the vector $(\kappa \mathbf{b})_i$ and the discrete integrated curvature κ_i both tend to approach zero while the discrete pointwise curvature $\hat{\kappa}_i \rightarrow \kappa$.

As discussed in Sect. 5.3, the components of the discrete integrated curvature vector $(\kappa \mathbf{b})_i$ at the vertex \mathbf{x}_i are used to measure the bending strains in the rod. In addition, the length $\|\mathbf{e}^k\|$ is used to measure stretching of the centerline of the rod.

3.3 An Orthogonal Triad at a Vertex

As shown in Fig. 3.3, an orthogonal triad of vectors at a vertex \mathbf{x}_k can be defined using the discrete binormal vector and the edge tangent vectors:

$$\{\Delta \mathbf{t}_k, \mathbf{b}_k, \mathbf{t}_{\gamma_k}\}, \quad (3.12)$$

where

$$\Delta \mathbf{t}_k = \mathbf{t}^k - \mathbf{t}^{k-1}, \quad \mathbf{t}_{\gamma_k} = \frac{1}{2} (\mathbf{t}^k + \mathbf{t}^{k-1}). \quad (3.13)$$

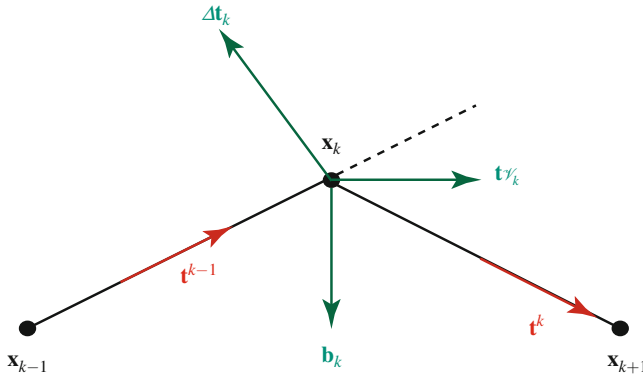


Fig. 3.3 The triad $\{\Delta \mathbf{t}_k, \mathbf{b}_k, \mathbf{t}_{\gamma_k}\}$ of vectors at a vertex \mathbf{x}_k . Although $\Delta \mathbf{t}_k$ and \mathbf{t}_{γ_k} are not necessarily unit vectors, we shall see from the example in Sect. 3.4, that this triad can be considered as a discrete analog of the Frenet triad

The vector \mathbf{t}_{γ_k} is known as the discrete vertex tangent. It is the average of the edge tangent vectors at a vertex. Closely related vectors appear in the literature, most notably $\tilde{\mathbf{t}}$ in [3, 4] and $\nabla^h \gamma$ in Hoffman [24, Definition 2.7]:

$$\tilde{\mathbf{t}} = \nabla^h \gamma = \frac{\mathbf{t}^{i-1} + \mathbf{t}^i}{1 + \mathbf{t}^{i-1} \cdot \mathbf{t}^i}. \quad (3.14)$$

The vectors $\{\Delta \mathbf{t}_k, \mathbf{b}_k, \mathbf{t}_{\gamma_k}\}$ lead to an appealing discrete analogue of the Serret–Frenet relation $\mathbf{e}'_t = \kappa \mathbf{e}_b \times \mathbf{e}_t$:

$$\Delta \mathbf{t}_i = (\kappa \mathbf{b})_i \times \mathbf{t}_{\gamma_i}. \quad (3.15)$$

We also note that

$$\tilde{\mathbf{t}} \times \Delta \mathbf{t}_i = (\kappa \mathbf{b})_i. \quad (3.16)$$

As illuminated by the forthcoming example in Sect. 3.4, the triad $\{\Delta \mathbf{t}_k, \mathbf{b}_k, \mathbf{t}_{\gamma_k}\}$ can be considered as a discrete analog of the Frenet triad.

3.4 The Discretized Helical Space Curve

To illustrate the previous results, we consider the example of a space curve which has the form of a segment of a helical space curve and is divided into n segments of equal length:

$$\begin{aligned} \mathbf{x}_0 &= R \mathbf{E}_1, \\ \mathbf{x}_k &= R \cos(k \Delta \theta) \mathbf{E}_1 + R \sin(k \Delta \theta) \mathbf{E}_2 + R k \Delta \theta \alpha \mathbf{E}_3, \\ \mathbf{x}_n &= R \cos(n \Delta \theta) \mathbf{E}_1 + R \sin(n \Delta \theta) \mathbf{E}_2 + R n \Delta \theta \alpha \mathbf{E}_3. \end{aligned} \quad (3.17)$$

In these expressions, $\Delta \theta$ represents a constant increment of θ . An example of the discretization (3.17) is shown in Fig. 3.4.

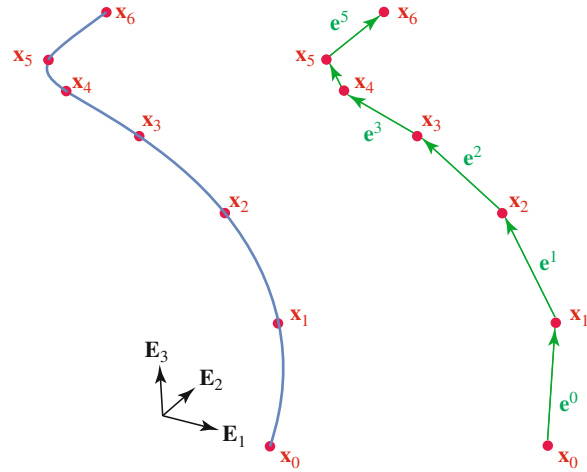
The edge vector for the k th edge is

$$\mathbf{e}^k = 2R \sin\left(\frac{\Delta \theta}{2}\right) \mathbf{e}_\theta^k + \alpha R \Delta \theta \mathbf{E}_3, \quad (3.18)$$

where we find it convenient to define edge and vertex vectors

$$\begin{aligned} \mathbf{e}_\theta^k &= \cos\left(k \Delta \theta + \frac{1}{2} \Delta \theta\right) \mathbf{E}_2 - \sin\left(k \Delta \theta + \frac{1}{2} \Delta \theta\right) \mathbf{E}_1, \\ \mathbf{e}_{\theta_k} &= \cos(k \Delta \theta) \mathbf{E}_2 - \sin(k \Delta \theta) \mathbf{E}_1, \end{aligned} \quad (3.19)$$

Fig. 3.4 A segment of a right-handed helix discretized into six segments according to Eq. (3.17) and the corresponding edge vectors \mathbf{e}^k



and their companions

$$\begin{aligned}\mathbf{e}_r^k &= \cos\left(k\Delta\theta + \frac{1}{2}\Delta\theta\right)\mathbf{E}_1 + \sin\left(k\Delta\theta + \frac{1}{2}\Delta\theta\right)\mathbf{E}_2, \\ \mathbf{e}_{r_k} &= \cos(k\Delta\theta)\mathbf{E}_1 + \sin(k\Delta\theta)\mathbf{E}_2.\end{aligned}\quad (3.20)$$

The edge vector \mathbf{e}^k has a constant magnitude:

$$\|\mathbf{e}^k\|^2 = R^2 \left(2(1 - \cos(\Delta\theta)) + \alpha^2 \Delta\theta^2\right). \quad (3.21)$$

The length ℓ_k of the Voronoi region in the neighborhood of a vertex for the discretization is constant:

$$\ell_k = R\sqrt{2(1 - \cos(\Delta\theta)) + \alpha^2 \Delta\theta^2}, \quad (3.22)$$

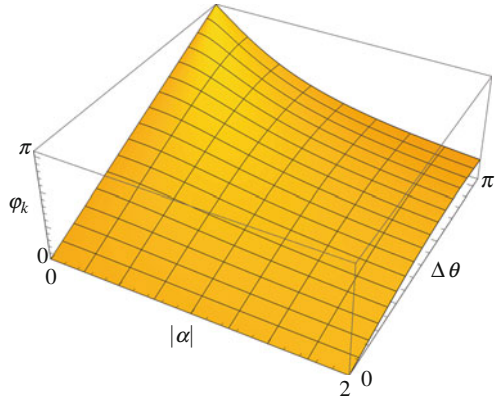
and approaches 0 as the discretization becomes finer and finer.

The turning angle at a vertex \mathbf{x}_i can be computed using the edge vectors:

$$\begin{aligned}\cos(\varphi_k) &= \frac{\alpha^2 \Delta\theta^2 + 2(1 - \cos(\Delta\theta)) \cos(\Delta\theta)}{2(1 - \cos(\Delta\theta)) + \alpha^2 \Delta\theta^2}, \\ |\sin(\varphi_k)| &= \frac{4 \sin^2\left(\frac{\Delta\theta}{2}\right) \sqrt{\alpha^2 \Delta\theta^2 + \sin^2(\Delta\theta)}}{2(1 - \cos(\Delta\theta)) + \alpha^2 \Delta\theta^2}.\end{aligned}\quad (3.23)$$

Setting $\alpha = 0$, it is easy to observe from these expressions that $\varphi_k = \Delta\theta$ for a discretized circle. The behavior of the turning angle for other values of α can be seen in Fig. 3.5.

Fig. 3.5 The turning angle φ_k as a function of the discretization angle $\Delta\theta$ and the parameter α for a helical space curve [cf. Eq. (3.23)]



An expression for the discrete binormal vector at the vertex \mathbf{x}_i can be computed with the help of Eqs. (3.10) and (3.19)₂. We also find it convenient to compute the other two vectors of the triad $\{\Delta \mathbf{t}_k, \mathbf{b}_k, \mathbf{t}_{v_k}\}$:

$$\begin{aligned} \Delta \mathbf{t}_k &= -\frac{4 \sin^2\left(\frac{\Delta\theta}{2}\right) \mathbf{e}_{r_k}}{\sqrt{2(1-\cos(\Delta\theta)) + \alpha^2 \Delta\theta^2}}, \\ \mathbf{b}_k &= \frac{\sin(\Delta\theta) \mathbf{E}_3 - \alpha \Delta\theta \mathbf{e}_{\theta_k}}{\sqrt{\sin^2(\Delta\theta) + \alpha^2 \Delta\theta^2}}, \\ \mathbf{t}_{v_k} &= \frac{\sin(\Delta\theta) \mathbf{e}_{\theta_k} + \alpha \Delta\theta \mathbf{E}_3}{\sqrt{2(1-\cos(\Delta\theta)) + \alpha^2 \Delta\theta^2}}. \end{aligned} \quad (3.24)$$

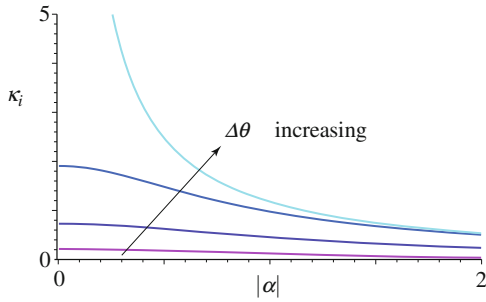
Observe that as $\Delta\theta \rightarrow 0$, then $\Delta \mathbf{t}_k \rightarrow \mathbf{0}$, $\frac{\Delta \mathbf{t}_k}{\|\Delta \mathbf{t}_k\|} \rightarrow \mathbf{e}_n$, $\mathbf{b}_k \rightarrow \mathbf{e}_b$, and $\mathbf{t}_{v_k} \rightarrow \mathbf{e}_t$.

It is illuminating to compute the discrete integrated curvature vector $(\kappa \mathbf{b})_i$ at the vertex \mathbf{x}_i . The most straightforward method to compute this quantity is to use Eqs. (3.11), (3.18), and (3.19)₂:

$$(\kappa \mathbf{b})_i = \frac{4 \sin^2\left(\frac{\Delta\theta}{2}\right) (\sin(\Delta\theta) \mathbf{E}_3 - \alpha \Delta\theta \mathbf{e}_{\theta_i})}{2 \sin^2\left(\frac{\Delta\theta}{2}\right) (1 + \cos(\Delta\theta)) + \alpha^2 \Delta\theta^2}. \quad (3.25)$$

As $\Delta\theta \rightarrow 0$, the vector $(\kappa \mathbf{b})_i$ and the discrete integrated curvature κ_i vanish (cf. Fig. 3.6). However, so too does ℓ_i . Hence, it can be shown that, in the limit as $\Delta\theta \rightarrow 0$, $\hat{\kappa}_i \mathbf{b}_i \rightarrow \kappa \mathbf{e}_b$ (as expected).

Fig. 3.6 The discrete integrated curvature κ_i as a function of the parameter α for the values of $\Delta\theta = 0.1\pi, 0.25\pi, 0.5\pi$, and π for a helical space curve [cf. Eqs. (3.9) and (3.23)]. In contrast to the curvature $\kappa = \frac{1}{R(1+\alpha^2)}$, the value of κ_i does not depend on the radius R of the circular helix



3.5 Closing Remarks

In this chapter, the notion of a discretized curve has been introduced. The tangent vectors \mathbf{t}^k that are parallel to the segments of the discretized curve can be used to define turning angles φ_i and a discrete integrated curvature vector $\kappa_i \mathbf{b}_i$ at the vertex \mathbf{x}_i . The next chapter will see the introduction of a pair of rotation operators. One of these operators rotates the tangent vector from one edge to its adjacent counterpart while the other transforms the tangent vector at time t to its evolved state at a later time. Both of these rotations play distinct roles in the sequel. Using the rotation operators, it is natural to associate a pair of vectors (that are orthogonal to tangent vectors) to edges of the discrete rod. One of these pairs of vectors is the counterpart to the Bishop vectors \mathbf{u} and \mathbf{v} discussed in Chap. 2.

Chapter 4

Bishop Frames and Reference Frames Along the Discretized Curve



4.1 Introduction

As we discuss in Sect. 5.3 of Chap. 5, a pair of components κ_{k_1} and κ_{k_2} of the discrete integrated curvature vector $\kappa_k \mathbf{b}_k$ associated with the discretized curve will be used to account for the bending strains of the rod. Additional information beyond the components of $\kappa_k \mathbf{b}_k$ is needed to account for the torsion of the rod-like body that the discrete elastic rod is modeling. A portion of this information will be provided by a set of material frame vectors \mathbf{m}_1^k and \mathbf{m}_2^k defined on each edge. The twist of the rod is related to the difference in the rotation of \mathbf{m}_1^k and \mathbf{m}_2^k between two successive edges. To measure the rotation, two different approaches have been used. In earlier work, such as [4], the rotation of the vectors \mathbf{m}_1^k and \mathbf{m}_2^k about \mathbf{t}^k was measured with the help of a Bishop frame on each edge, while in later works, such as [3, 29], a reference frame on each edge that is updated at each time step is used. The latter approach introduces an angle of twist m_{ref}^k into the formulation that can be challenging to comprehend.

In the present chapter, the aforementioned Bishop frames and reference frames are discussed. The material frames will be defined in Chap. 5. The number of angles introduced in this chapter can be challenging to track and we encourage the reader to refer to Tables 1.1 and 1.2 from Chap. 1 for additional guidance.

4.2 Space-Parallel and Time-Parallel Transport Operators

Central components in the theory of discrete elastic rods are the notions of an operator that transforms a tangent vector from one edge to its adjacent neighbor and another operator which transforms the tangent vector at an edge at time t to

its counterpart at time $t + \Delta t$. These operators are denoted by $P_{\mathbf{t}^{k-1}}^{\mathbf{t}^k}$ and $\bar{P}^k(t, \Delta t)$, respectively. Understanding these operators is a crucial step towards comprehending the discrete elastic rod formulation.

4.2.1 The Operator $P_{\mathbf{t}^{k-1}}^{\mathbf{t}^k}$ and Its Associated Darboux Vector $\kappa_k \mathbf{b}_k$

Because \mathbf{t}^k and \mathbf{t}^{k-1} are unit vectors, an operator, which is denoted by $P_{\mathbf{t}^{k-1}}^{\mathbf{t}^k}$, can be defined as the rotation that transforms \mathbf{t}^{k-1} to \mathbf{t}^k by rotating it about a unit vector \mathbf{b}_k that is parallel to $\mathbf{t}^k \times \mathbf{t}^{k-1}$ (i.e., the discrete version of the binormal vector):

$$P_{\mathbf{t}^{k-1}}^{\mathbf{t}^k} = \mathbf{R}(\varphi_k, \mathbf{b}_k). \quad (4.1)$$

For the reader's convenience, we recall that

$$\mathbf{b}_k = \frac{\mathbf{t}^{k-1} \times \mathbf{t}^k}{\|\mathbf{t}^{k-1} \times \mathbf{t}^k\|}, \quad \cos(\varphi_k) = \mathbf{t}^k \cdot \mathbf{t}^{k-1}, \quad (4.2)$$

and note that the rotation operator $\mathbf{R}(\varphi_k, \mathbf{b}_k)$ represents a counterclockwise rotation through an angle φ_k about an axis \mathbf{b}_k (cf. Fig. 4.1). Indeed, using the definition (3.11) of the discrete integrated curvature vector,

$$(\kappa \mathbf{b})_k = \kappa_k \mathbf{b}_k = \frac{2\mathbf{t}^{k-1} \times \mathbf{t}^k}{1 + \mathbf{t}^{k-1} \cdot \mathbf{t}^k}, \quad (4.3)$$

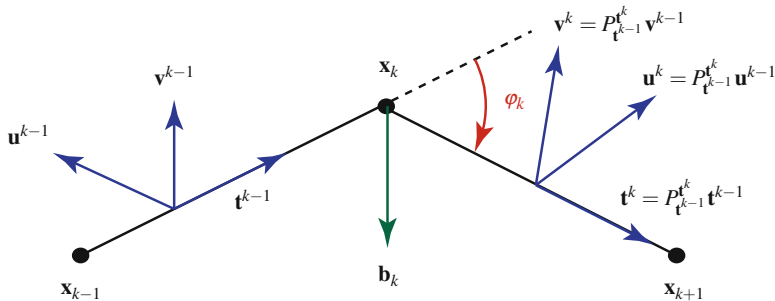


Fig. 4.1 Three vertices \mathbf{x}_{k-1} , \mathbf{x}_k , and \mathbf{x}_{k+1} , and the unit vectors associated with the edges. The frames $\{\mathbf{t}^{k-1}, \mathbf{u}^{k-1}, \mathbf{v}^{k-1} = \mathbf{t}^{k-1} \times \mathbf{u}^{k-1}\}$ and $\{\mathbf{t}^k, \mathbf{u}^k, \mathbf{v}^k = \mathbf{t}^k \times \mathbf{u}^k\}$ are Bishop frames. The frame on one edge is computed from the frame on the adjacent edge using the operator $P_{\mathbf{t}^{k-1}}^{\mathbf{t}^k}$: $\mathbf{t}^k = P_{\mathbf{t}^{k-1}}^{\mathbf{t}^k} \mathbf{t}^{k-1}$, $\mathbf{u}^k = P_{\mathbf{t}^{k-1}}^{\mathbf{t}^k} \mathbf{u}^{k-1}$, and $\mathbf{v}^k = P_{\mathbf{t}^{k-1}}^{\mathbf{t}^k} \mathbf{v}^{k-1}$ [cf. Eq. (4.18)].

we can associate a relative Darboux vector $\kappa_k \mathbf{b}_k$ with $P_{\mathbf{t}^{k-1}}^{\mathbf{t}^k}$. On a related intriguing note,

$$\kappa_k \mathbf{b}_k = 2 \tan\left(\frac{\varphi_k}{2}\right) \mathbf{b}_k \quad (4.4)$$

is twice the Rodrigues or Gibbs vector associated with the rotation $\mathbf{R}(\varphi_k, \mathbf{b}_k)$ (cf. Shuster [59, p. 469]).

The tensor $P_{\mathbf{t}^{k-1}}^{\mathbf{t}^k}$ is known as a space-parallel transport operator. A possible motivation for this terminology is provided by imagining the transformation of a vector \mathbf{t} from \mathbf{t}^{k-1} to \mathbf{t}^k as a continuous process performed at constant speed. Then, the path traced by the vector \mathbf{t} as it transforms from \mathbf{t}^{k-1} to \mathbf{t}^k will be an arc of a great circle on a unit sphere. The axis of rotation \mathbf{b}_k will be normal to the plane formed by the arc of the circle and the associated angular velocity vector will be constant. As discussed in great detail in [46], such rotational motions are geodesics of the rotation group $SO(3)$.¹ The operator $P_{\mathbf{t}^{k-1}}^{\mathbf{t}^k}$ will be a function of time but in the interests of keeping notation as compact as possible, this dependency is not explicitly emphasized in the sequel.

4.2.2 The Operator $\bar{P}^k(t, \Delta t)$ and Its Associated Angular Velocity Vector ${}_P\bar{\omega}^k(t)$

An alternative parallel transport operator can be defined by considering the configuration of an edge at time t . As shown in Figs. 4.2 and 4.3, consider the k th edge at time t and its evolved counterpart at time $t + \Delta t$. Given the tangent vectors $\mathbf{t}^k(t)$ and $\mathbf{t}^k(t + \Delta t)$, we can define a rotation $\bar{P}^k(t, \Delta t)$. This rotation transforms $\mathbf{t}^k(t)$ to $\mathbf{t}^k(t + \Delta t)$:

$$\bar{P}^k(t, \Delta t) \equiv P_{\mathbf{t}^k(t)}^{\mathbf{t}^k(t + \Delta t)} = \mathbf{R}(\alpha^k(t, \Delta t), \mathbf{h}^k(t, \Delta t)), \quad (4.5)$$

where the axis and angle of rotation are

$$\mathbf{h}^k(t, \Delta t) = \frac{\mathbf{t}^k(t) \times \mathbf{t}^k(t + \Delta t)}{\|\mathbf{t}^k(t) \times \mathbf{t}^k(t + \Delta t)\|}, \quad \cos(\alpha^k(t, \Delta t)) = \mathbf{t}^k(t) \cdot \mathbf{t}^k(t + \Delta t). \quad (4.6)$$

It is convenient to substitute for $\mathbf{h}^k(t, \Delta t)$ and $\alpha^k(t, \Delta t)$ into the representation (2.4) for a rotation tensor. After some manipulations, we find that

¹Our remarks here complement comments in [2, Appendix C].

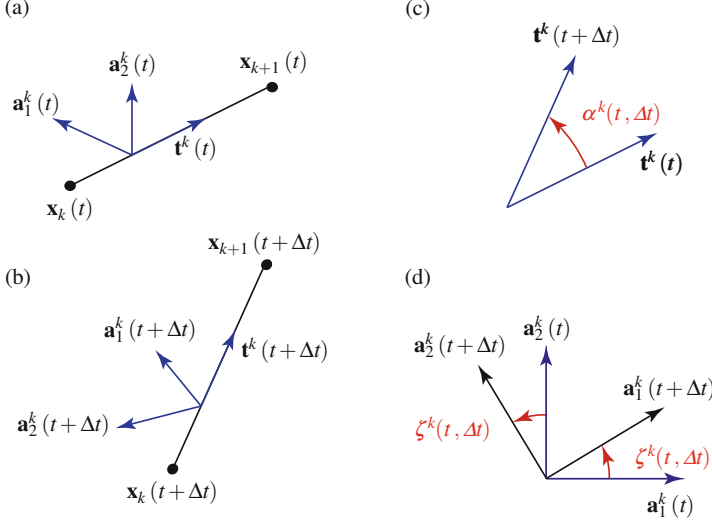


Fig. 4.2 Features of the time-parallel transport operator $\bar{P}^k(t, \Delta t)$. (a) The k th edge at time t . (b) The k th edge at time $t + \Delta t$. (c) The angle $\alpha^k(t, \Delta t)$ associated with the rotation $\bar{P}^k(t, \Delta t)$. (d) The rotation of the reference frame vectors. The angles of rotation ζ^k and α^k are distinct

$$\begin{aligned}\bar{P}^k(t, \Delta t) &= \cos(\alpha^k(t, \Delta t)) \mathbf{I} + \text{skewt}(\mathbf{t}^k(t) \times \mathbf{t}^k(t + \Delta t)) \\ &\quad + \frac{1}{1 + \cos(\alpha^k(t, \Delta t))} ((\mathbf{t}^k(t) \times \mathbf{t}^k(t + \Delta t)) \otimes (\mathbf{t}^k(t) \times \mathbf{t}^k(t + \Delta t))).\end{aligned}\quad (4.7)$$

This representation is well defined for all values of Δt and so it can be used to verify that

$$\bar{P}^k(t, 0) = \mathbf{I}. \quad (4.8)$$

For future purposes an angular velocity vector associated with $\bar{P}^k(t, \Delta t)$ will be of use. To compute this angular velocity vector, we define

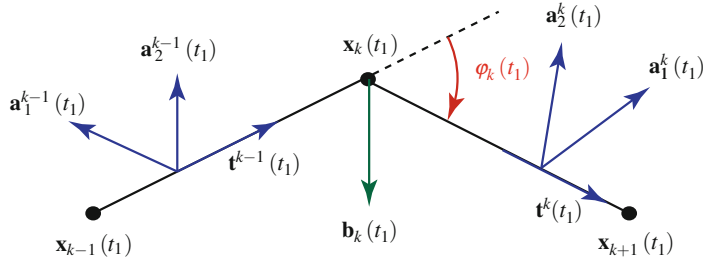
$$\dot{\bar{P}}^k(t) = \lim_{\Delta t \rightarrow 0} \frac{\bar{P}^k(t, \Delta t) - \bar{P}^k(t, 0)}{\Delta t}. \quad (4.9)$$

With the help of the representation (4.7) and the identities

$$\begin{aligned}\cos(\alpha^k(t, \Delta t)) - 1 &= \mathbf{t}^k(t + \Delta t) \cdot \mathbf{t}^k(t) - \mathbf{t}^k(t + \Delta t) \cdot \mathbf{t}^k(t + \Delta t) \\ &= -(\mathbf{t}^k(t + \Delta t) - \mathbf{t}^k(t)) \cdot \mathbf{t}^k(t + \Delta t),\end{aligned}$$

$$\lim_{\Delta t \rightarrow 0} \frac{1}{\Delta t} (\cos(\alpha^k(t, \Delta t)) - 1) = -\dot{\mathbf{t}}^k(t) \cdot \mathbf{t}^k(t) = 0, \quad (4.10)$$

$t = t_1$



$t = t_2$

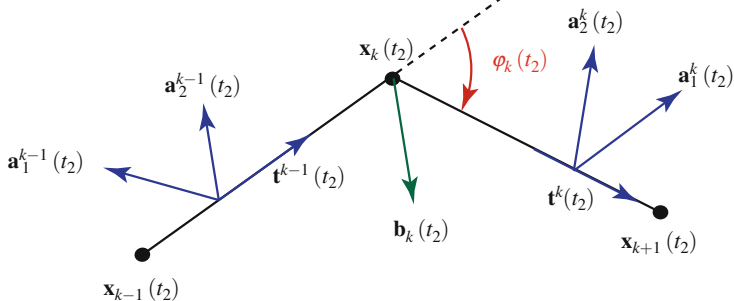


Fig. 4.3 Defining the reference frame vectors at time $t_2 = t + \Delta t$ by a time-parallel transport (4.21) from the configuration at time $t_1 = t$. For example, $\mathbf{a}_1^k(t_2) = \bar{P}^k(t_1, t_2 - t_1)\mathbf{a}_1^k(t_1)$ and $\mathbf{a}_1^{k-1}(t_2) = \bar{P}^{k-1}(t_1, t_2 - t_1)\mathbf{a}_1^{k-1}(t_1)$

and

$$\begin{aligned} \lim_{\Delta t \rightarrow 0} \frac{1}{\Delta t} & \left((\mathbf{t}^k(t) \times \dot{\mathbf{t}}^k(t + \Delta t)) \otimes (\mathbf{t}^k(t) \times \dot{\mathbf{t}}^k(t + \Delta t)) \right) \\ &= (\mathbf{t}^k(t) \times \dot{\mathbf{t}}^k(t)) \otimes (\mathbf{t}^k(t) \times \dot{\mathbf{t}}^k(t)) = \mathbf{0}, \end{aligned} \quad (4.11)$$

it can quickly be shown that

$$\dot{\bar{P}}^k(t) = \text{skewt}(\mathbf{t}^k(t) \times \dot{\mathbf{t}}^k(t)). \quad (4.12)$$

The angular velocity vector of interest is the following axial vector:

$${}_P\bar{\boldsymbol{\omega}}^k(t) = \text{ax}\left(\dot{\bar{P}}^k(t)\left(\bar{P}^k(t, 0)\right)^T\right). \quad (4.13)$$

As $\bar{P}^k(t, 0) = \mathbf{I}$, it immediately follows from Eq. (4.12) that

$${}_P\bar{\boldsymbol{\omega}}^k(t) = \mathbf{t}^k(t) \times \dot{\mathbf{t}}^k(t). \quad (4.14)$$

As anticipated, this representation for the angular velocity vector is in complete accord with the expression for the Darboux vector (2.19) associated with the Bishop frame that we encountered earlier in Chap. 2.

The angular velocity $P\bar{\omega}^k(t)$ can be expressed in terms of the motion of the vertices. To elaborate, differentiating

$$\mathbf{t}^k(t) = \frac{\mathbf{x}_{k+1}(t) - \mathbf{x}_k(t)}{\|\mathbf{x}_{k+1}(t) - \mathbf{x}_k(t)\|}, \quad (4.15)$$

and performing some minor rearranging we find that

$$\dot{\mathbf{t}}^k(t) = (\mathbf{I} - \mathbf{t}^k(t) \otimes \mathbf{t}^k(t)) \frac{\dot{\mathbf{x}}_{k+1}(t) - \dot{\mathbf{x}}_k(t)}{\|\mathbf{x}_{k+1}(t) - \mathbf{x}_k(t)\|}. \quad (4.16)$$

Whence one can substitute Eqs. (4.15) and (4.16) into Eq. (4.14) to obtain an expression for $P\bar{\omega}^k(t)$ in terms of the motion of the vertices.

4.3 Bishop Frames and Reference Frames

Associated with the zeroth edge, we can define a pair of vectors that are orthogonal to the tangent vector \mathbf{t}^0 (cf. Fig. 4.1). The pair of vectors and \mathbf{t}^0 constitute a (right-handed) Bishop triad:

$$\left\{ \mathbf{t}^0, \mathbf{u}^0, \mathbf{v}^0 = \mathbf{t}^0 \times \mathbf{u}^0 \right\}. \quad (4.17)$$

By associating the midpoint of the zeroth edge with this triad, we are able to define the Bishop frame associated with the zeroth edge. To compute the Bishop frame on subsequent edges, we use the operator $P_{\mathbf{t}^{k-1}}^{\mathbf{t}^k}$ to define the Bishop frame on the edge \mathbf{e}^k given the Bishop frame on the previous edge:

$$\mathbf{u}^k = P_{\mathbf{t}^{k-1}}^{\mathbf{t}^k} \mathbf{u}^{k-1}, \quad \mathbf{v}^k = P_{\mathbf{t}^{k-1}}^{\mathbf{t}^k} \mathbf{v}^{k-1}. \quad (4.18)$$

Exploiting the fact that the Bishop frame vectors form an orthonormal triad, we can conclude that $P_{\mathbf{t}^{k-1}}^{\mathbf{t}^k}$ has the representation

$$P_{\mathbf{t}^{k-1}}^{\mathbf{t}^k} = \mathbf{u}^k \otimes \mathbf{u}^{k-1} + \mathbf{v}^k \otimes \mathbf{v}^{k-1} + \mathbf{t}^k \otimes \mathbf{t}^{k-1}. \quad (4.19)$$

Referring to $P_{\mathbf{t}^{k-1}}^{\mathbf{t}^k}$ as a parallel transport operator is also consistent with the fact that the Bishop frame associated with a continuous curve is parallel-propagated along the curve. As with its continuous counterpart, the Bishop frame is also known as a twist-free frame.

The Bishop frame we have just discussed features prominently in Bergou et al. [4]. Later works, such as Bergou et al. [3] and Kaldor et al. [29], use a frame that is parallel-transported in time on an edge. The notation for the basis vectors associated with this orthonormal reference frame varies in the literature. Here, we denote the triad of vectors on the k th edge associated with this frame as $\{\mathbf{t}^k, \mathbf{a}_1^k, \mathbf{a}_2^k\}$.² Referring to Fig. 4.3, the (right-handed) frame is assigned to each edge initially and then propagated in time:

$$\mathbf{a}_1^k(t + \Delta t) = \bar{P}^k(t, \Delta t) \mathbf{a}_1^k(t), \quad \mathbf{a}_2^k(t + \Delta t) = \bar{P}^k(t, \Delta t) \mathbf{a}_2^k(t). \quad (4.20)$$

We can also conclude that $\bar{P}^k(t, \Delta t)$ has the representation

$$\bar{P}^k(t, \Delta t) = \mathbf{a}_1^k(t + \Delta t) \otimes \mathbf{a}_1^k(t) + \mathbf{a}_2^k(t + \Delta t) \otimes \mathbf{a}_2^k(t) + \mathbf{t}^k(t + \Delta t) \otimes \mathbf{t}^k(t). \quad (4.21)$$

We invite the reader to compare Eqs. (4.20) and (4.21) to Eqs. (4.18) and (4.19).

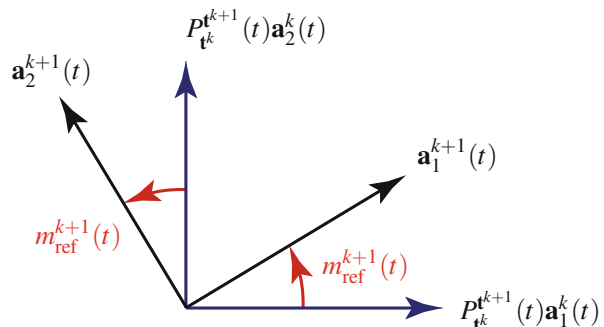
Unlike the Bishop frame, the reference frame is not space-parallel propagated along the discretized curve. That is,

$$\mathbf{a}_1^{k+1}(t) \neq P_{\mathbf{t}^k}^{\mathbf{t}^{k+1}}(t) \mathbf{a}_1^k(t), \quad \mathbf{a}_2^{k+1}(t) \neq P_{\mathbf{t}^k}^{\mathbf{t}^{k+1}}(t) \mathbf{a}_2^k(t). \quad (4.22)$$

However both of these pairs of vectors lie on a plane, and so we can define an angle m_{ref}^{k+1} that captures the difference between \mathbf{a}_1^{k+1} and its counterpart computed using the space-parallel transport operator $P_{\mathbf{t}^k}^{\mathbf{t}^{k+1}}$. Here, $\mathbf{a}_1^{k+1}, \mathbf{a}_2^{k+1}, \mathbf{t}^k, \mathbf{t}^{k+1}, P_{\mathbf{t}^k}^{\mathbf{t}^{k+1}}, \mathbf{a}_1^k$, and \mathbf{a}_2^k are each evaluated at the same instant in time. Referring to Fig. 4.4:

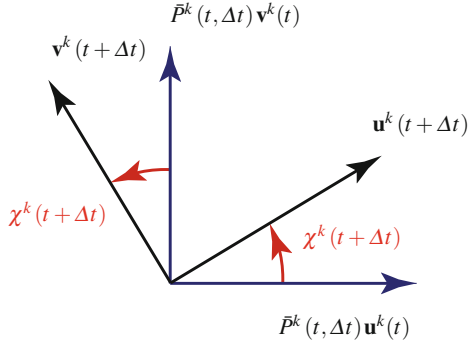
$$\begin{bmatrix} \mathbf{a}_1^{k+1}(t) \\ \mathbf{a}_2^{k+1}(t) \end{bmatrix} = \begin{bmatrix} \cos(m_{\text{ref}}^{k+1}(t)) & \sin(m_{\text{ref}}^{k+1}(t)) \\ -\sin(m_{\text{ref}}^{k+1}(t)) & \cos(m_{\text{ref}}^{k+1}(t)) \end{bmatrix} \begin{bmatrix} P_{\mathbf{t}^k}^{\mathbf{t}^{k+1}}(t) \mathbf{a}_1^k(t) \\ P_{\mathbf{t}^k}^{\mathbf{t}^{k+1}}(t) \mathbf{a}_2^k(t) \end{bmatrix}. \quad (4.23)$$

Fig. 4.4 The reference twist m_{ref}^{k+1} on the $(k+1)$ th edge at time t is defined by comparing the reference frame on an edge with its space-parallel transported counterpart from the adjacent edge



²In Bergou et al. [3], the triad is denoted by $\{\mathbf{t}^k, \underline{\mathbf{d}}_1^k, \underline{\mathbf{d}}_2^k\}$ while the triad is denoted by $\{\mathbf{t}^k, \mathbf{u}^k, \mathbf{v}^k\}$ in Kaldor et al. [29].

Fig. 4.5 The angle $\chi^k(t + \Delta t)$ relating the Bishop frame to its time-parallel propagated values on the k th edge at time $t + \Delta t$



The angle m_{ref}^i is known as the referential discrete (integrated) twist associated with the i th edge. For the zeroth edge, $m_{\text{ref}}^0 = 0$. We refer to m_{ref}^i as the reference twist in the sequel.

Complementing the angle m_{ref}^{k+1} , a related angle χ^k can be defined for the Bishop vectors and their time-parallel propagated counterparts. Referring to Fig. 4.5,

$$\begin{bmatrix} \mathbf{u}^k(t + \Delta t) \\ \mathbf{v}^k(t + \Delta t) \end{bmatrix} = \begin{bmatrix} \cos(\chi^k(t + \Delta t)) & \sin(\chi^k(t + \Delta t)) \\ -\sin(\chi^k(t + \Delta t)) & \cos(\chi^k(t + \Delta t)) \end{bmatrix} \begin{bmatrix} \bar{P}^k(t, \Delta t) \mathbf{u}^k(t) \\ \bar{P}^k(t, \Delta t) \mathbf{v}^k(t) \end{bmatrix}. \quad (4.24)$$

The angle χ^k and its space-parallel propagated counterpart are distinct. Indeed, because the Bishop frame vectors are space-parallel propagated, the latter angle is 0. An angle denoted $\psi_k(\epsilon)$ that is closely related to χ^k features in the work by Bergou et al. [4, Sect. 6]. The angle $\psi_k(\epsilon)$ represents the holonomy of a connection induced by parallel transporting \mathbf{t}^k around a closed circuit. We shall discuss this holonomy in further detail in Sect. 7.4.

The initial values of the Bishop vectors $\mathbf{u}^0(t_0)$ and $\mathbf{v}^0(t_0)$ at time $t = t_0$ are prescribed modulo a rotation about $\mathbf{t}^0(t_0)$. Once the initial values for this pair of vectors is selected, then the parallel propagation operators $P_{\mathbf{t}^0}^{\mathbf{t}^1}(t_0), \dots, P_{\mathbf{t}^{n-2}}^{\mathbf{t}^{n-1}}(t_0)$ define the Bishop triads throughout the rod at time $t = t_0$. By way of contrast, the initial values of the vectors $\mathbf{a}_1^k(t_0)$ and $\mathbf{a}_2^k(t_0)$ at time $t = t_0$ are prescribed modulo a rotation about $\mathbf{t}^k(t_0)$ for each edge and the operators $\bar{P}^k(t_0, \Delta t)$ are used to define the reference frame on the k th edge at time $t = t_0 + \Delta t$.

4.3.1 The Discretized Circular Space Curve

To further illustrate the results of this section, we return to the discretized helical space curve discussed in Sect. 3.4. The parallel transport operator $P_{\mathbf{t}^{k-1}}^{\mathbf{t}^k}$ for this curve can be computed with the help of Eqs. (3.23) and (3.24). The resulting lengthly expression is not very illuminating. However, when interest is restricted to a circle,

then the components of the rotation tensor simplify to that of a rotation about $\mathbf{b}_k = \mathbf{E}_3$ through a counterclockwise angle $\Delta\theta$:

$$\begin{aligned} P_{\mathbf{t}^{k-1}}^{\mathbf{t}^k} &= \cos(\Delta\theta) (\mathbf{e}_{r_k} \otimes \mathbf{e}_{r_k} + \mathbf{e}_{\theta_k} \otimes \mathbf{e}_{\theta_k}) \\ &\quad + \sin(\Delta\theta) (\mathbf{e}_{\theta_k} \otimes \mathbf{e}_{r_k} - \mathbf{e}_{r_k} \otimes \mathbf{e}_{\theta_k}) + \mathbf{E}_3 \otimes \mathbf{E}_3. \end{aligned} \quad (4.25)$$

With the help of Eqs. (3.19) and (3.20), we note that $\mathbf{t}^k = \mathbf{e}_\theta^k$ for a discretized circular curve. Choosing

$$\mathbf{u}^0 = \mathbf{E}_3, \quad \mathbf{v}^0 = -\mathbf{e}_r^0, \quad (4.26)$$

we find that

$$\mathbf{u}^k = \mathbf{E}_3, \quad \mathbf{v}^k = -\mathbf{e}_r^k. \quad (4.27)$$

In this case, it is transparent to see how the discrete Bishop frame approximates its continuous counterpart.

4.4 An Additional Representation for the Operator $P_{\mathbf{t}^{k-1}}^{\mathbf{t}^k}$

It is useful for future purposes to consider different representations of the space-parallel transport and time-parallel transport operators. First, we recall, from Eq. (4.19), the representation

$$P_{\mathbf{t}^{k-1}}^{\mathbf{t}^k} = \mathbf{u}^k \otimes \mathbf{u}^{k-1} + \mathbf{v}^k \otimes \mathbf{v}^{k-1} + \mathbf{t}^k \otimes \mathbf{t}^{k-1}. \quad (4.28)$$

After noting that the reference triad vectors and Bishop triad vectors are related by results of the form

$$\begin{aligned} \mathbf{a}_1^{k-1} &= \cos(\beta^{k-1}) \mathbf{u}^{k-1} + \sin(\beta^{k-1}) \mathbf{v}^{k-1}, \\ \mathbf{a}_2^{k-1} &= \cos(\beta^{k-1}) \mathbf{v}^{k-1} - \sin(\beta^{k-1}) \mathbf{u}^{k-1}, \end{aligned} \quad (4.29)$$

some straightforward manipulations can be used to show the representations

$$\begin{aligned} P_{\mathbf{t}^{k-1}}^{\mathbf{t}^k} &= \mathbf{u}^k \otimes \mathbf{u}^{k-1} + \mathbf{v}^k \otimes \mathbf{v}^{k-1} + \mathbf{t}^k \otimes \mathbf{t}^{k-1} \\ &= \cos(m_{\text{ref}}^k) (\mathbf{a}_1^k \otimes \mathbf{a}_1^{k-1} + \mathbf{a}_2^k \otimes \mathbf{a}_2^{k-1}) \\ &\quad + \sin(m_{\text{ref}}^k) (\mathbf{a}_1^k \otimes \mathbf{a}_2^{k-1} - \mathbf{a}_2^k \otimes \mathbf{a}_1^{k-1}) + \mathbf{t}^k \otimes \mathbf{t}^{k-1}, \end{aligned} \quad (4.30)$$

where

$$m_{\text{ref}}^k = \beta^k - \beta^{k-1}. \quad (4.31)$$

The representations (4.30) for $P_{\mathbf{t}^{k-1}}^{\mathbf{t}^k}$ enable a ready contrast between $P_{\mathbf{t}^{k-1}}^{\mathbf{t}^k} \mathbf{a}_1^{k-1}$ and $P_{\mathbf{t}^{k-1}}^{\mathbf{t}^k} \mathbf{u}^{k-1}$. They also show the privileged role occupied by the Bishop frame vectors \mathbf{u}^{k-1} and \mathbf{v}^{k-1} and how m_{ref}^k can be viewed as a rotation induced by the operator $P_{\mathbf{t}^{k-1}}^{\mathbf{t}^k}$.

As discussed previously, the rotation $\bar{P}^k(t, \Delta t)$ has the representation

$$\bar{P}^k(t, \Delta t) = \mathbf{a}_1^k(t + \Delta t) \otimes \mathbf{a}_1^k(t) + \mathbf{a}_2^k(t + \Delta t) \otimes \mathbf{a}_2^k(t) + \mathbf{t}^k(t + \Delta t) \otimes \mathbf{t}^k(t). \quad (4.32)$$

This tensor can be represented using the Bishop frame vectors $\mathbf{u}^k(t + \Delta t)$, $\mathbf{u}^k(t)$, $\mathbf{v}^k(t + \Delta t)$, and $\mathbf{v}^k(t)$ along with the angles $\beta^k(t + \Delta t)$ and $\beta^k(t)$ but the representation does not appear to be very illuminating.

4.5 Computation of Reference Twist in a Simple Rod

To illustrate many of the concepts introduced in this chapter, we consider a rod which has three vertices. The rod is subject to a motion parameterized by a scalar ϵ . This motion induces a reference twist m_{ref}^1 in the rod. Due to the simplicity of the model, the twist m_{ref}^1 along with the concomitant parallel transport operators can be explicitly computed. An alternative method of computing m_{ref}^1 for this rod, which exploits the Gauss–Bonnet theorem, will be discussed in Sect. 7.6.

Referring to Fig. 4.6, the initial configuration of the rod is defined by the vertices:

$$\mathbf{x}_0(\epsilon = 0) = \mathbf{0}, \quad \mathbf{x}_1(\epsilon = 0) = \mathbf{E}_1, \quad \mathbf{x}_2(\epsilon = 0) = 2\mathbf{E}_1 + \mathbf{E}_2. \quad (4.33)$$

During the deformation of the rod, the first edge remains stationary, while the second edge is stretched as its end node is raised upwards:

$$\mathbf{x}_0(\epsilon) = \mathbf{0}, \quad \mathbf{x}_1(\epsilon) = \mathbf{E}_1, \quad \mathbf{x}_2(\epsilon) = 2\mathbf{E}_1 + \mathbf{E}_2 + \epsilon\mathbf{E}_3. \quad (4.34)$$

It is straightforward to compute the edge and tangent vectors for this rod:

$$\begin{aligned} \mathbf{e}^0(\epsilon) &= \mathbf{E}_1, & \mathbf{e}^1(\epsilon) &= \mathbf{E}_1 + \mathbf{E}_2 + \epsilon\mathbf{E}_3, \\ \mathbf{t}^0(\epsilon) &= \mathbf{E}_1, & \mathbf{t}^1(\epsilon) &= \frac{1}{\sqrt{2 + \epsilon^2}} (\mathbf{E}_1 + \mathbf{E}_2 + \epsilon\mathbf{E}_3). \end{aligned} \quad (4.35)$$

We note for completeness that the discrete integrated curvature vector is

$$(\kappa\mathbf{b})_1 = \frac{2}{1 + \sqrt{2 + \epsilon^2}} (\mathbf{E}_3 - \epsilon\mathbf{E}_2). \quad (4.36)$$

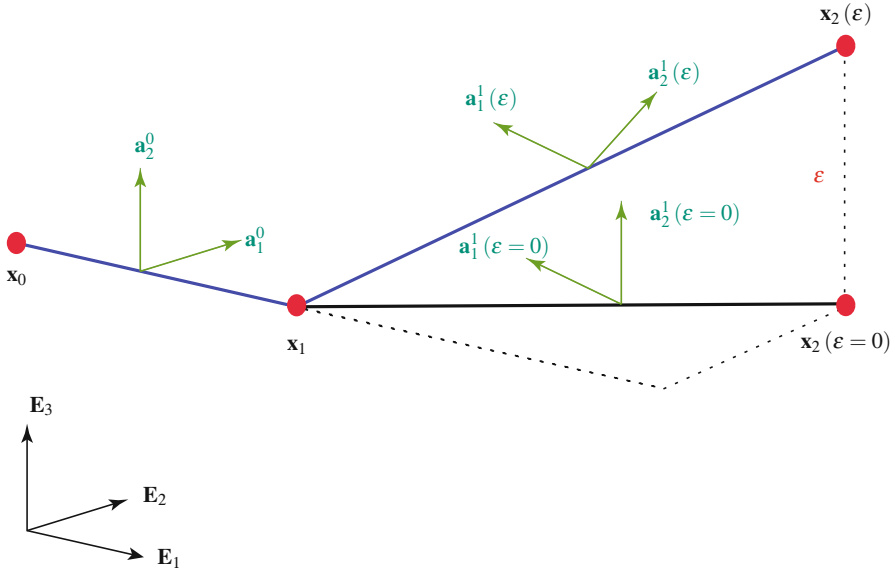


Fig. 4.6 The configurations of a rod which has three vertices. When $\epsilon = 0$, all of the vertices lie on a horizontal plane. As ϵ is increased from 0, the third vertex rises above this plane and a reference twist is induced in the second edge

Observe that as ϵ increases from zero, the discrete curvature κ_1 increases from a value $\frac{2}{1+\sqrt{2}}$.

The space-parallel transport operator can be defined as a function of the parameter ϵ :

$$P_{t_0^0}^{t^1}(\epsilon) = \mathbf{R}(\varphi_1(\epsilon), \mathbf{b}_1(\epsilon)). \quad (4.37)$$

With the help of Eq.(4.2), the turning angle φ_1 and axis of rotation \mathbf{b}_1 can be computed using the tangent vectors associated with the edges:

$$\begin{aligned} \cos(\varphi_1(\epsilon)) &= \frac{1}{\sqrt{2 + \epsilon^2}}, & \sin(\varphi_1(\epsilon)) &= \sqrt{\frac{1 + \epsilon^2}{2 + \epsilon^2}}, \\ \mathbf{b}_1(\epsilon) &= \frac{1}{\sqrt{1 + \epsilon^2}} (\mathbf{E}_3 - \epsilon \mathbf{E}_2). \end{aligned} \quad (4.38)$$

The time-parallel transport operators for the edges can be computed using Eq.(4.5):

$$\bar{P}^0(0, \epsilon) = \mathbf{I}, \quad \bar{P}^1(0, \epsilon) = \mathbf{R}(\alpha^1(\epsilon), \mathbf{h}^1(\epsilon)), \quad (4.39)$$

where

$$\begin{aligned}\mathbf{h}^1(0, \epsilon) &= \frac{1}{\sqrt{2}} (\mathbf{E}_1 - \mathbf{E}_2), \\ \cos(\alpha^1(0, \epsilon)) &= \sqrt{\frac{2}{2 + \epsilon^2}}, \quad \sin(\alpha^1(0, \epsilon)) = \frac{\epsilon}{\sqrt{2 + \epsilon^2}}.\end{aligned}\quad (4.40)$$

In the definition of the time-parallel transport operators $\bar{P}^k(t, \Delta t)$, we have taken time $t = 0$ and used ϵ in place of Δt . When $\epsilon = 0$, both of these operators simplify to the identity tensor.

The reference frame vectors on the first edge when $\epsilon = 0$ are chosen to be

$$\mathbf{a}_1^0(\epsilon = 0) = \mathbf{E}_2, \quad \mathbf{a}_2^0(\epsilon = 0) = \mathbf{E}_3. \quad (4.41)$$

Because the time-parallel operator for the first edge is the identity tensor, these vectors remain constant:

$$\mathbf{a}_1^0(\epsilon) = \mathbf{E}_2, \quad \mathbf{a}_2^0(\epsilon) = \mathbf{E}_3. \quad (4.42)$$

The reference frame vectors on the second edge at $\epsilon = 0$ are computed using the space-parallel transport operator $P_{t^0}^{t^1}(\epsilon = 0)$:

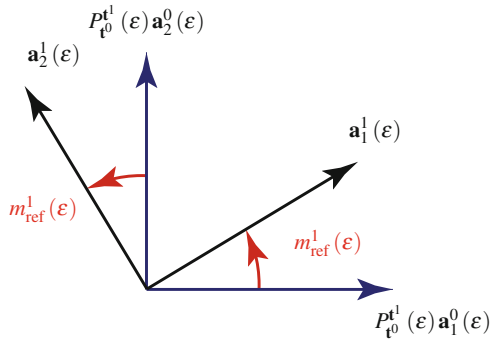
$$\begin{aligned}\mathbf{a}_1^1(\epsilon = 0) &= P_{t^0}^{t^1}(\epsilon = 0) \mathbf{a}_1^0(\epsilon = 0) \\ &= P_{t^0}^{t^1}(\epsilon = 0) \mathbf{E}_2 \\ &= \frac{1}{\sqrt{2}} (\mathbf{E}_2 - \mathbf{E}_1), \\ \mathbf{a}_2^1(\epsilon = 0) &= P_{t^0}^{t^1}(\epsilon = 0) \mathbf{a}_2^0(\epsilon = 0) \\ &= P_{t^0}^{t^1}(\epsilon = 0) \mathbf{E}_3 \\ &= \mathbf{E}_3.\end{aligned}\quad (4.43)$$

It is important to observe that the initial values of the reference vectors \mathbf{a}_1^k and \mathbf{a}_2^k are obtained by specifying \mathbf{a}_1^0 and \mathbf{a}_2^0 and then using the initial space-parallel transport operators to determine the initial values of \mathbf{a}_1^k and \mathbf{a}_2^k . At later instances of time, \mathbf{a}_1^k and \mathbf{a}_2^k are updated using the time-parallel transport operator.

For $\epsilon \neq 0$, the reference frame vectors on the second edge are computed using the time-parallel transport operator associated with the second edge:

$$\begin{aligned}\mathbf{a}_1^1(\epsilon) &= \bar{P}^1(0, \epsilon) \mathbf{a}_1^1(\epsilon = 0) \\ &= \frac{1}{\sqrt{2}} (\mathbf{E}_2 - \mathbf{E}_1),\end{aligned}$$

Fig. 4.7 The angle $m_{\text{ref}}^1(\epsilon)$ relating the reference frame vectors to their space-parallel propagated values on the second edge. When $\epsilon = 0$ for the example of interest in this section of the Brief, $m_{\text{ref}}^1 = 0$



$$\begin{aligned}\mathbf{a}_2^1(\epsilon) &= \bar{P}^1(0, \epsilon) \mathbf{a}_2^1(\epsilon = 0) \\ &= \cos(\alpha^1(0, \epsilon)) \mathbf{E}_3 - \frac{\sin(\alpha^1(0, \epsilon))}{\sqrt{2}} (\mathbf{E}_2 + \mathbf{E}_1).\end{aligned}\quad (4.44)$$

The computation of $\mathbf{a}_1^1(\epsilon)$ is greatly simplified by noting that this vector is parallel to the axis of rotation of $\bar{P}^1(0, \epsilon)$.

The reference twist m_{ref}^0 for the first edge is identically 0. As shown in Fig. 4.7, for the second edge, the reference twist m_{ref}^1 is the angle between $P_{t^0}^{t^1}(\epsilon) \mathbf{a}_1^0(\epsilon)$ and $\mathbf{a}_1^1(\epsilon)$:

$$\begin{aligned}c^1(\epsilon) &\equiv \cos(m_{\text{ref}}^1) = (P_{t^0}^{t^1}(\epsilon) \mathbf{a}_1^0(\epsilon)) \cdot \mathbf{a}_1^1(\epsilon) \\ &= (P_{t^0}^{t^1}(\epsilon) \mathbf{E}_2) \cdot \mathbf{a}_1^1(\epsilon), \\ s^1(\epsilon) &\equiv \sin(m_{\text{ref}}^1) = (P_{t^0}^{t^1}(\epsilon) \mathbf{a}_1^0(\epsilon)) \cdot \mathbf{a}_1^1(\epsilon) \\ &= (P_{t^0}^{t^1}(\epsilon) \mathbf{E}_3) \cdot \mathbf{a}_1^1(\epsilon).\end{aligned}\quad (4.45)$$

Computing the dot products and expanding the resulting expressions, we find the following representations for the respective functions $\cos(m_{\text{ref}}^1)$ and $\sin(m_{\text{ref}}^1)$:

$$\begin{aligned}c^1(\epsilon) &= \frac{\sin(\varphi_1(\epsilon))}{\sqrt{2}\sqrt{1+\epsilon^2}} + \frac{1}{\sqrt{2}} \left(\cos(\varphi_1(\epsilon)) + \frac{\epsilon^2(1-\cos(\varphi_1(\epsilon)))}{1+\epsilon^2} \right) \\ &= \frac{2+\epsilon^2(1+\sqrt{2+\epsilon^2})}{\sqrt{2}(1+\epsilon^2)\sqrt{2+\epsilon^2}},\end{aligned}\quad (4.46)$$

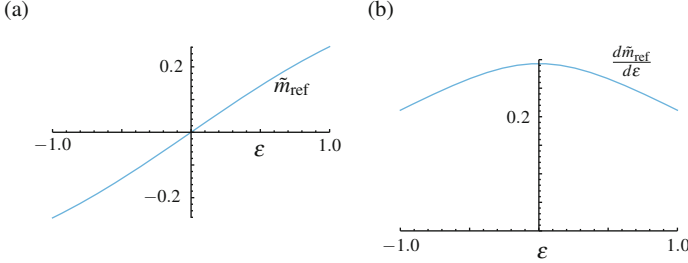


Fig. 4.8 (a) The reference twist $m_{\text{ref}}^1 = \tilde{m}_{\text{ref}}$ as a function of ϵ computed using Eq. (4.48) for the rod with two edges shown in Fig. 4.6. (b) The corresponding value of $\frac{d\tilde{m}_{\text{ref}}}{d\epsilon}$ computed by differentiating the lengthy expression for the function \tilde{m}_{ref}

and

$$\begin{aligned} s^1(\epsilon) &= \epsilon \cos(\alpha_1(0, \epsilon)) \left(\frac{1 - \cos(\varphi_1(\epsilon))}{1 + \epsilon^2} \right) \\ &+ \frac{\sin(\alpha_1(0, \epsilon))}{\sqrt{2}} \left(\cos(\varphi_1(\epsilon)) + \frac{\epsilon^2(1 - \cos(\varphi_1(\epsilon)))}{1 + \epsilon^2} \right) \\ &- \frac{\sin(\alpha_1(0, \epsilon))}{\sqrt{2}} \left(\frac{\sin(\varphi_1(\epsilon))}{\sqrt{2}\sqrt{1 + \epsilon^2}} \right). \end{aligned} \quad (4.47)$$

In contrast to the expression for $c^1(\epsilon)$, the explicit expression for $s^1(\epsilon)$ is lengthy and not very illuminating and so it is omitted.

Using the functions $c^1(\epsilon)$ and $s^1(\epsilon)$, the reference twist as a function of ϵ can be determined. We denote the resulting function by $\tilde{m}_{\text{ref}}(\epsilon)$:

$$m_{\text{ref}}^1 = \tilde{m}_{\text{ref}}(\epsilon). \quad (4.48)$$

The graph of $\tilde{m}_{\text{ref}}(\epsilon)$ is shown in Fig. 4.8a. We observe that

$$\tilde{m}_{\text{ref}}(-1) = -\frac{\pi}{12}, \quad \tilde{m}_{\text{ref}}(0) = 0, \quad \tilde{m}_{\text{ref}}(1) = \frac{\pi}{12}, \quad (4.49)$$

and note that $m_{\text{ref}}(\epsilon)$ is a monotonically increasing function of ϵ . Thus, the simple motion of lifting one of the edges of the rod induces a reference twist in the rod.

In Sect. 7.6 of this Brief, the reference twist and its derivative will be computed using a construction from spherical trigonometry. As can be seen by comparing Fig. 4.8 and Fig. 7.9, the results from the two distinct methods are equivalent when $\epsilon \geq 0$.

Chapter 5

Material Frames and Measures of Twists



5.1 Introduction

To model the deformation of a long slender (i.e., rod-like) body, the behavior of the cross-sections must be accounted for. In modern theories of rods, deformable vector fields, which are known as directors, are associated with each point on the material curve that is used to model the centerline of the rod. In the discrete elastic rod formulation, a pair of directors (or material vectors) is associated with each edge of the discretized curve (cf. Fig. 5.1). While the discrete integrated curvature vector $\kappa_k \mathbf{b}_k$ associated with the discretized curve accounts for the bending of the rod, the directors are needed to measure the twist of the rod. Here, the twist of the rod is related to the difference in the rotation of the directors between two successive edges. To measure the rotation, two different approaches have been used. In earlier works, such as [4], the rotation was measured with the help of a Bishop frame on each edge while later works, such as [3, 29], use a reference frame on each edge that is updated at each time step. The latter approach introduces an angle of twist into the formulation that can be difficult to comprehend.

In the present chapter, the director (material) frames and their associated triad $\{\mathbf{t}^k, \mathbf{m}_1^k, \mathbf{m}_2^k\}$ are introduced. Our discussion provides a considerable elaboration on the outlines presented in [3, 4, 29], but it is not complete. In particular, we need to postpone discussing how a reference twist m_{ref}^k can be related to a geometrical concept, which known as a holonomy, until Chap. 7. To illustrate some of the developments in the present chapter, the problem of a rod uncoiling from a helical state under its own weight is presented in Sect. 5.9. As with the previous chapter, we encourage the reader to refer to Tables 1.1 and 1.2 from Chap. 1 for added guidance.

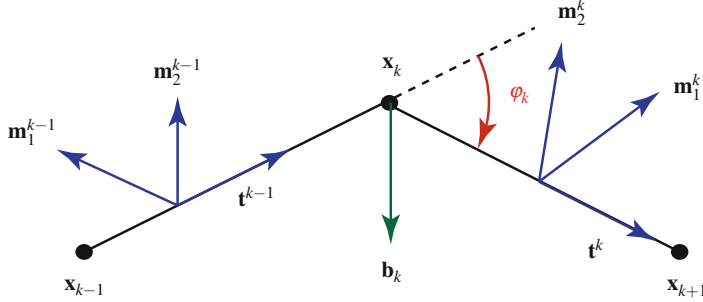


Fig. 5.1 Three vertices x_{k-1} , x_k , and x_{k+1} , and some of the unit vectors associated with the edges. The triads $\{t^{k-1}, m_1^{k-1}, m_2^{k-1} = t^{k-1} \times m_1^{k-1}\}$ and $\{t^k, m_1^k, m_2^k = t^k \times m_1^k\}$ are material triads. Each triad can be associated with the midpoint of its associated edge to constitute a material frame

5.2 The Material Triad

The most popular nonlinear rod theory that captures three-dimensional motions of the centerline, torsion of the cross-sections, and a pair of flexures of the centerline, dates to Kirchhoff [31] in 1859. In modern formulations of this theory, a pair of unit vectors, known as directors, \mathbf{d}_1 and \mathbf{d}_2 , are associated with each point on the centerline of the rod. These vectors are assumed to remain normal to the unit tangent vector to the centerline of the rod (cf. the textbooks [1, 51]). Kirchhoff's rod theory assumes that the cross-sections of the rod remain plane and normal to the centerline while the rod is deforming. Thus, the deformation of the triad $\{\mathbf{d}_1, \mathbf{d}_2, \mathbf{d}_3 = \mathbf{e}_t\}$ can be modeled using a rotation tensor and three strains can be defined with the help of the rotation and its partial derivative with respect to s . As discussed in Sect. 2.3, this trio of strains are related to the curvature κ and geometric torsion τ of the centerline, and the twist of the cross-section relative to the Frenet frame. It is important to keep in mind that while the behavior of the Bishop and Frenet triads do not generally capture the three strains in Kirchhoff's rod theory, the director triad $\{\mathbf{d}_1, \mathbf{d}_2, \mathbf{d}_3 = \mathbf{e}_t\}$ does.

In the theory of discrete elastic rods, the counterpart to the director triad is a material triad $\{t^k, m_1^k, m_2^k\}$ associated with an edge. The unit vectors m_1^k and m_2^k are coplanar with the Bishop frame vectors \mathbf{u}^k and \mathbf{v}^k and can be related to them by a rotation ϑ^k about t^k as shown in Fig. 5.2a.¹ The initial prescription for the material vectors at time $t = t_0$ are such that $\{t^k, m_1^k, m_2^k\}$ form a right-handed orthonormal triad on each edge of the rod.

¹In some works, the material vectors are identified as the discrete directors: $\mathbf{m}_1^k = \mathbf{d}_1^k$ and $\mathbf{m}_2^k = \mathbf{d}_2^k$.

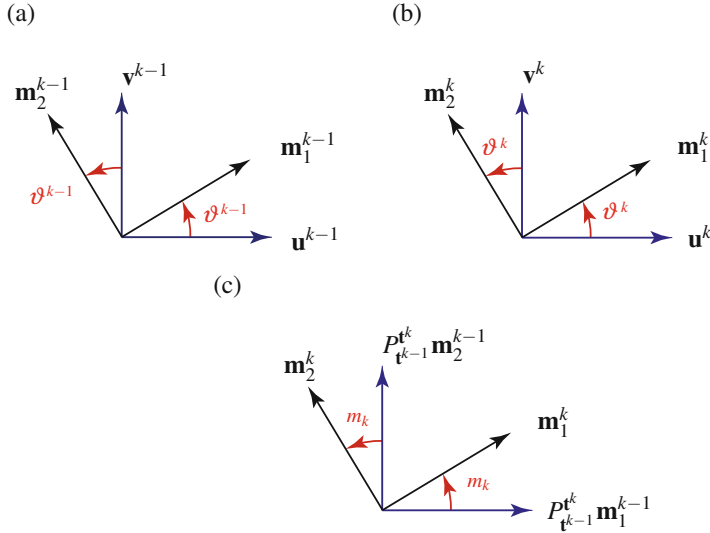


Fig. 5.2 (a) Schematic of the angle ϑ^{k-1} defining the rotation between the Bishop frame vectors and the material vectors along the edge \mathbf{e}^{k-1} . (b) Schematic of the angle ϑ^k defining the rotation between the Bishop frame vectors and the material vectors along the edge \mathbf{e}^k . (c) The discrete integrated twist $m_k = \vartheta^k - \vartheta^{k-1}$ and its relation to space-parallel transport

5.2.1 The Operators $M_{\mathbf{t}^{k-1}}^{\mathbf{t}^k}$ and $\bar{M}^k(t, \Delta t)$

The rotation of the material triad from one edge to its adjacent counterpart at an instant t can be defined by a rotation tensor:

$$M_{\mathbf{t}^{k-1}}^{\mathbf{t}^k} = \mathbf{m}_1^k \otimes \mathbf{m}_1^{k-1} + \mathbf{m}_2^k \otimes \mathbf{m}_2^{k-1} + \mathbf{t}^k \otimes \mathbf{t}^{k-1}. \quad (5.1)$$

Referring to Fig. 5.2b, c, the tensor $M_{\mathbf{t}^{k-1}}^{\mathbf{t}^k}$ and the parallel transport operator $P_{\mathbf{t}^{k-1}}^{\mathbf{t}^k}$ are related:

$$\begin{aligned} M_{\mathbf{t}^{k-1}}^{\mathbf{t}^k} &= \mathbf{R}(\vartheta^k, \mathbf{t}^k) P_{\mathbf{t}^{k-1}}^{\mathbf{t}^k} \mathbf{R}^T(\vartheta^{k-1}, \mathbf{t}^{k-1}) \\ &= \mathbf{R}(\vartheta^k, \mathbf{t}^k) P_{\mathbf{t}^{k-1}}^{\mathbf{t}^k} \mathbf{R}(-\vartheta^{k-1}, \mathbf{t}^{k-1}). \end{aligned} \quad (5.2)$$

It should be obvious from Eq. (5.2) that $\mathbf{t}^k = M_{\mathbf{t}^{k-1}}^{\mathbf{t}^k} \mathbf{t}^{k-1}$. The operator $M_{\mathbf{t}^{k-1}}^{\mathbf{t}^k}$ plays a seminal role in determining the twist of the rod.

Complementing the rotation $M_{\mathbf{t}^{k-1}}^{\mathbf{t}^k}$, we also define an operator that transforms the material frame at an instant t to its counterpart at $t + \Delta t$:

$$\bar{M}^k(t, \Delta t) = \mathbf{m}_1^k(t + \Delta t) \otimes \mathbf{m}_1^k(t) + \mathbf{m}_2^k(t + \Delta t) \otimes \mathbf{m}_2^k(t) + \mathbf{t}^k(t + \Delta t) \otimes \mathbf{t}^k(t). \quad (5.3)$$

Thus, for example, $\mathbf{m}_1^k(t + \Delta t) = \bar{M}^k(t, \Delta t) \mathbf{m}_1^k(t)$. The operator $\bar{M}^k(t, \Delta t)$ will feature in computing the kinetics of the discrete elastic rod and has numerous representations. However, for ease of exposition, we postpone discussion of these representations until Sect. 5.7.

5.3 Bending Strains and Curvatures

The components of the discrete integrated curvature vector $(\kappa \mathbf{b})_k$ at the vertex \mathbf{x}_k are used to quantify the bending strains of the rod. Recalling from Eq. (3.11) that

$$(\kappa \mathbf{b})_k = \frac{2\mathbf{t}^{k-1} \times \mathbf{t}^k}{1 + \mathbf{t}^{k-1} \cdot \mathbf{t}^k}, \quad (5.4)$$

we observe that $(\kappa \mathbf{b})_k$ is orthonormal to \mathbf{t}^k and \mathbf{t}^{k-1} . This implies that we can construct a basis for \mathbb{E}^3 where $(\kappa \mathbf{b})_k$ has one zero component. The basis is

$$\left\{ \frac{1}{2} (\mathbf{t}^{k-1} + \mathbf{t}^k), \frac{1}{2} (\mathbf{m}_1^{k-1} + \mathbf{m}_1^k), \frac{1}{2} (\mathbf{m}_2^{k-1} + \mathbf{m}_2^k) \right\}. \quad (5.5)$$

The non-zero components of $(\kappa \mathbf{b})_k$ are used to define the curvatures associated with the material frame at the k th vertex:

$$\begin{aligned} \kappa_{k_1} &= \frac{1}{2} (\mathbf{m}_2^{k-1} + \mathbf{m}_2^k) \cdot (\kappa \mathbf{b})_k, \\ \kappa_{k_2} &= -\frac{1}{2} (\mathbf{m}_1^{k-1} + \mathbf{m}_1^k) \cdot (\kappa \mathbf{b})_k. \end{aligned} \quad (5.6)$$

These curvatures were introduced in Bergou et al. [3] and are known as vertex-based material curvatures. The pair of curvatures will be used as the bending strains of the discrete elastic rod (see Sect. 8.3).

To provide additional motivation for κ_{k_1} and κ_{k_2} , we note that they are discretized versions of the continuous case:

$$\begin{aligned} \kappa_{D_1} &= \mathbf{e}'_t \cdot \mathbf{d}_1 = \mathbf{v}_D \cdot \mathbf{d}_2 = \kappa \mathbf{e}_b \cdot \mathbf{d}_2, \\ \kappa_{D_2} &= \mathbf{e}'_t \cdot \mathbf{d}_2 = -\mathbf{v}_D \cdot \mathbf{d}_1 = -\kappa \mathbf{e}_b \cdot \mathbf{d}_1. \end{aligned} \quad (5.7)$$

When comparing the discrete and continuous cases, one also needs to be cognizant of the length ℓ_k of the Voronoi region of the vertex \mathbf{x}_k that is used to scale $(\kappa \mathbf{b})_k$.

5.4 Discrete Integrated Twist

As discussed earlier [cf. Eq. (4.18)], the Bishop triad vectors on an edge can be computed from the previous edge using the rotation (space-parallel transport operator) $P_{\mathbf{t}^{k-1}}^{\mathbf{t}^k}$. Thus, at each instant in time, the propagation of the Bishop frame vectors \mathbf{u}^{k-1} and \mathbf{v}^{k-1} from the $(k-1)$ th edge to the vectors \mathbf{u}^k and \mathbf{v}^k on the k th edge using $P_{\mathbf{t}^{k-1}}^{\mathbf{t}^k}$ is known as space-parallel transport. The rotation of the material vectors relative to the Bishop vectors defines a discrete twist. By appropriately accommodating the rotation $P_{\mathbf{t}^{k-1}}^{\mathbf{t}^k}$, the relative rotation of the material vectors between adjacent edges can be computed. The resulting relative rotation is a measure of the torsional strain in the rod.

To elaborate on our previous remarks, we refer the reader to Fig. 5.2c and observe that

$$\begin{aligned}\mathbf{m}_1^{k-1} &= \cos(\vartheta^{k-1}) \mathbf{u}^{k-1} + \sin(\vartheta^{k-1}) \mathbf{v}^{k-1}, \\ \mathbf{m}_2^{k-1} &= \cos(\vartheta^{k-1}) \mathbf{v}^{k-1} - \sin(\vartheta^{k-1}) \mathbf{u}^{k-1}.\end{aligned}\quad (5.8)$$

Whence,

$$\begin{aligned}P_{\mathbf{t}^{k-1}}^{\mathbf{t}^k} \mathbf{m}_1^{k-1} &= \cos(\vartheta^{k-1}) \mathbf{u}^k + \sin(\vartheta^{k-1}) \mathbf{v}^k, \\ P_{\mathbf{t}^{k-1}}^{\mathbf{t}^k} \mathbf{m}_2^{k-1} &= \cos(\vartheta^{k-1}) \mathbf{v}^k - \sin(\vartheta^{k-1}) \mathbf{u}^k,\end{aligned}\quad (5.9)$$

and

$$\begin{aligned}\mathbf{m}_1^k &= \cos(\vartheta^k - \vartheta^{k-1}) P_{\mathbf{t}^{k-1}}^{\mathbf{t}^k} \mathbf{m}_1^{k-1} + \sin(\vartheta^k - \vartheta^{k-1}) P_{\mathbf{t}^{k-1}}^{\mathbf{t}^k} \mathbf{m}_2^{k-1}, \\ \mathbf{m}_2^k &= \cos(\vartheta^k - \vartheta^{k-1}) P_{\mathbf{t}^{k-1}}^{\mathbf{t}^k} \mathbf{m}_2^{k-1} - \sin(\vartheta^k - \vartheta^{k-1}) P_{\mathbf{t}^{k-1}}^{\mathbf{t}^k} \mathbf{m}_1^{k-1}.\end{aligned}\quad (5.10)$$

The latter identity leads to the definition of the discrete integrated twist m_k on the edge \mathbf{e}^k :

$$m_k = \vartheta^k - \vartheta^{k-1}. \quad (5.11)$$

As noted in Bergou et al. [4, Sect. 4.2.2] and summarized in Fig. 5.2c, the twist m_k can be interpreted as the difference between a material frame on the k th edge and the corresponding parallel transported frame from the $(k-1)$ th edge.

In the interests of reducing computational cost, use of the relative twist m_k as a measure of torsional strain was modified following the 2008 paper [4]. In later works, such as [3, 29], the Bishop frame vectors \mathbf{u}^k and \mathbf{v}^k are not explicitly used to compute m_k , rather the reference frame vectors \mathbf{a}_1^k and \mathbf{a}_2^k are used. In this case,

it is necessary to supplement m_k with a measure known as the referential discrete (integrated) twist (or reference twist) m_{ref}^k . This modification will be discussed in further detail in Sect. 5.6.

5.5 Decompositions of the Rotation $M_{\mathbf{t}^{k-1}}^{\mathbf{t}^k}$

As presented in Audoly et al. [2, Eq.(C.8), Appendix C.2], the relative twist m_k can be used to provide decompositions of the rotation $M_{\mathbf{t}^{k-1}}^{\mathbf{t}^k}$. The resulting decomposition shows a relationship between the space-parallel transport operator and a rotation through the relative twist about a tangent vector to one of the edges. The resulting decompositions can be useful when computing angular velocity vectors and Darboux vectors.

To establish the decompositions, one starts by noting that

$$\begin{aligned} P_{\mathbf{t}^{k-1}}^{\mathbf{t}^k} \mathbf{R}(m_k, \mathbf{t}^{k-1}) \left(P_{\mathbf{t}^{k-1}}^{\mathbf{t}^k} \right)^T \mathbf{t}^k &= \mathbf{t}^k, \\ P_{\mathbf{t}^{k-1}}^{\mathbf{t}^k} \mathbf{R}(m_k, \mathbf{t}^{k-1}) \left(P_{\mathbf{t}^{k-1}}^{\mathbf{t}^k} \right)^T \mathbf{u}^k &= \cos(m_k) \mathbf{u}^k + \sin(m_k) \mathbf{v}^k, \\ P_{\mathbf{t}^{k-1}}^{\mathbf{t}^k} \mathbf{R}(m_k, \mathbf{t}^{k-1}) \left(P_{\mathbf{t}^{k-1}}^{\mathbf{t}^k} \right)^T \mathbf{v}^k &= -\sin(m_k) \mathbf{u}^k + \cos(m_k) \mathbf{v}^k. \end{aligned} \quad (5.12)$$

These results enable one to find a simple expression for a compound rotation:

$$P_{\mathbf{t}^{k-1}}^{\mathbf{t}^k} \mathbf{R}(m_k, \mathbf{t}^{k-1}) \left(P_{\mathbf{t}^{k-1}}^{\mathbf{t}^k} \right)^T = \mathbf{R}(m_k, \mathbf{t}^k). \quad (5.13)$$

Examining the action of $P_{\mathbf{t}^{k-1}}^{\mathbf{t}^k} \mathbf{R}(m_k, \mathbf{t}^{k-1})$ on \mathbf{m}_1^{k-1} and \mathbf{m}_2^{k-1} results in the conclusion that

$$M_{\mathbf{t}^{k-1}}^{\mathbf{t}^k} = P_{\mathbf{t}^{k-1}}^{\mathbf{t}^k} \mathbf{R}(m_k, \mathbf{t}^{k-1}) = \mathbf{R}(m_k, \mathbf{t}^k) P_{\mathbf{t}^{k-1}}^{\mathbf{t}^k}, \quad (5.14)$$

where the rotation $M_{\mathbf{t}^{k-1}}^{\mathbf{t}^k}$ was defined previously by Eq. (5.2).

5.6 Discrete Integrated Twist and Induced Reference Twist

In later versions of the discrete elastic rod formulation, the reference frame vectors \mathbf{a}_1^k and \mathbf{a}_2^k are used to compute the twist of the rod. As shall be elaborated upon below, the resulting formulation introduces a so-called reference twist into the measure of torsional strain. In our examination of the literature on discrete elastic rods, we found the notion of induced reference twist to be exceptionally difficult to comprehend. We hope the explanation provided below contributes to clarifying the concept of induced reference twist.

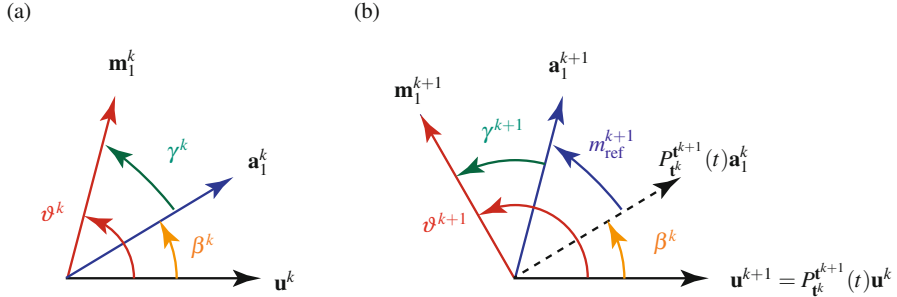


Fig. 5.3 The angles and unit vectors employed in the definition of the discrete reference twist m_{ref}^{k+1} . (a) The vectors on the k th edge. (b) The vectors associated with the $(k+1)$ th edge. It is important to observe that the angle β^k between \mathbf{a}_1^k and \mathbf{u}^k is identical to the angle between $P_{\mathbf{t}_k^k}(t)\mathbf{a}_1^k$ and $\mathbf{u}^{k+1} = P_{\mathbf{t}_{k-1}^k}(t)\mathbf{u}^k$. The angle $\beta^{k+1} = \beta^k + m_{\text{ref}}^{k+1}$ is not explicitly shown

To discuss the formulation of twist featuring the reference frame, it is convenient to assume that the reference frame and the Bishop frame are both being computed for the deformed discrete curve. Consider the k th edge. The vectors \mathbf{m}_1^k , \mathbf{u}^k , and \mathbf{a}_1^k can be used to define the three angles ϑ^k , γ^k , and β^k shown in Fig. 5.3a:

$$\vartheta^k = \beta^k + \gamma^k. \quad (5.15)$$

Each of these angles can be associated with a measure of twisting of the rod. The angle β^k is the signed angle formed by \mathbf{a}_1^k and \mathbf{u}^k , is identical to the angle formed by \mathbf{a}_1^k and \mathbf{v}^k , and can be considered as the twist angle of the reference frame. The angles γ^k and ϑ^k are the signed angles formed by \mathbf{m}_1^k and \mathbf{a}_1^k and \mathbf{m}_1^k and \mathbf{u}^k , respectively. The change in the angle β^k from one edge to the preceding edge is the induced reference twist:

$$m_{\text{ref}}^{k+1} = \beta^{k+1} - \beta^k. \quad (5.16)$$

This interpretation of the induced reference twist is consistent with our earlier discussion on Page 39 [cf. Eq. (4.23)]. The reference twist m_{ref}^k in [3] and [29] is denoted by m_k and $\hat{\vartheta}^k$, respectively.

If we next consider the $(k+1)$ th edge, then it is straightforward to argue that the angle between \mathbf{u}^{k+1} and $P_{\mathbf{t}_k^k}(t)\mathbf{a}_1^k$ will be β^k . The argument relies on the facts that for any pair of vectors \mathbf{a} and \mathbf{b} and a rotation tensor \mathbf{R} , the following identities hold:

$$\begin{aligned} (\mathbf{Ra}) \cdot (\mathbf{Rb}) &= \mathbf{a} \cdot \mathbf{b}, \\ (\mathbf{Ra}) \times (\mathbf{Rb}) &= \mathbf{R}(\mathbf{a} \times \mathbf{b}). \end{aligned} \quad (5.17)$$

Referring to Fig. 4.4 and Eq. (4.23), we observe that

$$\vartheta^{k+1} = \beta^k + \gamma^{k+1} + m_{\text{ref}}^{k+1}, \quad \beta^{k+1} = \beta^k + m_{\text{ref}}^{k+1}. \quad (5.18)$$

With the added help of Eq. (5.11), we note that the discrete integrated twist on the $(k+1)$ th edge has the representations

$$\begin{aligned} m_{k+1} &= \vartheta^{k+1} - \vartheta^k \\ &= (\gamma^{k+1} + m_{\text{ref}}^{k+1} + \beta^k) - (\gamma^k + \beta^k) \\ &= \gamma^{k+1} - \gamma^k + m_{\text{ref}}^{k+1}. \end{aligned} \quad (5.19)$$

The final representation $m_{k+1} = \gamma^{k+1} - \gamma^k + m_{\text{ref}}^{k+1}$ features in works by Bergou et al. [3] and Kaldor et al. [29] where the reference triad is parallel transported in time. We observe also from the relation $m_{k+1} = \gamma^{k+1} - \gamma^k + m_{\text{ref}}^{k+1}$ that it is not necessary to compute the Bishop frame in order for m_{k+1} to be computed. Indeed, the Bishop frame is not explicitly needed in the most recent discrete elastic rod formulations.

In the code for the discrete elastic rod formulation, $m_{\text{ref}}^{k+1}(t + \Delta t)$ is computed using a recursive scheme which assumes that $m_{\text{ref}}^{k+1}(t)$ is known:

$$m_{\text{ref}}^{k+1}(t + \Delta t) = m_{\text{ref}}^{k+1}(t) + \Delta m_{\text{ref}}^{k+1}(t + \Delta t). \quad (5.20)$$

To compute the increment $\Delta m_{\text{ref}}^{k+1}(t + \Delta t)$, the angle $m_{\text{ref}}^{k+1}(t)$ is used to rotate $P_{t^k}^{t^{k+1}} \mathbf{a}_1^k(t + \Delta t)$ about $\mathbf{t}^{k+1}(t + \Delta t)$ to define the vector $\mathbf{R}(m_{\text{ref}}^k(t), \mathbf{t}^{k+1}) P_{t^k}^{t^{k+1}} \mathbf{a}_1^k(t + \Delta t)$. Then, the angle between $\mathbf{R}(m_{\text{ref}}^k(t), \mathbf{t}^{k+1}) P_{t^k}^{t^{k+1}} \mathbf{a}_1^k(t + \Delta t)$ and $\mathbf{a}_1^{k+1}(t + \Delta t)$ is computed. As summarized in Fig. 5.4, this angle is $\Delta m_{\text{ref}}^{k+1}(t + \Delta t)$.²

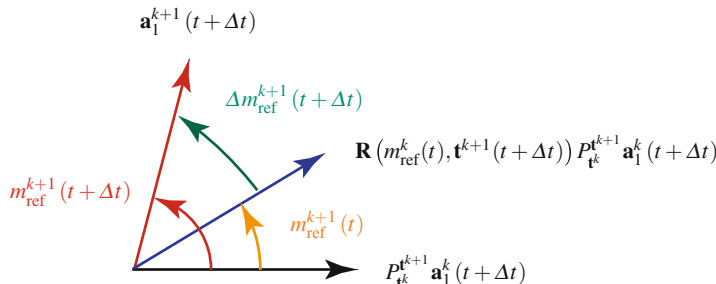


Fig. 5.4 Schematic of the angle $\Delta m_{\text{ref}}^{k+1}(t + \Delta t)$ between $\mathbf{a}_1^{k+1}(t + \Delta t)$ and $\mathbf{R}(m_{\text{ref}}^k(t), \mathbf{t}^{k+1}(t + \Delta t)) P_{t^k}^{t^{k+1}} \mathbf{a}_1^k(t + \Delta t)$

²In the code, $\Delta m_{\text{ref}}^{k+1}$ is known by the variable name SIGNANG.

5.7 Representations for the Operator $\bar{M}^k(t, \Delta t)$ and the Vector $\bar{\omega}^k(t)$

The operator $\bar{M}^k(t, \Delta t)$ was defined previously as an operator that transformed the material frame on the k th edge from a time t to a later instant $t + \Delta t$ [cf. Eq. (5.3)]. Recalling the representation (4.21) from Page 39,

$$\bar{P}^k(t, \Delta t) = \mathbf{a}_1^k(t + \Delta t) \otimes \mathbf{a}_1^k(t) + \mathbf{a}_2^k(t + \Delta t) \otimes \mathbf{a}_2^k(t) + \mathbf{t}^k(t + \Delta t) \otimes \mathbf{t}^k(t), \quad (5.21)$$

and then paralleling the developments for $M_{t^{k-1}}^{\mathbf{t}^k}$ in Sect. 5.5, it is straightforward to show that the operator $\bar{M}^k(t, \Delta t)$ has the following representations:

$$\begin{aligned} \bar{M}^k(t, \Delta t) &= \mathbf{m}_1^k(t + \Delta t) \otimes \mathbf{m}_1^k(t) + \mathbf{m}_2^k(t + \Delta t) \otimes \mathbf{m}_2^k(t) + \mathbf{t}^k(t + \Delta t) \otimes \mathbf{t}^k(t) \\ &= \bar{P}^k(t, \Delta t) \mathbf{R}\left(\gamma^k(t + \Delta t) - \gamma^k(t), \mathbf{t}^k(t)\right) \\ &= \mathbf{R}\left(\gamma^k(t + \Delta t) - \gamma^k(t), \mathbf{t}^k(t + \Delta t)\right) \bar{P}^k(t, \Delta t). \end{aligned} \quad (5.22)$$

The angle γ^k in these representations is the angle between \mathbf{a}_1^k and \mathbf{m}_1^k at an instant in time (cf. Fig. 5.3).

An angular velocity vector $\bar{\omega}^k(t)$ associated with $\bar{M}^k(t, \Delta t)$ will be of use later in computing expressions for the variations of the material vectors, mechanical power of moments, and the kinetic energy of the discrete elastic rod. To compute $\bar{\omega}^k(t)$, we define

$$\dot{\bar{M}}^k(t) = \lim_{\Delta t \rightarrow 0} \frac{\bar{M}^k(t, \Delta t) - \bar{M}^k(t, 0)}{\Delta t}. \quad (5.23)$$

The angular velocity vector of interest is the following axial vector:

$$\bar{\omega}^k(t) = \text{ax} \left(\dot{\bar{M}}^k(t) \left(\bar{M}^k(t, 0) \right)^T \right). \quad (5.24)$$

It is straightforward to compute a representation for this angular velocity vector using Eqs. (4.14) and (5.22)₃³:

$$\bar{\omega}^k(t) = \dot{\gamma}^k(t) \mathbf{t}^k(t) + \mathbf{t}^k(t) \times \dot{\mathbf{t}}^k(t). \quad (5.25)$$

³The easiest method to compute this representation is to use the relative angular velocity vector proposed in Casey and Lam [7]. This relative angular velocity vector was discussed earlier in Sect. 2.3.

In this representation, $\dot{\gamma}^k(t) \mathbf{t}^k(t)$ can be interpreted as the angular velocity vector of $\mathbf{R}(\gamma^k(t), \mathbf{t}^k(t))$ relative to $\bar{P}^k(t)$ while $\mathbf{t}^k(t) \times \dot{\mathbf{t}}^k(t)$ is the angular velocity vector associated with $\bar{P}^k(t)$.

5.8 Velocity Vectors of the Material Vectors \mathbf{m}_1^k and \mathbf{m}_2^k

To compute expressions for $\dot{\mathbf{m}}_1^k$ and $\dot{\mathbf{m}}_2^k$, we recall that

$$\mathbf{m}_1^k(t + \Delta t) = \bar{M}^k(t, \Delta t) \mathbf{m}_1^k(t), \quad \mathbf{m}_2^k(t + \Delta t) = \bar{M}^k(t, \Delta t) \mathbf{m}_2^k(t), \quad (5.26)$$

and

$$\bar{\omega}^k(t) = \text{ax} \left(\dot{\bar{M}}^k(t) \left(\bar{M}^k(t, 0) \right)^T \right) = \dot{\gamma}^k(t) \mathbf{t}^k(t) + \mathbf{t}^k(t) \times \dot{\mathbf{t}}^k(t). \quad (5.27)$$

Whence,

$$\begin{aligned} \dot{\mathbf{m}}_1^k(t) &= \bar{\omega}^k(t) \times \mathbf{m}_1^k(t) \\ &= \dot{\gamma}^k(t) \mathbf{m}_2^k(t) - \left(\mathbf{m}_1^k(t) \cdot \dot{\mathbf{t}}^k(t) \right) \mathbf{t}^k(t), \\ \dot{\mathbf{m}}_2^k(t) &= \bar{\omega}^k(t) \times \mathbf{m}_2^k(t) \\ &= -\dot{\gamma}^k(t) \mathbf{m}_1^k(t) - \left(\mathbf{m}_2^k(t) \cdot \dot{\mathbf{t}}^k(t) \right) \mathbf{t}^k(t). \end{aligned} \quad (5.28)$$

Observe that the velocity vectors $\dot{\mathbf{m}}_1^k$ and $\dot{\mathbf{m}}_2^k$ each have two components: one due to the twist $\dot{\gamma}^k$ and the other due to the motion of the edge vector \mathbf{e}^k (i.e., bending). As discussed earlier, the latter component is determined by the motion of the vertices [cf. Eqs. (4.15) and (4.16)].

5.9 Uncoiling of a Twisted Rod

To illustrate the evolution of the reference twist m_{ref}^k , we consider a uniform rod whose centerline is bent into a helical space curve and cantilevered at one of its ends to a fixed point O . The rod is then released from rest and falls under gravity as shown in the inset images in Fig. 5.5. This example was inspired by a study on the mechanics of the self-burial of the seeds of a small flowering plant known as a filaree published by Evangelista et al. [12].

The rod is assumed to have a length of 1 m, a circular cross-section of radius 1 mm, a Young's modulus of 1 MPa, a Poisson's ratio of 0.5, and a mass density of 1000 kg/m³. Initially, the rod is coiled into a right-handed circular helix of radius

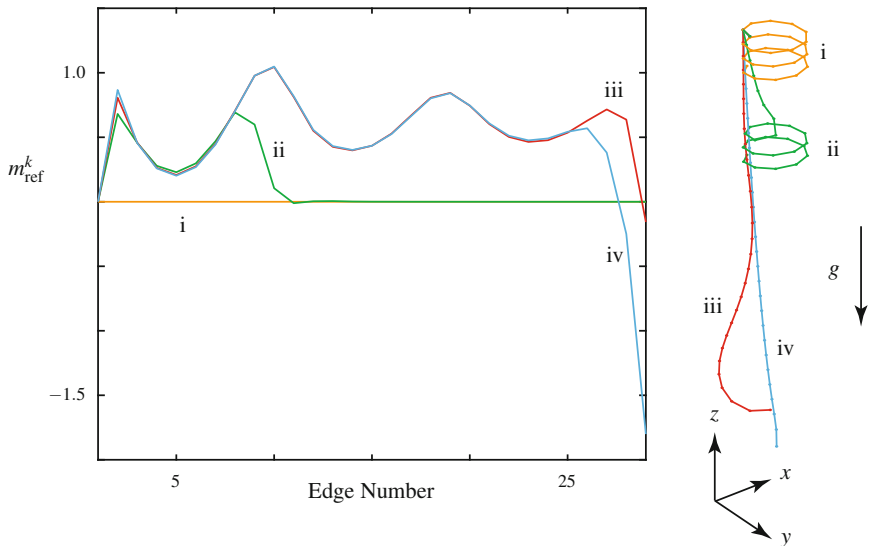
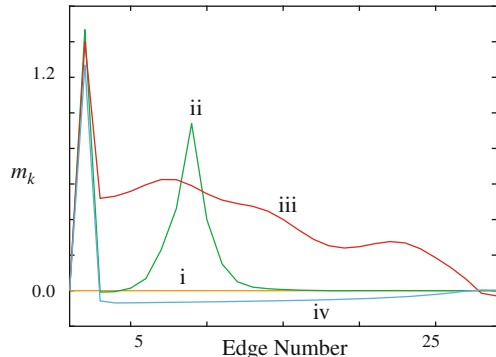


Fig. 5.5 Evolution of the reference twist m_{ref}^k in a coiled rod which is released from rest at time $t = 0$ and unwinds due to a gravitational force: i, $t = 0$; ii, $t = 0.2$ s; iii, $t = 0.5$ s; and iv, $t = 10$ s

Fig. 5.6 Evolution of the twist $m_k = \gamma^k - \gamma^{k-1} + m_{\text{ref}}^k$ in a coiled rod which is released from rest at time $t = 0$ and unwinds due to a gravitational force: i, $t = 0$; ii, $t = 0.2$ s; iii, $t = 0.5$ s; and iv, $t = 10$ s



$R = 5$ cm and $\alpha = 0.1$ [cf. Eq. (2.29)]. For the discrete elastic formulation, the rod is modeled as a discrete curve with 30 vertices. To account for the cantilevered boundary conditions, the first two vertices of the rod are fixed: i.e., \mathbf{x}_0 and \mathbf{x}_1 are constant.

Referring to Figs. 5.5 and 5.6, as the rod unwinds, the discrete integrated twist m_k changes as does the reference twist m_{ref}^k in each of the edges. After the transients have died down, the centerline of the rod will be vertical and the rod will be stationary and in a state of tension. As we shall see later in Chap. 7, the formula used to compute the reference twist can also be established using a concept known as holonomy.

Chapter 6

Variations, Gradients, and Hessians



6.1 Introduction

Expressions for changes to several kinematical quantities, including the discrete integrated curvature vector $\kappa_k \mathbf{b}_k$ and the material frame vectors \mathbf{m}_1^k and \mathbf{m}_2^k , as the vertices are varied will be needed both to compute elastic forces in the discrete rod and to compute Hessians for Newton's method. The changes to the position vectors of the vertices are described by the variations $\delta \mathbf{x}_i$:

$$\mathbf{x}_0 \rightarrow \mathbf{x}_0 + \delta \mathbf{x}_0, \quad \dots, \quad \mathbf{x}_k \rightarrow \mathbf{x}_k + \delta \mathbf{x}_k, \quad \dots, \quad \mathbf{x}_{n-1} \rightarrow \mathbf{x}_{n-1} + \delta \mathbf{x}_{n-1}. \quad (6.1)$$

Among others, the variations in the vertices induce changes to tangent vectors, edge vectors, turning angles, curvatures, and referential twist m_{ref}^k . For instance, the variations (6.1) result in

$$\mathbf{e}^{k-1} \rightarrow \mathbf{e}^{k-1} + \delta \mathbf{e}^{k-1}, \quad \mathbf{e}^k \rightarrow \mathbf{e}^k + \delta \mathbf{e}^k, \quad (6.2)$$

and

$$\mathbf{t}^{k-1} \rightarrow \mathbf{t}^{k-1} + \delta \mathbf{t}^{k-1}, \quad \mathbf{t}^k \rightarrow \mathbf{t}^k + \delta \mathbf{t}^k. \quad (6.3)$$

After computing expressions for the variations induced by Eq. (6.1), we will establish representations for the gradients and Hessians of various kinematical quantities including m_{ref}^k . Our exposition in this chapter provides detailed commentary on several results that are summarized in the papers by Bergou et al. [3, 4] and Kaldor et al. [29].

6.2 Notation for Gradients and Hessians

Given a scalar-valued function A and vectors $\mathbf{w} = \sum_{r=1}^3 w_r \mathbf{E}_r$ and $\mathbf{z} = \sum_{s=1}^3 z_s \mathbf{E}_s$, we use the following representations for the gradient of the scalar-valued function $A(\mathbf{w}, \mathbf{z})$ with respect to \mathbf{w} and the second partial derivative of the scalar-valued function $A(\mathbf{w}, \mathbf{z})$ with respect to a pair of vectors:

$$\frac{\partial A}{\partial \mathbf{w}} = \sum_{r=1}^3 \frac{\partial A}{\partial w_r} \mathbf{E}_r, \quad \frac{\partial^2 A}{\partial \mathbf{w} \partial \mathbf{z}} = \sum_{r=1}^3 \sum_{s=1}^3 \frac{\partial^2 A}{\partial w_s \partial z_r} \mathbf{E}_r \otimes \mathbf{E}_s. \quad (6.4)$$

The Hessian of A is the following 6×6 matrix:

$$\mathcal{H} = \begin{bmatrix} \left(\frac{\partial^2 A}{\partial \mathbf{w} \partial \mathbf{w}} \mathbf{E}_r \right) \cdot \mathbf{E}_s & \left(\frac{\partial^2 A}{\partial \mathbf{z} \partial \mathbf{w}} \mathbf{E}_r \right) \cdot \mathbf{E}_s \\ \left(\frac{\partial^2 A}{\partial \mathbf{w} \partial \mathbf{z}} \mathbf{E}_r \right) \cdot \mathbf{E}_s & \left(\frac{\partial^2 A}{\partial \mathbf{z} \partial \mathbf{z}} \mathbf{E}_r \right) \cdot \mathbf{E}_s \end{bmatrix}. \quad (6.5)$$

In this expression, the indices r and s range from 1 to 3. When computing Hessians, we invoke the facts that $\frac{\partial^2 A}{\partial \mathbf{w} \partial \mathbf{w}}$ and $\frac{\partial^2 A}{\partial \mathbf{z} \partial \mathbf{z}}$ are symmetric while

$$\frac{\partial^2 A}{\partial \mathbf{w} \partial \mathbf{z}} = \left(\frac{\partial^2 A}{\partial \mathbf{z} \partial \mathbf{w}} \right)^T. \quad (6.6)$$

In the interests of brevity, we only record non-zero components of a Hessian.

Consider a vector-valued function $\mathbf{A} = \mathbf{A}(\mathbf{w}) = \sum_{r=1}^3 A_r \mathbf{E}_r$ where the vector $\mathbf{w} = \sum_{s=1}^3 w_s \mathbf{E}_s$. The gradient of the vector-valued function $\mathbf{A}(\mathbf{w})$ with respect to \mathbf{w} is a second-order tensor with the representation

$$\nabla_{\mathbf{w}} \mathbf{A} = \frac{\partial \mathbf{A}}{\partial \mathbf{w}} = \sum_{r=1}^3 \sum_{s=1}^3 \frac{\partial A_r}{\partial w_s} \mathbf{E}_r \otimes \mathbf{E}_s. \quad (6.7)$$

In addition, the following relation exists between the variation of \mathbf{A} and the variation of \mathbf{w} : $\delta \mathbf{A} = \nabla_{\mathbf{w}} \mathbf{A} \delta \mathbf{w}$.

6.3 Variations of the Tangent Vectors

For the variation of the tangent vectors, we find, with the help of Taylor series expansions of $\|\mathbf{e}^{k-1} + \delta \mathbf{e}^{k-1}\|^{-1}$ and $\|\mathbf{e}^k + \delta \mathbf{e}^k\|^{-1}$ about $\delta \mathbf{e}^k = \mathbf{0}$ and $\delta \mathbf{e}^{k-1} = \mathbf{0}$, that

$$\begin{aligned}\delta \mathbf{t}^{k-1} &= \frac{\delta \mathbf{e}^{k-1}}{\|\mathbf{e}^{k-1}\|} - \left(\frac{\delta \mathbf{e}^{k-1} \cdot \mathbf{t}^{k-1}}{\|\mathbf{e}^{k-1}\|} \right) \mathbf{t}^{k-1} \\ &= (\mathbf{I} - \mathbf{t}^{k-1} \otimes \mathbf{t}^{k-1}) \frac{\delta \mathbf{e}^{k-1}}{\|\mathbf{e}^{k-1}\|}. \end{aligned} \quad (6.8)$$

The corresponding representations for $\delta \mathbf{t}^k$, $\delta \mathbf{t}^{k+1}$, $\delta \Delta \mathbf{t}_k$, and $\delta \mathbf{t}_{\gamma_k}$ are easily inferred. In the sequel, we will make extensive use of the fact that the variation of a unit vector is orthogonal to the vector. That is, if $\mathbf{t} \cdot \mathbf{t} = 1$, then $\delta \mathbf{t} \cdot \mathbf{t} = 0$.

6.4 Variation of the Turning Angle Between Two Edge Vectors

Consider the angle φ_k formed by two vectors \mathbf{e}^{k-1} and \mathbf{e}^k . For this angle, we have the relations

$$\cos(\varphi_k) = \frac{\mathbf{e}^{k-1} \cdot \mathbf{e}^k}{\|\mathbf{e}^{k-1}\| \|\mathbf{e}^k\|} = \mathbf{t}^{k-1} \cdot \mathbf{t}^k, \quad (6.9)$$

and

$$\begin{aligned}\sin(\varphi_k) &= \frac{\mathbf{e}^{k-1} \times \mathbf{e}^k}{\|\mathbf{e}^{k-1} \times \mathbf{e}^k\|} \cdot \left(\frac{\mathbf{e}^{k-1} \times \mathbf{e}^k}{\|\mathbf{e}^{k-1}\| \|\mathbf{e}^k\|} \right) \\ &= \frac{\|\mathbf{e}^{k-1} \times \mathbf{e}^k\|}{\|\mathbf{e}^{k-1}\| \|\mathbf{e}^k\|} \\ &= \|\mathbf{t}^{k-1} \times \mathbf{t}^k\|. \end{aligned} \quad (6.10)$$

We also note that

$$\|\mathbf{e}^{k-1} \times \mathbf{e}^k\|^2 = \|\mathbf{e}^{k-1}\|^2 \|\mathbf{e}^k\|^2 - (\mathbf{e}^{k-1} \cdot \mathbf{e}^k)^2. \quad (6.11)$$

Differentiating $\cos(\varphi_k)$ with respect to \mathbf{e}^{k-1} we find that

$$-\sin(\varphi_k) \frac{\partial \varphi_k}{\partial \mathbf{e}^{k-1}} = \frac{\mathbf{e}^k}{\|\mathbf{e}^{k-1}\| \|\mathbf{e}^k\|} - \frac{\mathbf{e}^{k-1}}{\|\mathbf{e}^{k-1}\|^2} \left(\frac{\mathbf{e}^{k-1} \cdot \mathbf{e}^k}{\|\mathbf{e}^{k-1}\| \|\mathbf{e}^k\|} \right). \quad (6.12)$$

Substituting the expression $\sin(\varphi_k) = \|\mathbf{t}^{k-1} \times \mathbf{t}^k\|$, we conclude that

$$\begin{aligned}\frac{\partial \varphi_k}{\partial \mathbf{e}^{k-1}} &= -\frac{\mathbf{e}^k}{\|\mathbf{e}^{k-1} \times \mathbf{e}^k\|} + \frac{\mathbf{e}^{k-1}}{\|\mathbf{e}^{k-1}\|^2} \left(\frac{\mathbf{e}^{k-1} \cdot \mathbf{e}^k}{\|\mathbf{e}^{k-1} \times \mathbf{e}^k\|} \right) \\ &= \frac{(\mathbf{e}^{k-1} \cdot \mathbf{e}^k) \mathbf{e}^{k-1} - \|\mathbf{e}^{k-1}\|^2 \mathbf{e}^k}{\|\mathbf{e}^{k-1}\|^2 \|\mathbf{e}^{k-1} \times \mathbf{e}^k\|} \\ &= \frac{\mathbf{e}^{k-1} \times (\mathbf{e}^{k-1} \times \mathbf{e}^k)}{\|\mathbf{e}^{k-1}\|^2 \|\mathbf{e}^{k-1} \times \mathbf{e}^k\|}.\end{aligned}\tag{6.13}$$

That is,

$$\frac{\partial \varphi_k}{\partial \mathbf{e}^{k-1}} = \frac{\mathbf{t}^{k-1}}{\|\mathbf{e}^{k-1}\|} \times \left(\frac{\mathbf{e}^{k-1} \times \mathbf{e}^k}{\|\mathbf{e}^{k-1} \times \mathbf{e}^k\|} \right).\tag{6.14}$$

Similarly,

$$\frac{\partial \varphi_k}{\partial \mathbf{e}^k} = -\frac{\mathbf{t}^k}{\|\mathbf{e}^k\|} \times \left(\frac{\mathbf{e}^{k-1} \times \mathbf{e}^k}{\|\mathbf{e}^{k-1} \times \mathbf{e}^k\|} \right).\tag{6.15}$$

As kindly communicated to us by Etienne Vouga [65], it is straightforward to use the results (6.14) and (6.15) to compute the derivatives $\frac{\partial \vartheta}{\partial \mathbf{a}^1}$ and $\frac{\partial \vartheta}{\partial \mathbf{a}^2}$ for the angle ϑ formed by two vectors \mathbf{a}^1 and \mathbf{a}^2 : $\|\mathbf{a}^1\| \|\mathbf{a}^2\| \cos(\vartheta) = \mathbf{a}^1 \cdot \mathbf{a}^2$.

Because the turning angle φ_k is defined by the edge vectors \mathbf{e}^{k-1} and \mathbf{e}^k , we can combine the representations (6.14) and (6.15) to conclude that

$$\begin{aligned}\delta \varphi_k &= \left(\frac{\mathbf{t}^{k-1}}{\|\mathbf{e}^{k-1}\|} \times \left(\frac{\mathbf{e}^{k-1} \times \mathbf{e}^k}{\|\mathbf{e}^{k-1} \times \mathbf{e}^k\|} \right) \right) \cdot \delta \mathbf{e}^{k-1} - \left(\frac{\mathbf{t}^k}{\|\mathbf{e}^k\|} \times \left(\frac{\mathbf{e}^{k-1} \times \mathbf{e}^k}{\|\mathbf{e}^{k-1} \times \mathbf{e}^k\|} \right) \right) \cdot \delta \mathbf{e}^k \\ &= \left(\frac{\mathbf{e}^{k-1} \times \mathbf{e}^k}{\|\mathbf{e}^{k-1} \times \mathbf{e}^k\|} \right) \cdot \left(\frac{\mathbf{t}^k}{\|\mathbf{e}^k\|} \times \delta \mathbf{e}^k - \frac{\mathbf{t}^{k-1}}{\|\mathbf{e}^{k-1}\|} \times \delta \mathbf{e}^{k-1} \right).\end{aligned}\tag{6.16}$$

This representation will be used in Chap. 7 to compute the variation of the interior angles of a spherical quadrilateral and a spherical triangle.

6.5 Variation of the Vector $(\kappa \mathbf{b})_k$

Using the representation (3.11) for $(\kappa \mathbf{b})_k$ that features the edge vectors and representations of the form (6.8) for the tangent vector, a representation for the variation of $(\kappa \mathbf{b})_k$ due to a variation of the edge vectors \mathbf{e}^{k-1} and \mathbf{e}^k can be found:

$$\begin{aligned} \delta(\kappa \mathbf{b})_k &= \frac{2\delta \mathbf{e}^{k-1} \times \mathbf{e}^k}{\|\mathbf{e}^{k-1}\| \|\mathbf{e}^k\| + \mathbf{e}^{k-1} \cdot \mathbf{e}^k} + \frac{2\mathbf{e}^{k-1} \times \delta \mathbf{e}^k}{\|\mathbf{e}^{k-1}\| \|\mathbf{e}^k\| + \mathbf{e}^{k-1} \cdot \mathbf{e}^k} \\ &\quad - \underbrace{\frac{(\mathbf{e}^k + \|\mathbf{e}^k\| \mathbf{t}^{k-1}) \cdot \delta \mathbf{e}^{k-1}}{(\|\mathbf{e}^{k-1}\| \|\mathbf{e}^k\| + \mathbf{e}^{k-1} \cdot \mathbf{e}^k)} (\kappa \mathbf{b})_k}_{-} - \underbrace{\frac{(\mathbf{e}^{k-1} + \|\mathbf{e}^{k-1}\| \mathbf{t}^k) \cdot \delta \mathbf{e}^k}{(\|\mathbf{e}^{k-1}\| \|\mathbf{e}^k\| + \mathbf{e}^{k-1} \cdot \mathbf{e}^k)} (\kappa \mathbf{b})_k}_{-}. \end{aligned} \quad (6.17)$$

Manipulating this expression further by dividing by the magnitude of the edge vectors results in the following expressions:

$$\begin{aligned} \frac{1}{2} \delta(\kappa \mathbf{b})_k &= \frac{\frac{\delta \mathbf{e}^{k-1}}{\|\mathbf{e}^{k-1}\|} \times \mathbf{t}^k}{1 + \mathbf{t}^{k-1} \cdot \mathbf{t}^k} + \frac{\mathbf{t}^{k-1} \times \frac{\delta \mathbf{e}^k}{\|\mathbf{e}^k\|}}{1 + \mathbf{t}^{k-1} \cdot \mathbf{t}^k} \\ &\quad - \left(\frac{(\kappa \mathbf{b})_k}{1 + \mathbf{t}^{k-1} \cdot \mathbf{t}^k} \right) \mathbf{t}_{\gamma_k} \cdot \left(\frac{\delta \mathbf{e}^{k-1}}{\|\mathbf{e}^{k-1}\|} + \frac{\delta \mathbf{e}^k}{\|\mathbf{e}^k\|} \right). \end{aligned} \quad (6.18)$$

Substituting for the variations of the vertices, we find that

$$\begin{aligned} \frac{1}{2} \delta(\kappa \mathbf{b})_k &= \frac{\frac{\delta \mathbf{x}_k - \delta \mathbf{x}_{k-1}}{\|\mathbf{e}^{k-1}\|} \times \mathbf{t}^k}{1 + \mathbf{t}^{k-1} \cdot \mathbf{t}^k} + \frac{\mathbf{t}^{k-1} \times \frac{\delta \mathbf{x}_{k+1} - \delta \mathbf{x}_k}{\|\mathbf{e}^k\|}}{1 + \mathbf{t}^{k-1} \cdot \mathbf{t}^k} \\ &\quad - \left(\frac{(\kappa \mathbf{b})_k}{1 + \mathbf{t}^{k-1} \cdot \mathbf{t}^k} \right) f \end{aligned} \quad (6.19)$$

where

$$f = \frac{(\mathbf{t}^k + \mathbf{t}^{k-1})}{2} \cdot \left(\frac{\delta \mathbf{x}_k - \delta \mathbf{x}_{k-1}}{\|\mathbf{e}^{k-1}\|} + \frac{\delta \mathbf{x}_{k+1} - \delta \mathbf{x}_k}{\|\mathbf{e}^k\|} \right). \quad (6.20)$$

With the help of Eq. (6.7), the representation (6.19) for the variation of the curvature vector can be used to determine the tensors

$$\begin{aligned} \mathbf{G}_{k-1} &= \nabla_{k-1} (\kappa \mathbf{b})_k = \frac{\partial (\kappa \mathbf{b})_k}{\partial \mathbf{x}_{k-1}}, \\ \mathbf{G}_k &= \nabla_k (\kappa \mathbf{b})_k = \frac{\partial (\kappa \mathbf{b})_k}{\partial \mathbf{x}_k}, \\ \mathbf{G}_{k+1} &= \nabla_{k+1} (\kappa \mathbf{b})_k = \frac{\partial (\kappa \mathbf{b})_k}{\partial \mathbf{x}_{k+1}}, \end{aligned} \quad (6.21)$$

which appear in Bergou et al. [4, Sect. 7]. For example,

$$\mathbf{G}_{k-1} = \frac{2\text{skewt}(\mathbf{e}^k)}{\|\mathbf{e}^{k-1}\| \|\mathbf{e}^k\| + \mathbf{e}^{k-1} \cdot \mathbf{e}^k} + \frac{(\kappa \mathbf{b})_k \otimes \left(\underbrace{\mathbf{e}^k + \|\mathbf{e}^k\| \mathbf{t}^{k-1}}_{\mathbf{t}_{\gamma_k}} \right)}{\|\mathbf{e}^{k-1}\| \|\mathbf{e}^k\| + \mathbf{e}^{k-1} \cdot \mathbf{e}^k}. \quad (6.22)$$

The underbraced term $(\mathbf{e}^k + \|\mathbf{e}^k\| \mathbf{t}^{k-1})$ in this expression differs from that presented in Bergou et al. [4, Sect. 7]. The difference can be traced to the underbraced terms in Eq. (6.17). Related remarks pertain to \mathbf{G}_k and \mathbf{G}_{k+1} . It is also easy to observe from Eq. (6.19) that

$$\nabla_k (\kappa \mathbf{b})_k = -\nabla_{k+1} (\kappa \mathbf{b})_k - \nabla_{k-1} (\kappa \mathbf{b})_k. \quad (6.23)$$

That is, $\mathbf{G}_{k-1} + \mathbf{G}_k + \mathbf{G}_{k+1} = \mathbf{0}$.

The derivatives of $(\kappa \mathbf{b})_k$ with respect to the edge vectors will be needed to compute gradients of force vector \mathbf{F}_{t_i} in Sect. 8.5. From (6.19), we find that

$$\frac{\partial (\kappa \mathbf{b})_k}{\partial \mathbf{e}^{k-1}} = -\mathbf{G}_{k-1}, \quad \frac{\partial (\kappa \mathbf{b})_k}{\partial \mathbf{e}^k} = \mathbf{G}_k. \quad (6.24)$$

From the definition of the vector $(\kappa \mathbf{b})_k$, it is straightforward to conclude the remaining gradients of this vector, such as

$$\frac{\partial (\kappa \mathbf{b})_k}{\partial \mathbf{e}^{k-3}}, \quad \frac{\partial (\kappa \mathbf{b})_k}{\partial \mathbf{e}^{k-2}}, \quad \frac{\partial (\kappa \mathbf{b})_k}{\partial \mathbf{e}^{k+1}}, \quad \frac{\partial (\kappa \mathbf{b})_k}{\partial \mathbf{e}^{k+2}}, \quad (6.25)$$

et cetera, are all identically $\mathbf{0}$.

6.6 Variation of the Material Vectors \mathbf{m}_1^k and \mathbf{m}_2^k

The variations of the vertices rigidly rotates the material vectors, the reference frame vectors, and the Bishop frame vectors. On each edge, the angles subtended by these vectors are unaltered. For instance, the angle ϑ^k between \mathbf{u}^k and \mathbf{m}_1^k and the angle γ^k between \mathbf{a}_1^k and \mathbf{m}_1^k are unchanged: $\delta\gamma^k = 0$ and $\delta\vartheta^k = 0$, among others.

To compute the variation of the material vectors due to variations of the edges, we recall Eq. (5.28):

$$\begin{aligned} \dot{\mathbf{m}}_1^k(t) &= \bar{\omega}^k(t) \times \mathbf{m}_1^k(t) \\ &= \dot{\gamma}^k(t) \mathbf{m}_2^k(t) - (\mathbf{m}_1^k(t) \cdot \dot{\mathbf{t}}^k(t)) \mathbf{t}^k(t), \\ \dot{\mathbf{m}}_2^k(t) &= \bar{\omega}^k(t) \times \mathbf{m}_2^k(t) \\ &= -\dot{\gamma}^k(t) \mathbf{m}_1^k(t) - (\mathbf{m}_2^k(t) \cdot \dot{\mathbf{t}}^k(t)) \mathbf{t}^k(t). \end{aligned} \quad (6.26)$$

Noting that the variations of the edges does not alter the angle γ^k , enables us to conclude that

$$\begin{aligned}
\delta \mathbf{m}_1^k &= - \left(\mathbf{m}_1^k \cdot \delta \mathbf{t}^k \right) \mathbf{t}^k \\
&= \left(-\mathbf{t}^k \otimes \mathbf{m}_1^k \right) \delta \mathbf{t}^k, \\
\delta \mathbf{m}_2^k &= - \left(\mathbf{m}_2^k \cdot \delta \mathbf{t}^k \right) \mathbf{t}^k \\
&= \left(-\mathbf{t}^k \otimes \mathbf{m}_2^k \right) \delta \mathbf{t}^k.
\end{aligned} \tag{6.27}$$

It is important to note that $\delta \mathbf{m}_1^k$ and $\delta \mathbf{m}_2^k$ both lie in the direction of the tangent \mathbf{t}^k and as a result are orthogonal to $(\kappa \mathbf{b})_{k-1}$, $(\kappa \mathbf{b})_k$, and $(\kappa \mathbf{b})_{k+1}$.

6.7 Variations and Gradients of the Curvatures κ_{k_1} and κ_{k_2}

The curvatures associated with the material frame at the k th vertex were defined in Eq. (5.6):

$$\begin{aligned}
\kappa_{k_1} &= \frac{1}{2} \left(\mathbf{m}_2^{k-1} + \mathbf{m}_2^k \right) \cdot (\kappa \mathbf{b})_k, \\
\kappa_{k_2} &= -\frac{1}{2} \left(\mathbf{m}_1^{k-1} + \mathbf{m}_1^k \right) \cdot (\kappa \mathbf{b})_k.
\end{aligned} \tag{6.28}$$

As mentioned previously, the curvatures κ_{k_1} and κ_{k_2} were introduced in Bergou et al. [3] and are known as vertex-based material curvatures. They are used as the bending strains of the discrete elastic rod.

The variations of the curvatures κ_{k_1} and κ_{k_2} due to the variation of the vertices are

$$\begin{aligned}
\delta \kappa_{k_1} &= \frac{1}{2} \left(\mathbf{m}_2^{k-1} + \mathbf{m}_2^k \right) \cdot \delta (\kappa \mathbf{b})_k + \frac{1}{2} \left(\delta \mathbf{m}_2^{k-1} + \delta \mathbf{m}_2^k \right) \cdot (\kappa \mathbf{b})_k, \\
\delta \kappa_{k_2} &= -\frac{1}{2} \left(\mathbf{m}_1^{k-1} + \mathbf{m}_1^k \right) \cdot \delta (\kappa \mathbf{b})_k - \frac{1}{2} \left(\delta \mathbf{m}_1^{k-1} + \delta \mathbf{m}_1^k \right) \cdot (\kappa \mathbf{b})_k.
\end{aligned} \tag{6.29}$$

From the representations (6.27), we observe that $\delta \mathbf{m}_1^k$ is parallel to \mathbf{t}^k and $\delta \mathbf{m}_1^{k-1}$ is parallel to \mathbf{t}^{k-1} . Consequently, both of these variations are orthogonal to \mathbf{b}_k . Identical remarks apply to $\delta \mathbf{m}_2^k$ and $\delta \mathbf{m}_2^{k-1}$. It follows that we can simplify the expressions for the variations to

$$\begin{aligned}
\delta \kappa_{k_1} &= \frac{1}{2} \left(\mathbf{m}_2^{k-1} + \mathbf{m}_2^k \right) \cdot \delta (\kappa \mathbf{b})_k, \\
\delta \kappa_{k_2} &= -\frac{1}{2} \left(\mathbf{m}_1^{k-1} + \mathbf{m}_1^k \right) \cdot \delta (\kappa \mathbf{b})_k.
\end{aligned} \tag{6.30}$$

These final expressions are identical to those in the literature (cf. Bergou et al. [3]).¹

To compute the gradient of a scalar v with respect to a vector \mathbf{u} , we make use of the identities

$$\dot{v} = \frac{\partial v}{\partial \mathbf{u}} \cdot \dot{\mathbf{u}}, \quad \delta v = \frac{\partial v}{\partial \mathbf{u}} \cdot \delta \mathbf{u}. \quad (6.31)$$

Thus, to compute $\frac{\partial \kappa_{k_1}}{\partial \mathbf{e}^{k-1}}$ and $\frac{\partial \kappa_{k_1}}{\partial \mathbf{e}^k}$, we appeal to the expression (6.29)₁ for $\delta \kappa_{k_1}$ and then invoke the representation (6.18) for $\delta(\kappa \mathbf{b})_k$ with $\delta \mathbf{e}^k$ and $\delta \mathbf{e}^{k-1}$ set to zero, respectively. The resulting intermediate expressions for $\frac{\partial \kappa_{k_1}}{\partial \mathbf{e}^{k-1}}$ and $\frac{\partial \kappa_{k_1}}{\partial \mathbf{e}^k}$ are exceptionally lengthy:

$$\begin{aligned} \frac{\partial \kappa_{k_1}}{\partial \mathbf{e}^{k-1}} \cdot \delta \mathbf{e}^{k-1} &= \frac{1}{2} \left(\mathbf{m}_2^{k-1} + \mathbf{m}_2^k \right) \cdot \left(\frac{2 \frac{\delta \mathbf{e}^{k-1}}{\|\mathbf{e}^{k-1}\|} \times \mathbf{t}^k}{1 + \mathbf{t}^{k-1} \cdot \mathbf{t}^k} \right. \\ &\quad \left. - \frac{(\kappa \mathbf{b})_k}{1 + \mathbf{t}^{k-1} \cdot \mathbf{t}^k} (\mathbf{t}^k + \mathbf{t}^{k-1}) \cdot \left(\frac{\delta \mathbf{e}^{k-1}}{\|\mathbf{e}^{k-1}\|} \right) \right) \\ &= - \left(\frac{1}{2} \left(\mathbf{m}_2^{k-1} + \mathbf{m}_2^k \right) \times \left(\frac{2 \mathbf{t}^k}{1 + \mathbf{t}^{k-1} \cdot \mathbf{t}^k} \right) + \kappa_{k_1} \tilde{\mathbf{t}} \right) \cdot \frac{\delta \mathbf{e}^{k-1}}{\|\mathbf{e}^{k-1}\|}, \end{aligned} \quad (6.32)$$

and

$$\begin{aligned} \frac{\partial \kappa_{k_1}}{\partial \mathbf{e}^k} \cdot \delta \mathbf{e}^k &= \frac{1}{2} \left(\mathbf{m}_2^{k-1} + \mathbf{m}_2^k \right) \cdot \left(\frac{2 \mathbf{t}^{k-1} \times \frac{\delta \mathbf{e}^k}{\|\mathbf{e}^k\|}}{1 + \mathbf{t}^{k-1} \cdot \mathbf{t}^k} \right. \\ &\quad \left. - \frac{(\kappa \mathbf{b})_k}{1 + \mathbf{t}^{k-1} \cdot \mathbf{t}^k} (\mathbf{t}^k + \mathbf{t}^{k-1}) \cdot \left(\frac{\delta \mathbf{e}^k}{\|\mathbf{e}^k\|} \right) \right) \\ &= \left(\frac{1}{2} \left(\mathbf{m}_2^{k-1} + \mathbf{m}_2^k \right) \times \left(\frac{2 \mathbf{t}^{k-1}}{1 + \mathbf{t}^{k-1} \cdot \mathbf{t}^k} \right) - \kappa_{k_1} \tilde{\mathbf{t}} \right) \cdot \frac{\delta \mathbf{e}^k}{\|\mathbf{e}^k\|}. \end{aligned} \quad (6.33)$$

To simplify these expressions we have used the definition (3.14) of the vector

¹It is tempting to assume (in error) that the material vectors are unaltered by the change in the vertices. However, as the variations in \mathbf{m}_1^{k-1} , \mathbf{m}_2^{k-1} , \mathbf{m}_1^k , and \mathbf{m}_2^k induced by variations in the vertices are orthogonal to $(\kappa \mathbf{b})_k$, the variations $\delta \mathbf{m}_1^{k-1}$, $\delta \mathbf{m}_2^{k-1}$, $\delta \mathbf{m}_1^k$, and $\delta \mathbf{m}_2^k$ are absent in the final expressions for $\delta \kappa_{k_1}$ and $\delta \kappa_{k_2}$.

$$\tilde{\mathbf{t}} = \frac{\mathbf{t}^{k-1} + \mathbf{t}^k}{1 + \mathbf{t}^{k-1} \cdot \mathbf{t}^k}. \quad (6.34)$$

In conclusion, we find the following representations for the gradients of κ_{k_1} :

$$\begin{aligned} \frac{\partial \kappa_{k_1}}{\partial \mathbf{e}^{k-1}} &= \frac{1}{\|\mathbf{e}^{k-1}\|} \left(-\kappa_{k_1} \tilde{\mathbf{t}} + \mathbf{t}^k \times \left(\frac{\mathbf{m}_2^{k-1} + \mathbf{m}_2^k}{1 + \mathbf{t}^{k-1} \cdot \mathbf{t}^k} \right) \right), \\ \frac{\partial \kappa_{k_1}}{\partial \mathbf{e}^k} &= \frac{1}{\|\mathbf{e}^k\|} \left(-\kappa_{k_1} \tilde{\mathbf{t}} - \mathbf{t}^{k-1} \times \left(\frac{\mathbf{m}_2^{k-1} + \mathbf{m}_2^k}{1 + \mathbf{t}^{k-1} \cdot \mathbf{t}^k} \right) \right). \end{aligned} \quad (6.35)$$

These results agree with the expressions presented in Bergou et al. [3, Appendix A]. The corresponding results for κ_{k_2} are

$$\begin{aligned} \frac{\partial \kappa_{k_2}}{\partial \mathbf{e}^{k-1}} &= \frac{1}{\|\mathbf{e}^{k-1}\|} \left(-\kappa_{k_2} \tilde{\mathbf{t}} - \mathbf{t}^k \times \left(\frac{\mathbf{m}_1^{k-1} + \mathbf{m}_1^k}{1 + \mathbf{t}^{k-1} \cdot \mathbf{t}^k} \right) \right), \\ \frac{\partial \kappa_{k_2}}{\partial \mathbf{e}^k} &= \frac{1}{\|\mathbf{e}^k\|} \left(-\kappa_{k_2} \tilde{\mathbf{t}} + \mathbf{t}^{k-1} \times \left(\frac{\mathbf{m}_1^{k-1} + \mathbf{m}_1^k}{1 + \mathbf{t}^{k-1} \cdot \mathbf{t}^k} \right) \right). \end{aligned} \quad (6.36)$$

We shall shortly use these expressions to compute Hessians.

6.8 Gradients and Time Derivative of the Reference Twist m_{ref}^k

As shall be discussed in Chap. 7 [cf. Eq. (7.48)], the variation of the reference twist is the component of the discrete curvature vector along the variation in the averaged tangent vector:

$$\frac{dm_{\text{ref}}^k}{d\epsilon} = (\kappa \mathbf{b})_k \cdot \frac{d\mathbf{t}_{\gamma_k}}{d\epsilon}, \quad (6.37)$$

where ϵ is a scalar used to parameterize the change in the vector \mathbf{t}_{γ_k} . It is interesting to note an immediate implication of this result: If the vertices are only displaced in the plane normal to \mathbf{b}_k , there will be no change to the reference twist.

Invoking expressions such as Eq. (6.8) to compute $\delta \mathbf{t}_{\gamma_k} = \frac{d\mathbf{t}_{\gamma_k}}{d\epsilon} \delta \epsilon$, we find that

$$\delta m_{\text{ref}}^k = \frac{\mathbf{t}^{k-1} \times \mathbf{t}^k}{1 + \mathbf{t}^{k-1} \cdot \mathbf{t}^k} \cdot \left(\frac{\delta \mathbf{e}^{k-1}}{\|\mathbf{e}^{k-1}\|} + \frac{\delta \mathbf{e}^k}{\|\mathbf{e}^k\|} \right), \quad (6.38)$$

where $\delta m_{\text{ref}}^k = \frac{dm_{\text{ref}}^k}{d\epsilon} \delta\epsilon$. Whence,

$$\begin{aligned}\frac{\partial m_{\text{ref}}^k}{\partial \mathbf{e}^{k-1}} &= \left(\frac{1}{2 \|\mathbf{e}^{k-1}\|} \right) (\kappa \mathbf{b})_k, \\ \frac{\partial m_{\text{ref}}^k}{\partial \mathbf{e}^k} &= \left(\frac{1}{2 \|\mathbf{e}^k\|} \right) (\kappa \mathbf{b})_k, \\ \frac{\partial m_{\text{ref}}^k}{\partial \mathbf{x}_{k-1}} &= - \left(\frac{1}{2 \|\mathbf{e}^{k-1}\|} \right) (\kappa \mathbf{b})_k, \\ \frac{\partial m_{\text{ref}}^k}{\partial \mathbf{x}_{k+1}} &= \left(\frac{1}{2 \|\mathbf{e}^k\|} \right) (\kappa \mathbf{b})_k, \\ \frac{\partial m_{\text{ref}}^k}{\partial \mathbf{x}_k} &= - \left(\frac{1}{2 \|\mathbf{e}^k\|} - \frac{1}{2 \|\mathbf{e}^{k-1}\|} \right) (\kappa \mathbf{b})_k.\end{aligned}\tag{6.39}$$

These representations for the gradients of m_{ref}^k agree with expressions for the variation of an angle m in Bergou et al. [3, Appendix A], and modulo a sign difference (which we believe to be a typographical error) for the variation of an angle ψ_k in Bergou et al. [4, Sect. 6, Eq. (9)] and a related expression in Kaldor et al. [29, Appendix A] for the derivatives of an angle $\hat{\theta}^k$. Referring to Eq. (5.19), the quantity m in [3] corresponds to $m_k = \gamma^k - \gamma^{k-1} + m_{\text{ref}}^k$. The angle $\hat{\theta}^k$ in Kaldor et al. [29, Appendix A] corresponds to the angle m_{ref}^k .

For future purposes, we will also need to compute \dot{m}_{ref}^k . Appealing to Eq. (6.38), after replacing the variation with the time derivative, we quickly find that

$$\dot{m}_{\text{ref}}^k = \frac{\mathbf{t}^{k-1} \times \mathbf{t}^k}{1 + \mathbf{t}^{k-1} \cdot \mathbf{t}^k} \cdot \left(\frac{\dot{\mathbf{e}}^{k-1}}{\|\mathbf{e}^{k-1}\|} + \frac{\dot{\mathbf{e}}^k}{\|\mathbf{e}^k\|} \right).\tag{6.40}$$

Substituting for the curvature vector and the time derivatives of the edge vectors, it can be shown that the time derivative has the following representation:

$$\begin{aligned}\dot{m}_{\text{ref}}^k &= - \frac{1}{2 \|\mathbf{e}^{k-1}\|} (\kappa \mathbf{b})_k \cdot \dot{\mathbf{x}}_{k-1} + \frac{1}{2 \|\mathbf{e}^k\|} (\kappa \mathbf{b})_k \cdot \dot{\mathbf{x}}_{k+1} \\ &\quad + \left(\frac{1}{2 \|\mathbf{e}^{k-1}\|} - \frac{1}{2 \|\mathbf{e}^k\|} \right) (\kappa \mathbf{b})_k \cdot \dot{\mathbf{x}}_k.\end{aligned}\tag{6.41}$$

This representation will be used in Sect. 8.4 when constitutive relations for forces and moments are established.

6.9 Preliminary Results for Computing Hessians

We now turn to computing the Hessians of the twist m_k and the curvatures κ_{k_1} and κ_{k_2} . The reader is referred to Sect. 6.2 for details on the notation used in defining these second order tensors. As a preliminary calculation, we note that

$$\begin{aligned} \frac{\partial}{\partial \mathbf{e}^i} \left(\frac{1}{\|\mathbf{e}^k\|} \right) &= -\frac{\mathbf{e}^i}{\|\mathbf{e}^i\|^3} \delta_i^k, \\ \frac{\partial}{\partial \mathbf{e}^i} \left(\mathbf{t}^k = \frac{\mathbf{e}^k}{\|\mathbf{e}^k\|} \right) &= \frac{1}{\|\mathbf{e}^k\|} \left(\mathbf{I} - \frac{\mathbf{e}^k}{\|\mathbf{e}^k\|} \otimes \frac{\mathbf{e}^k}{\|\mathbf{e}^k\|} \right) \delta_i^k, \\ \frac{\partial}{\partial \mathbf{e}^i} \left(\frac{\mathbf{e}^k}{\|\mathbf{e}^k\|} \times \mathbf{a} \right) &= -\frac{1}{\|\mathbf{e}^k\|} \left(\left(\frac{\mathbf{e}^k}{\|\mathbf{e}^k\|} \times \mathbf{a} \right) \otimes \frac{\mathbf{e}^k}{\|\mathbf{e}^k\|} + \text{skewt}(\mathbf{a}) \right) \delta_i^k \\ &= -\frac{1}{\|\mathbf{e}^k\|} \left((\mathbf{t}^k \times \mathbf{a}) \otimes \mathbf{t}^k + \text{skewt}(\mathbf{a}) \right) \delta_i^k, \\ \frac{\partial}{\partial \mathbf{e}^i} ((\kappa \mathbf{b})_k \times \mathbf{a}) &= \left(\frac{\partial (\kappa \mathbf{b})_k}{\partial \mathbf{e}^i} \right)^T \mathbf{a}. \end{aligned} \tag{6.42}$$

The vector \mathbf{a} in Eq. (6.42)_{3,4} is assumed to be constant, δ_i^k is the Kronecker delta, and the gradient of $(\kappa \mathbf{b})_k$ can be inferred from Eq. (6.18). The identities (6.42) are appealed to extensively in the sequel.

It is convenient to define a scalar χ :

$$\chi = 1 + \mathbf{t}^{k-1} \cdot \mathbf{t}^k. \tag{6.43}$$

Whence,

$$\begin{aligned} \frac{\partial \chi}{\partial \mathbf{e}^{k-1}} &= \frac{1}{\|\mathbf{e}^{k-1}\|} \left(\mathbf{I} - \mathbf{t}^{k-1} \otimes \mathbf{t}^{k-1} \right) \mathbf{t}^k, \\ \frac{\partial \chi}{\partial \mathbf{e}^k} &= \frac{1}{\|\mathbf{e}^k\|} \left(\mathbf{I} - \mathbf{t}^k \otimes \mathbf{t}^k \right) \mathbf{t}^{k-1}, \end{aligned} \tag{6.44}$$

and

$$\begin{aligned} \frac{\partial \tilde{\mathbf{t}}}{\partial \mathbf{e}^{k-1}} &= \frac{1}{\chi \|\mathbf{e}^{k-1}\|} \left(\left(\mathbf{I} - \mathbf{t}^{k-1} \otimes \mathbf{t}^{k-1} \right) - \tilde{\mathbf{t}} \otimes \left(\left(\mathbf{I} - \mathbf{t}^{k-1} \otimes \mathbf{t}^{k-1} \right) \mathbf{t}^k \right) \right), \\ \frac{\partial \tilde{\mathbf{t}}}{\partial \mathbf{e}^k} &= \frac{1}{\chi \|\mathbf{e}^k\|} \left(\left(\mathbf{I} - \mathbf{t}^k \otimes \mathbf{t}^k \right) - \tilde{\mathbf{t}} \otimes \left(\left(\mathbf{I} - \mathbf{t}^k \otimes \mathbf{t}^k \right) \mathbf{t}^{k-1} \right) \right), \end{aligned} \tag{6.45}$$

where it might be helpful for some readers to recall that $\chi \tilde{\mathbf{t}} = \mathbf{t}^{k-1} + \mathbf{t}^k$.

6.10 Hessians of the Reference Twist m_{ref}^k

The first Hessian we compute pertains to m_{ref}^k . To proceed, we recall from Eq. (6.39) that

$$\frac{\partial m_{\text{ref}}^k}{\partial \mathbf{e}^{k-1}} = \left(\frac{1}{2 \|\mathbf{e}^{k-1}\|} \right) (\kappa \mathbf{b})_k, \quad \frac{\partial m_{\text{ref}}^k}{\partial \mathbf{e}^k} = \left(\frac{1}{2 \|\mathbf{e}^k\|} \right) (\kappa \mathbf{b})_k. \quad (6.46)$$

Using Eq. (6.42)₁, we find that

$$\frac{\partial^2 m_{\text{ref}}^k}{\partial \mathbf{e}^k \partial \mathbf{e}^k} = -\text{sym} \left(\frac{1}{2 \|\mathbf{e}^k\|^3} (\kappa \mathbf{b})_k \otimes \mathbf{e}^k - \frac{1}{2 \|\mathbf{e}^k\|} \frac{\partial (\kappa \mathbf{b})_k}{\partial \mathbf{e}^k} \right). \quad (6.47)$$

Referring to Eq. (6.18), we previously computed the variation of $(\kappa \mathbf{b})_k$ and this expression can be used to infer a representation for $\frac{\partial (\kappa \mathbf{b})_k}{\partial \mathbf{e}^k}$:

$$\frac{\partial (\kappa \mathbf{b})_k}{\partial \mathbf{e}^k} = -\frac{2}{\|\mathbf{e}^k\|} \left(\frac{(\kappa \mathbf{b})_k}{1 + \mathbf{t}^{k-1} \cdot \mathbf{t}^k} \right) \otimes \mathbf{t}_{\gamma_k} + \frac{2 \text{skewt}(\mathbf{t}^{k-1})}{\|\mathbf{e}^k\| (1 + \mathbf{t}^k \cdot \mathbf{t}^{k-1})}. \quad (6.48)$$

Substituting this expression in Eq. (6.47) and noting that the symmetric part of a skew-symmetric tensor is $\mathbf{0}$, we conclude that a portion of the Hessian has the following representations:

$$\begin{aligned} \frac{\partial^2 m_{\text{ref}}^k}{\partial \mathbf{e}^k \partial \mathbf{e}^k} &= -\frac{1}{\|\mathbf{e}^k\|^2} \text{sym} \left(\frac{1}{2} (\kappa \mathbf{b})_k \otimes \mathbf{t}^k + \left(\frac{(\kappa \mathbf{b})_k}{1 + \mathbf{t}^{k-1} \cdot \mathbf{t}^k} \right) \otimes \mathbf{t}_{\gamma_k} \right) \\ &= -\frac{1}{2 \|\mathbf{e}^k\|^2} \text{sym} \left((\kappa \mathbf{b})_k \otimes \mathbf{t}^k + (\kappa \mathbf{b})_k \otimes \tilde{\mathbf{t}} \right). \end{aligned} \quad (6.49)$$

In writing the second representation, we used the definition (3.14) of the vector $\tilde{\mathbf{t}}$. A similar line of argument yields the representations

$$\begin{aligned} \frac{\partial^2 m_{\text{ref}}^k}{\partial \mathbf{e}^{k-1} \partial \mathbf{e}^{k-1}} &= -\frac{1}{\|\mathbf{e}^{k-1}\|^2} \text{sym} \left(\frac{1}{2} (\kappa \mathbf{b})_k \otimes \mathbf{t}^{k-1} + \left(\frac{(\kappa \mathbf{b})_k}{1 + \mathbf{t}^{k-1} \cdot \mathbf{t}^k} \right) \otimes \mathbf{t}_{\gamma_k} \right) \\ &= -\frac{1}{2 \|\mathbf{e}^{k-1}\|^2} \text{sym} \left((\kappa \mathbf{b})_k \otimes \mathbf{t}^{k-1} + (\kappa \mathbf{b})_k \otimes \tilde{\mathbf{t}} \right). \end{aligned} \quad (6.50)$$

The third part of the Hessian is the easiest to compute:

$$\begin{aligned}
 \left(\frac{\partial^2 m_{\text{ref}}^k}{\partial \mathbf{e}^{k-1} \partial \mathbf{e}^k} \right)^T &= \frac{\partial^2 m_{\text{ref}}^k}{\partial \mathbf{e}^k \partial \mathbf{e}^{k-1}} \\
 &= \frac{1}{2 \|\mathbf{e}^{k-1}\|} \frac{\partial (\kappa \mathbf{b})_k}{\partial \mathbf{e}^k} \\
 &= \frac{\text{skewt}(\mathbf{t}^{k-1})}{\|\mathbf{e}^{k-1}\| \|\mathbf{e}^k\| (1 + \mathbf{t}^k \cdot \mathbf{t}^{k-1})} - \frac{1}{\|\mathbf{e}^{k-1}\| \|\mathbf{e}^k\|} \left(\frac{(\kappa \mathbf{b})_k}{1 + \mathbf{t}^{k-1} \cdot \mathbf{t}^k} \right) \otimes \mathbf{t}_{\gamma_k}
 \end{aligned} \tag{6.51}$$

Observe that we appealed to Eq. (6.48) to establish the final form of the representation. For completeness, we note that the representations (6.49), (6.50), and (6.51) are identical to the expressions for the Hessian of m recorded in Bergou et al. [3, Appendix A].

6.11 Hessians of the Curvatures κ_{k_1} and κ_{k_2}

The computation of the Hessians for the curvatures κ_{k_1} and κ_{k_2} are considerably lengthier than the corresponding calculations for the twist. We restrict ourselves to a brief summary of the computations and invite the reader to compare our expressions [cf. Eqs. (6.55), (6.57), and (6.58)] to those recorded in Bergou et al. [3, Appendix A]. Unfortunately, only partial agreement will be found between the expressions in [3, Appendix A] and those recorded in the present paper.

Starting from Eq. (6.35)₁:

$$\begin{aligned}
 \frac{\partial \kappa_{k_1}}{\partial \mathbf{e}^{k-1}} &= \frac{1}{\|\mathbf{e}^{k-1}\|} \left(-\kappa_{k_1} \tilde{\mathbf{t}} + \frac{1}{\chi} \mathbf{t}^k \times (\mathbf{m}_2^{k-1} + \mathbf{m}_2^k) \right) \\
 &= \frac{1}{\|\mathbf{e}^{k-1}\|} \left(-\kappa_{k_1} \tilde{\mathbf{t}} + \mathbf{t}^k \times \tilde{\mathbf{m}}_2 \right),
 \end{aligned} \tag{6.52}$$

where

$$\tilde{\mathbf{m}}_2 = \frac{1}{\chi} \left(\mathbf{m}_2^{k-1} + \mathbf{m}_2^k \right). \tag{6.53}$$

Hence,

$$\begin{aligned}
\frac{\partial \kappa_{k_1}}{\partial \mathbf{e}^{k-1} \partial \mathbf{e}^{k-1}} &= -\frac{1}{\|\mathbf{e}^{k-1}\|} \text{sym} \left(\tilde{\mathbf{t}} \otimes \underbrace{\frac{\partial \kappa_{k_1}}{\partial \mathbf{e}^{k-1}}}_{(6.52)} + \underbrace{\frac{\partial \kappa_{k_1}}{\partial \mathbf{e}^{k-1}} \otimes \mathbf{t}^k}_{(6.52)} + \kappa_{k_1} \underbrace{\frac{\partial \tilde{\mathbf{t}}}{\partial \mathbf{e}^{k-1}}}_{(6.45)} \right) \\
&\quad - \frac{1}{\|\mathbf{e}^{k-1}\|} \text{sym} \left(\frac{1}{\chi^2} \left(\mathbf{t}^k \times (\mathbf{m}_2^{k-1} + \mathbf{m}_2^k) \right) \otimes \underbrace{\frac{\partial \chi}{\partial \mathbf{e}^{k-1}}}_{(6.44)} \right) \\
&\quad - \frac{1}{\|\mathbf{e}^{k-1}\|} \text{sym} \left(\frac{1}{\chi} \underbrace{\left(\frac{\partial \mathbf{t}^k}{\partial \mathbf{e}^{k-1}} \right)^T}_{=0} (\mathbf{m}_2^{k-1} + \mathbf{m}_2^k) \right). \tag{6.54}
\end{aligned}$$

The equations numbers below the underbrace indicate the substitutions that we can use to evaluate an expression. After combining terms in the above expression, we find that

$$\begin{aligned}
\frac{\partial \kappa_{k_1}}{\partial \mathbf{e}^{k-1} \partial \mathbf{e}^{k-1}} &= -\frac{1}{\|\mathbf{e}^{k-1}\|} \text{sym} \left((\tilde{\mathbf{t}} + \mathbf{t}^k) \otimes \underbrace{\frac{\partial \kappa_{k_1}}{\partial \mathbf{e}^{k-1}}}_{(6.52)} + \kappa_{k_1} \underbrace{\frac{\partial \tilde{\mathbf{t}}}{\partial \mathbf{e}^{k-1}}}_{(6.45)} \right) \\
&\quad - \frac{1}{\|\mathbf{e}^{k-1}\|} \text{sym} \left(\frac{1}{\chi} (\mathbf{t}^k \times \tilde{\mathbf{m}}_2) \otimes \underbrace{\frac{\partial \chi}{\partial \mathbf{e}^{k-1}}}_{(6.44)} \right). \tag{6.55}
\end{aligned}$$

To find the second set of terms for the Hessian, we start from Eq. (6.35)₂:

$$\frac{\partial \kappa_{k_1}}{\partial \mathbf{e}^k} = -\frac{1}{\|\mathbf{e}^k\|} (\kappa_{k_1} \tilde{\mathbf{t}} + \mathbf{t}^{k-1} \times \tilde{\mathbf{m}}_2). \tag{6.56}$$

Paralleling the previous set of calculations, we find the following representation:

$$\begin{aligned}
\frac{\partial \kappa_{k_1}}{\partial \mathbf{e}^k \partial \mathbf{e}^k} &= -\frac{1}{\|\mathbf{e}^k\|} \text{sym} \left((\tilde{\mathbf{t}} + \mathbf{t}^{k-1}) \otimes \underbrace{\frac{\partial \kappa_{k_1}}{\partial \mathbf{e}^k}}_{(6.56)} + \kappa_{k_1} \underbrace{\frac{\partial \tilde{\mathbf{t}}}{\partial \mathbf{e}^k}}_{(6.45)} \right) \\
&\quad - \frac{1}{\|\mathbf{e}^k\|} \text{sym} \left(\frac{1}{\chi} (\mathbf{t}^{k-1} \times \tilde{\mathbf{m}}_2) \otimes \underbrace{\frac{\partial \chi}{\partial \mathbf{e}^k}}_{(6.44)} \right). \tag{6.57}
\end{aligned}$$

To compute the final components of the Hessian, we again start from the expression (6.52) for $\frac{\partial \kappa_{k_1}}{\partial \mathbf{e}^{k-1}}$ and take the derivative of this expression with respect to \mathbf{e}^k . With some minor rearranging, we find that

$$\begin{aligned} \frac{\partial \kappa_{k_1}}{\partial \mathbf{e}^k \partial \mathbf{e}^{k-1}} &= -\frac{1}{\|\mathbf{e}^{k-1}\|} \left(\tilde{\mathbf{t}} \otimes \underbrace{\frac{\partial \kappa_{k_1}}{\partial \mathbf{e}^k}}_{(6.56)} + \kappa_{k_1} \underbrace{\frac{\partial \tilde{\mathbf{t}}}{\partial \mathbf{e}^k}}_{(6.45)} \right) \\ &\quad - \frac{1}{\|\mathbf{e}^{k-1}\|} \left(\frac{1}{\chi} \left(\mathbf{t}^k \times \tilde{\mathbf{m}}_2 \right) \otimes \underbrace{\frac{\partial \chi}{\partial \mathbf{e}^k}}_{(6.44)} + \underbrace{\left(\frac{\partial \mathbf{t}^k}{\partial \mathbf{e}^k} \right)^T}_{(6.42)} \tilde{\mathbf{m}}_2 \right). \end{aligned} \quad (6.58)$$

The corresponding expressions for the Hessian of κ_{k_2} are obtained from Eqs. (6.55), (6.57), and (6.58) by setting $\kappa_{k_1} \rightarrow \kappa_{k_2}$ and $\tilde{\mathbf{m}}_2 \rightarrow \tilde{\mathbf{m}}_1$.

6.12 Closing Remarks

This concludes our presentation of the gradients and Hessians of various kinematical quantities. The resulting representations for the Hessians of κ_{k_1} , κ_{k_2} , m_{ref}^k , and $\|\mathbf{e}^k\|$ will be used in Chap. 8 to compute expressions for internal forces and moments. In addition, the representation for the variation of the turning angle φ_k will play a key role in Chap. 7.

Chapter 7

Spherical Excess and Reference Twist



7.1 Introduction

The method by which a component of the rotation of the cross-section is computed in discrete elastic rods is exceptional and exploits a phenomenon in differential geometry known as a holonomy. In particular, a classic result from spherical geometry is used to show that the change in the reference twist can be related to a solid angle or, as it is also known in this context, spherical excess:

$$f^k(\epsilon) = \Delta m_{\text{ref}}^k(\epsilon) = m_{\text{ref}}^k(\epsilon) - m_{\text{ref}}^k(0). \quad (7.1)$$

In addition, the following expression for the variation of the reference twist is employed in [3, 29]:

$$\frac{dm_{\text{ref}}^k}{d\epsilon} = (\kappa \mathbf{b})_k \cdot \frac{d\mathbf{t}_{\gamma_k}}{d\epsilon}. \quad (7.2)$$

The purpose of the present chapter is to provide details on the calculations needed to establish these representations for $\Delta m_{\text{ref}}^k(\epsilon)$ and its derivative.

By way of background, the method used to establish the aforementioned representations has its genesis in the following remarkable result which can be found in Kelvin and Tait's Treatise on Natural Philosophy [30, 63, Sect. 123]. Imagine a line element in a rigid body which we define by a unit vector $\mathbf{e} = \mathbf{e}(t)$ that is fixed to the rigid body. Suppose after a time interval $t_1 - t_0$, $\mathbf{e}(t_1) = \mathbf{e}(t_0)$. Then, the rotation $\Delta\nu$ of the body about $\mathbf{e}(t_0)$ during the time interval can be determined modulo 2π by computing the solid angle A enclosed by the path traced out by $\mathbf{e}(t)$ on the unit

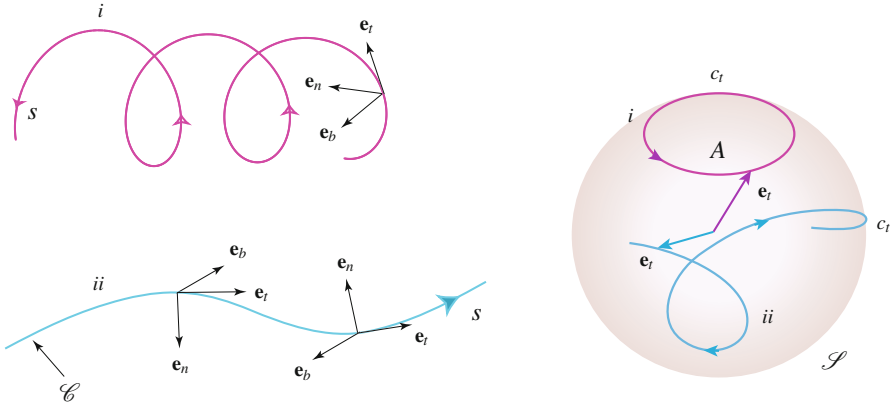


Fig. 7.1 A pair of space curves \mathcal{C} and their tangent indicatrices on the unit sphere \mathcal{S} . The solid angle A enclosed by the tangent indicatrix c_t (or tantrix) of the unit tangent vector \mathbf{e}_t on \mathcal{S} is intimately related to the rotation of the cross-section of a rod which has a centerline \mathcal{C} . The arrow indicates the direction of increasing arclength parameter s

sphere and the integral of a component of the angular velocity vector $\boldsymbol{\omega}$ of the rigid body:

$$\Delta\nu = \int_{t_0}^{t_1} \boldsymbol{\omega} \cdot \mathbf{e}(\tau) d\tau + A \quad \text{modulo } 2\pi. \quad (7.3)$$

The proof of this result employs the Gauss-Bonnet theorem to relate a line integral to A .¹ The solid angle (or spherical excess) A is known as a holonomy.

In the theory of rods, the unit vector of interest is the unit tangent vector \mathbf{e}_t and the curve it traces out on the unit sphere is known as the tangent indicatrix or tantrix c_t (cf. Fig. 7.1). Suppose after an interval $s_1 - s_0$ of the arclength parameter s , $\mathbf{e}_t(s_1) = \mathbf{e}_t(s_0)$, then Eq. (7.3) can be used to determine the relative rotation of the cross-section of the rod about \mathbf{e}_t in the interval $s_1 - s_0$. We also note that Fuller, in a celebrated paper [14], combines Eq. (7.3) with Călugăreanu's theorem relating the linking number L_k , twist T_w , and writhe W_r of a ribbon to show that the writhe of a closed non-self-intersecting curve satisfies the identity

$$2\pi + 2\pi W_r = A \quad \text{modulo } 2\pi. \quad (7.4)$$

For the ribbon used in Fuller's argument, $\Delta\nu = 0$ modulo 2π .

¹As discussed in [42, 44, 48, 68], Kelvin and Tait's result has been independently rediscovered several times since 1867. The most notable instance lies in a wonderful paper by Goodman and Robinson [15] where it is used to compute drift in navigation estimates.

In the discrete elastic rod formulation, the reference twist m_{ref}^k along the k th edge and its variation are determined by measuring the solid angle traced by the tangent vector \mathbf{t}^k on the unit sphere. The computations exploit results from spherical geometry and the calculations are related to Eqs. (7.3) and (7.4). Several readers may find it more helpful to simply start with the example discussed in Sect. 7.6 where the computation of a solid angle is used to determine the reference twist, before exploring the earlier sections of this chapter. We also take this opportunity to recommend the texts of Henderson [23] and Pressley [53] for additional background on the classic differential geometry used in this chapter.

7.2 Background from Spherical Geometry

Consider the closed path on the unit sphere shown in Fig. 7.2a. The quadrilateral is formed by four points on the unit sphere connected by arcs of great circles and is known as a spherical quadrilateral. From classic results in spherical trigonometry (cf. [62, 64]), it is known that the Gaussian curvature of the unit sphere $K = 1$ and that the solid angle (or spherical excess) E formed by the quadrilateral on the unit sphere is

$$E = \Theta_1 + \Theta_2 + \Theta_3 + \Theta_4 - 2\pi. \quad (7.5)$$

The angles $\Theta_1, \dots, \Theta_4$ are known as interior angles. Referring to Fig. 7.2b, it is convenient for future purposes to use the unit vectors $\mathbf{v}_1, \dots, \mathbf{v}_4$ to define the interior angles. To do so, we note that the geodesic connecting **1** to **2**, say, lies on a plane perpendicular to $\mathbf{v}_1 \times \mathbf{v}_2$. Whence, we can define unit vectors that are normal to the sides of the quadrilateral as follows:

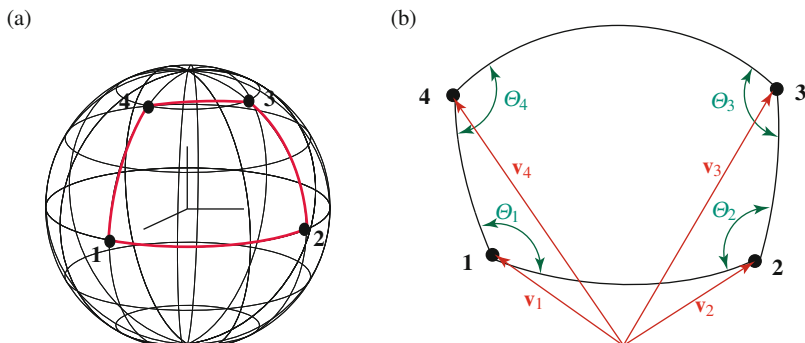
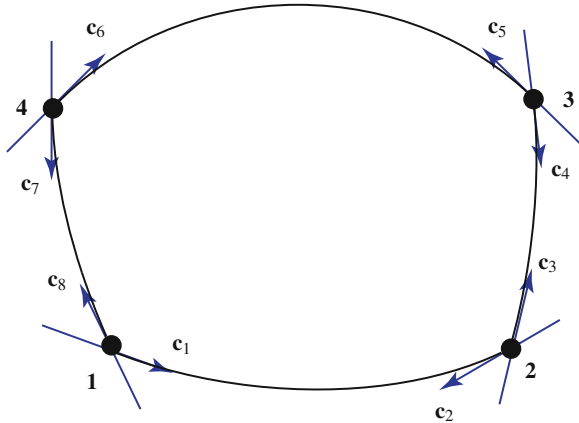


Fig. 7.2 (a) The four vertices of a spherical quadrilateral on a sphere of unit radius. The sides of the quadrilateral are great circles connecting the vertices. (b) Schematic of the unit vectors $\mathbf{v}_1, \dots, \mathbf{v}_4$ defining the respective vertices **1**, **2**, **3**, **4** and labelling of the interior angles $\Theta_1, \dots, \Theta_4$

Fig. 7.3 Schematic of the unit tangent vectors $\mathbf{c}_1, \dots, \mathbf{c}_8$ that are tangent to the arcs forming a spherical quadrilateral on the unit sphere



$$\begin{aligned}\mathbf{n}_1 &= \frac{\mathbf{v}_1 \times \mathbf{v}_2}{\|\mathbf{v}_1 \times \mathbf{v}_2\|}, & \mathbf{n}_2 &= -\frac{\mathbf{v}_1 \times \mathbf{v}_2}{\|\mathbf{v}_1 \times \mathbf{v}_2\|}, \\ \mathbf{n}_3 &= \frac{\mathbf{v}_2 \times \mathbf{v}_3}{\|\mathbf{v}_2 \times \mathbf{v}_3\|}, \quad \dots, & \mathbf{n}_8 &= -\frac{\mathbf{v}_4 \times \mathbf{v}_1}{\|\mathbf{v}_4 \times \mathbf{v}_1\|}.\end{aligned}\quad (7.6)$$

In addition, referring to Fig. 7.3, the unit tangent vectors to the sides of the spherical quadrilateral at the vertices are

$$\begin{aligned}\mathbf{c}_1 &= \frac{(\mathbf{v}_1 \times \mathbf{v}_2) \times \mathbf{v}_1}{\|(\mathbf{v}_1 \times \mathbf{v}_2) \times \mathbf{v}_1\|}, & \mathbf{c}_2 &= -\frac{(\mathbf{v}_1 \times \mathbf{v}_2) \times \mathbf{v}_2}{\|(\mathbf{v}_1 \times \mathbf{v}_2) \times \mathbf{v}_2\|}, \\ \mathbf{c}_3 &= \frac{(\mathbf{v}_2 \times \mathbf{v}_3) \times \mathbf{v}_2}{\|(\mathbf{v}_2 \times \mathbf{v}_3) \times \mathbf{v}_2\|}, \quad \dots, & \mathbf{c}_8 &= -\frac{(\mathbf{v}_4 \times \mathbf{v}_1) \times \mathbf{v}_1}{\|(\mathbf{v}_4 \times \mathbf{v}_1) \times \mathbf{v}_1\|}.\end{aligned}\quad (7.7)$$

The expressions for these unit tangent vectors can be simplified using identities of the form

$$(\mathbf{v}_1 \times \mathbf{v}_2) \times \mathbf{v}_1 = \mathbf{v}_2 - (\mathbf{v}_1 \cdot \mathbf{v}_2) \mathbf{v}_1. \quad (7.8)$$

The angle Θ_1 can be defined using \mathbf{c}_1 and \mathbf{c}_8 :

$$\cos(\Theta_1) = \mathbf{c}_1 \cdot \mathbf{c}_8. \quad (7.9)$$

However, because

$$((\mathbf{v}_1 \times \mathbf{v}_2) \times \mathbf{v}_1) \cdot ((\mathbf{v}_1 \times \mathbf{v}_4) \times \mathbf{v}_1) = (\mathbf{v}_1 \times \mathbf{v}_2) \cdot (\mathbf{v}_1 \times \mathbf{v}_4) \quad (7.10)$$

and

$$\|(\mathbf{v}_1 \times \mathbf{v}_2) \times \mathbf{v}_1\|^2 = 1 - (\mathbf{v}_1 \cdot \mathbf{v}_2)^2 = \|\mathbf{v}_1 \times \mathbf{v}_2\|^2, \quad (7.11)$$

we can also use the normal vectors \mathbf{n}_1 and \mathbf{n}_8 to define the angle Θ_1 :

$$\begin{aligned}\cos(\Theta_1) &= \mathbf{c}_1 \cdot \mathbf{c}_8 = \mathbf{n}_1 \cdot \mathbf{n}_8 \\ &= \left(\frac{\mathbf{v}_1 \times \mathbf{v}_2}{\|\mathbf{v}_1 \times \mathbf{v}_2\|} \right) \cdot \left(\frac{\mathbf{v}_1 \times \mathbf{v}_4}{\|\mathbf{v}_1 \times \mathbf{v}_4\|} \right).\end{aligned}\quad (7.12)$$

This observation greatly facilitates the forthcoming computations. For future reference, we note that it is straightforward to establish the following expressions:

$$\begin{aligned}\cos(\Theta_2) &= \left(\frac{\mathbf{v}_2 \times \mathbf{v}_1}{\|\mathbf{v}_2 \times \mathbf{v}_1\|} \right) \cdot \left(\frac{\mathbf{v}_2 \times \mathbf{v}_3}{\|\mathbf{v}_2 \times \mathbf{v}_3\|} \right), \\ \cos(\Theta_3) &= \left(\frac{\mathbf{v}_3 \times \mathbf{v}_2}{\|\mathbf{v}_3 \times \mathbf{v}_2\|} \right) \cdot \left(\frac{\mathbf{v}_3 \times \mathbf{v}_4}{\|\mathbf{v}_3 \times \mathbf{v}_4\|} \right), \\ \cos(\Theta_4) &= \left(\frac{\mathbf{v}_4 \times \mathbf{v}_3}{\|\mathbf{v}_4 \times \mathbf{v}_3\|} \right) \cdot \left(\frac{\mathbf{v}_4 \times \mathbf{v}_1}{\|\mathbf{v}_4 \times \mathbf{v}_1\|} \right).\end{aligned}\quad (7.13)$$

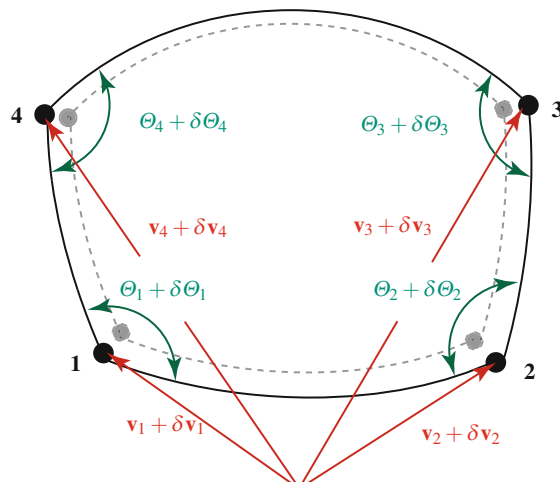
We take this opportunity to remark that expressions for interior angles in terms of normal vectors are also used to compute the writhing of DNA molecules which are modeled as polymer chains (see, e.g., [33]).

7.2.1 An Expression for the Variation in the Spherical Excess

As shown in Fig. 7.4, we now consider the case where each of the vertices are displaced by an incremental amount:

$$\mathbf{v}_1 \rightarrow \mathbf{v}_1 + \delta\mathbf{v}_1, \quad \mathbf{v}_2 \rightarrow \mathbf{v}_2 + \delta\mathbf{v}_2, \quad \mathbf{v}_3 \rightarrow \mathbf{v}_3 + \delta\mathbf{v}_3, \quad \mathbf{v}_4 \rightarrow \mathbf{v}_4 + \delta\mathbf{v}_4. \quad (7.14)$$

Fig. 7.4 The perturbed spherical quadrilateral formed by displacing the vertices



To compute the resulting change δE in E , we consider the respective changes $\delta\Theta_1, \dots, \delta\Theta_4$ in the interior angles. We start with the change in the angle Θ_1 as the changes in the other three angles can be established easily once an expression for $\delta\Theta_1$ has been found.

The interior angle Θ_1 is formed by the tangent vectors \mathbf{c}_1 and \mathbf{c}_8 and is equal to the angle formed by \mathbf{n}_1 and \mathbf{n}_8 . The latter pair of unit vectors are parallel to $\mathbf{v}_1 \times \mathbf{v}_2$ and $\mathbf{v}_1 \times \mathbf{v}_4$. Thus, an expression for the variation of Θ_1 can be computed starting from the expression (7.12) for $\cos(\Theta_1)$:

$$\delta\Theta_1 = \frac{\partial\Theta_1}{\partial(\mathbf{v}_1 \times \mathbf{v}_2)} \cdot \delta(\mathbf{v}_1 \times \mathbf{v}_2) + \frac{\partial\Theta_1}{\partial(\mathbf{v}_1 \times \mathbf{v}_4)} \cdot \delta(\mathbf{v}_1 \times \mathbf{v}_4). \quad (7.15)$$

With the help of Eqs. (6.14) and (6.15), we find that

$$\begin{aligned} \delta\Theta_1 = & - \left(\frac{(\mathbf{v}_1 \times \mathbf{v}_2) \times (\mathbf{v}_1 \times \mathbf{v}_4)}{\|(\mathbf{v}_1 \times \mathbf{v}_2) \times (\mathbf{v}_1 \times \mathbf{v}_4)\|} \right) \cdot \left(\left(\frac{\mathbf{v}_1 \times \mathbf{v}_2}{\|\mathbf{v}_1 \times \mathbf{v}_2\|^2} \right) \times (\delta\mathbf{v}_1 \times \mathbf{v}_2 + \mathbf{v}_1 \times \delta\mathbf{v}_2) \right) \\ & + \left(\frac{(\mathbf{v}_1 \times \mathbf{v}_2) \times (\mathbf{v}_1 \times \mathbf{v}_4)}{\|(\mathbf{v}_1 \times \mathbf{v}_2) \times (\mathbf{v}_1 \times \mathbf{v}_4)\|} \right) \cdot \left(\left(\frac{\mathbf{v}_1 \times \mathbf{v}_4}{\|\mathbf{v}_1 \times \mathbf{v}_4\|^2} \right) \times (\delta\mathbf{v}_1 \times \mathbf{v}_4 + \mathbf{v}_1 \times \delta\mathbf{v}_4) \right). \end{aligned} \quad (7.16)$$

Noting that \mathbf{v}_1 is a unit vector,

$$(\mathbf{v}_1 \times \mathbf{v}_2) \times (\mathbf{v}_1 \times \mathbf{v}_4) = ((\mathbf{v}_1 \times \mathbf{v}_2) \cdot \mathbf{v}_4) \mathbf{v}_1, \quad (7.17)$$

and that the triad $\{\mathbf{v}_1, \mathbf{v}_2, \mathbf{v}_4\}$ is right-handed, we can conclude that

$$\left(\frac{(\mathbf{v}_1 \times \mathbf{v}_2) \times (\mathbf{v}_1 \times \mathbf{v}_4)}{\|(\mathbf{v}_1 \times \mathbf{v}_2) \times (\mathbf{v}_1 \times \mathbf{v}_4)\|} \right) = \mathbf{v}_1. \quad (7.18)$$

This conclusion dramatically simplifies the expression for $\delta\Theta_1$:

$$\begin{aligned} \delta\Theta_1 = & -\mathbf{v}_1 \cdot \left(\left(\frac{\mathbf{v}_1 \times \mathbf{v}_2}{\|\mathbf{v}_1 \times \mathbf{v}_2\|^2} \right) \times (\delta\mathbf{v}_1 \times \mathbf{v}_2 + \mathbf{v}_1 \times \delta\mathbf{v}_2) \right) \\ & + \mathbf{v}_1 \cdot \left(\left(\frac{\mathbf{v}_1 \times \mathbf{v}_4}{\|\mathbf{v}_1 \times \mathbf{v}_4\|^2} \right) \times (\delta\mathbf{v}_1 \times \mathbf{v}_4 + \mathbf{v}_1 \times \delta\mathbf{v}_4) \right). \end{aligned} \quad (7.19)$$

Repeatedly invoking triple product identities and noting that $\delta\mathbf{v} \cdot \mathbf{v} = 0$ for any unit vector \mathbf{v} , we arrive at the expression

$$\begin{aligned} \delta\Theta_1 = & - \left(\frac{\mathbf{v}_1 \times \mathbf{v}_2}{\|\mathbf{v}_1 \times \mathbf{v}_2\|^2} \right) \cdot (\delta\mathbf{v}_2 - (\mathbf{v}_1 \cdot \mathbf{v}_2) \delta\mathbf{v}_1) \\ & + \left(\frac{\mathbf{v}_1 \times \mathbf{v}_4}{\|\mathbf{v}_1 \times \mathbf{v}_4\|^2} \right) \cdot (\delta\mathbf{v}_4 - (\mathbf{v}_1 \cdot \mathbf{v}_4) \delta\mathbf{v}_1). \end{aligned} \quad (7.20)$$

The corresponding expressions for the other three angles are

$$\begin{aligned}\delta\Theta_2 &= \left(\frac{\mathbf{v}_2 \times \mathbf{v}_3}{\|\mathbf{v}_2 \times \mathbf{v}_3\|^2} \right) \cdot ((\mathbf{v}_2 \cdot \mathbf{v}_3) \delta\mathbf{v}_2 - \delta\mathbf{v}_3) \\ &\quad - \left(\frac{\mathbf{v}_2 \times \mathbf{v}_1}{\|\mathbf{v}_2 \times \mathbf{v}_1\|^2} \right) \cdot ((\mathbf{v}_2 \cdot \mathbf{v}_1) \delta\mathbf{v}_2 - \delta\mathbf{v}_1), \\ \delta\Theta_3 &= \left(\frac{\mathbf{v}_3 \times \mathbf{v}_4}{\|\mathbf{v}_3 \times \mathbf{v}_4\|^2} \right) \cdot ((\mathbf{v}_3 \cdot \mathbf{v}_4) \delta\mathbf{v}_3 - \delta\mathbf{v}_4) \\ &\quad - \left(\frac{\mathbf{v}_3 \times \mathbf{v}_2}{\|\mathbf{v}_3 \times \mathbf{v}_2\|^2} \right) \cdot ((\mathbf{v}_3 \cdot \mathbf{v}_2) \delta\mathbf{v}_3 - \delta\mathbf{v}_2), \\ \delta\Theta_4 &= \left(\frac{\mathbf{v}_4 \times \mathbf{v}_1}{\|\mathbf{v}_4 \times \mathbf{v}_1\|^2} \right) \cdot ((\mathbf{v}_4 \cdot \mathbf{v}_1) \delta\mathbf{v}_4 - \delta\mathbf{v}_1) \\ &\quad - \left(\frac{\mathbf{v}_4 \times \mathbf{v}_3}{\|\mathbf{v}_4 \times \mathbf{v}_3\|^2} \right) \cdot ((\mathbf{v}_4 \cdot \mathbf{v}_3) \delta\mathbf{v}_4 - \delta\mathbf{v}_3).\end{aligned}\tag{7.21}$$

Adding these expressions together and using identities such as $\|\mathbf{v}_3 \times \mathbf{v}_4\|^2 = 1 - (\mathbf{v}_3 \cdot \mathbf{v}_4)^2$, we find that

$$\begin{aligned}\delta E &= \delta\Theta_1 + \delta\Theta_2 + \delta\Theta_3 + \delta\Theta_4 \\ &= - \left(\frac{\mathbf{v}_1 \times \mathbf{v}_2}{1 + (\mathbf{v}_1 \cdot \mathbf{v}_2)} \right) \cdot (\delta\mathbf{v}_1 + \delta\mathbf{v}_2) - \left(\frac{\mathbf{v}_2 \times \mathbf{v}_3}{1 + (\mathbf{v}_2 \cdot \mathbf{v}_3)} \right) \cdot (\delta\mathbf{v}_2 + \delta\mathbf{v}_3) \\ &\quad - \left(\frac{\mathbf{v}_3 \times \mathbf{v}_4}{1 + (\mathbf{v}_3 \cdot \mathbf{v}_4)} \right) \cdot (\delta\mathbf{v}_3 + \delta\mathbf{v}_4) - \left(\frac{\mathbf{v}_4 \times \mathbf{v}_1}{1 + (\mathbf{v}_4 \cdot \mathbf{v}_1)} \right) \cdot (\delta\mathbf{v}_4 + \delta\mathbf{v}_1).\end{aligned}\tag{7.22}$$

This expression for the variation of the spherical excess is the basis for the central result of this chapter [cf. Eq. (7.48)].

7.3 Spherical Excess and an Angle of Rotation for a Compound Rotation

7.3.1 A Composition of Parallel Transports

To examine one aspect of how the twist is computed in discrete elastic rods, we consider a set of configurations of the discrete elastic rod that are parameterized by a single parameter ϵ :

$$\mathbf{x}_0(\epsilon), \dots, \mathbf{x}_{n-1}(\epsilon),\tag{7.23}$$

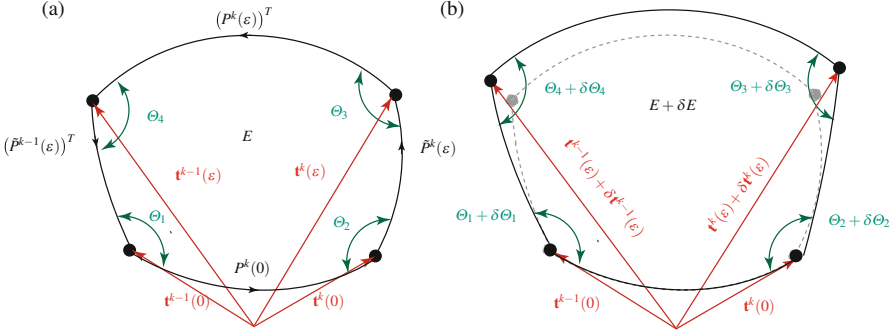


Fig. 7.5 (a) The four vertices of a quadrilateral on a sphere of unit radius. The vertices are defined by the unit vectors $\mathbf{t}^{k-1}(0)$, $\mathbf{t}^k(0)$, $\mathbf{t}^{k-1}(\epsilon)$, and $\mathbf{t}^k(\epsilon)$ and the sides of the quadrilateral are great circles connecting the vertices. (b) The perturbed quadrilateral which is obtained by displacing the vertices: $\mathbf{x}_{k-1}(\epsilon) \rightarrow \mathbf{x}_{k-1}(\epsilon) + \delta \mathbf{x}_{k-1}(\epsilon)$, $\mathbf{x}_k(\epsilon) \rightarrow \mathbf{x}_k(\epsilon) + \delta \mathbf{x}_k(\epsilon)$, and $\mathbf{x}_{k+1}(\epsilon) \rightarrow \mathbf{x}_{k+1}(\epsilon) + \delta \mathbf{x}_{k+1}(\epsilon)$

with concomitant expressions for the tangent vectors and edge vectors. The parameter ϵ will be used to track a variation of the discrete curve. Next, we consider a pair of connected edges, $\mathbf{e}^{k-1}(0) = \mathbf{e}^{k-1}(\epsilon = 0)$ and $\mathbf{e}^k(0) = \mathbf{e}^k(\epsilon = 0)$, and imagine their associated tangent vectors mapped to the unit sphere (cf. Fig. 7.5a). We recall from Chap. 4 that the pair of tangent vectors are related by the rotation $P_{\mathbf{t}^{k-1}(\epsilon=0)}^{\mathbf{t}^k(\epsilon=0)}$:

$$P^k(0) \equiv P_{\mathbf{t}^{k-1}(0)}^{\mathbf{t}^k(0)} = \mathbf{R}(\varphi_k(0), \mathbf{b}_k(0)), \quad (7.24)$$

where the discretized binormal vector at $\mathbf{x}_k(0)$ and the turning angle are defined by

$$\mathbf{b}_k(0) = \frac{\mathbf{t}^{k-1}(0) \times \mathbf{t}^k(0)}{\|\mathbf{t}^{k-1}(0) \times \mathbf{t}^k(0)\|}, \quad \cos(\varphi_k(0)) = \mathbf{t}^k(0) \cdot \mathbf{t}^{k-1}(0). \quad (7.25)$$

The axis of rotation is orthogonal to $\mathbf{t}^{k-1}(0) = \mathbf{t}^{k-1}(\epsilon = 0)$ and $\mathbf{t}^k(0) = \mathbf{t}^k(\epsilon = 0)$ and thus the path connecting the trace of $\mathbf{t}^{k-1}(0)$ to $\mathbf{t}^k(0)$ can be considered an arc of a great circle (i.e., a geodesic on the sphere).

If we now imagine the same edges as displaced, then it is easy to see that the ends of the tangent vectors $\mathbf{t}^{k-1}(\epsilon)$ and $\mathbf{t}^k(\epsilon)$ will occupy new points on the unit sphere, where ϵ is non-zero. We recall that the tangent vectors $\mathbf{t}^{k-1}(\epsilon)$ and $\mathbf{t}^k(\epsilon)$ are related by a rotation:

$$P^k(\epsilon) \equiv P_{\mathbf{t}^{k-1}(\epsilon)}^{\mathbf{t}^k(\epsilon)} = \mathbf{R}(\varphi_k(\epsilon), \mathbf{b}_k(\epsilon)), \quad (7.26)$$

where the discretized binormal vector at $\mathbf{x}_k(\epsilon)$ and the turning angle are defined by

$$\mathbf{b}_k(\epsilon) = \frac{\mathbf{t}^{k-1}(\epsilon) \times \mathbf{t}^k(\epsilon)}{\|\mathbf{t}^{k-1}(\epsilon) \times \mathbf{t}^k(\epsilon)\|}, \quad \cos(\varphi_k(\epsilon)) = \mathbf{t}^k(\epsilon) \cdot \mathbf{t}^{k-1}(\epsilon). \quad (7.27)$$

Again, the path joining $\mathbf{t}^{k-1}(\epsilon)$ and $\mathbf{t}^k(\epsilon)$ on the unit sphere is a great circle.

We recall from Chap. 4 that the rotations $P^k(0)$ and $P^k(\epsilon)$ were associated with space-parallel transport and were used to define the Bishop triads on edges. The next pair of rotations we employ are examples of the time-parallel transport operators that were used to define the reference frames in Chap. 4. The first of these rotations, which we denote by $\tilde{P}^{k-1}(\epsilon)$ transforms $\mathbf{t}^{k-1}(0)$ to $\mathbf{t}^{k-1}(\epsilon)$ and the second rotation, which we denote by $\tilde{P}^k(\epsilon)$ transforms $\mathbf{t}^k(0)$ to $\mathbf{t}^k(\epsilon)$ (cf. Fig. 4.2 on Page 36). The latter rotation is defined by

$$\tilde{P}^k(\epsilon) \equiv P_{\mathbf{t}^k(0)}^{\mathbf{t}^k(\epsilon)} = \mathbf{R}(\alpha^k(\epsilon), \mathbf{h}^k(\epsilon)), \quad (7.28)$$

where the axis and angle of rotation are

$$\mathbf{h}^k(\epsilon) = \frac{\mathbf{t}^k(0) \times \mathbf{t}^k(\epsilon)}{\|\mathbf{t}^k(\epsilon) \times \mathbf{t}^k(0)\|}, \quad \cos(\alpha^k(\epsilon)) = \mathbf{t}^k(0) \cdot \mathbf{t}^k(\epsilon). \quad (7.29)$$

The corresponding representation for $\tilde{P}^{k-1}(\epsilon)$ is readily inferred from Eq. (7.28). Again, the presumed paths connecting the respective tangent vectors on the sphere are great circles (cf. Fig. 7.5a).

Now consider the product

$$\hat{P}^k(\epsilon) = (\tilde{P}^{k-1}(\epsilon))^T (P^k(\epsilon))^T \tilde{P}^k(\epsilon) P^k(0). \quad (7.30)$$

To understand this product, note that

$$\begin{aligned} \mathbf{t}^k(0) &= P^k(0) \mathbf{t}^{k-1}(0), & \mathbf{t}^k(\epsilon) &= \tilde{P}^k(\epsilon) \mathbf{t}^k(0), \\ \mathbf{t}^{k-1}(\epsilon) &= (P^k(\epsilon))^T \mathbf{t}^k(\epsilon), & \mathbf{t}^{k-1}(0) &= (\tilde{P}^{k-1}(\epsilon))^T \mathbf{t}^{k-1}(\epsilon). \end{aligned} \quad (7.31)$$

Thus, the product of the four rotations (parallel transports) is a rotation about $\mathbf{t}^{k-1}(0)$ through an angle $f^k(\epsilon)$:

$$(\tilde{P}^{k-1}(\epsilon))^T (P^k(\epsilon))^T \tilde{P}^k(\epsilon) P^k(0) = \mathbf{R}(f^k(\epsilon), \mathbf{t}^{k-1}(0)). \quad (7.32)$$

While \mathbf{t}^{k-1} is transported back to its original location, the angle $f^k(\epsilon)$ may not be zero.

7.3.2 Computing the Angle $f^k(\epsilon)$

There are two approaches that we can use to explain the computation of the angle $f^k(\epsilon)$. Both are intimately related to the concept of the holonomy of a connection induced by parallel transport of a vector around a closed path. The first approach uses the kinetic analogy and compares the rotation of the Bishop triad to a corotational frame on a rigid body. Here we imagine a rigid body that is free to rotate about a fixed point. We choose a set of material points in the rigid body and use them to define a unit vector \mathbf{r} . We then align the rigid body at time t_0 such that $\mathbf{r}(t_0) = \mathbf{t}^k(0)$. In a thought experiment, we now move the rigid body so that $\mathbf{r}(t)$ traces out the boundary of the quadrilateral shown in Fig. 7.5a and the motion of the body is such that $\omega \cdot \mathbf{r}(t) = 0$. In other words, the corotational basis that is fixed to the rigid body is equivalent to a Bishop frame. After a time $t_1 - t_0$, $\mathbf{r}(t_1) = \mathbf{r}(t_0) = \mathbf{t}^k(0)$ and the rigid body will have rotated about $\mathbf{r}(t_0)$ through an

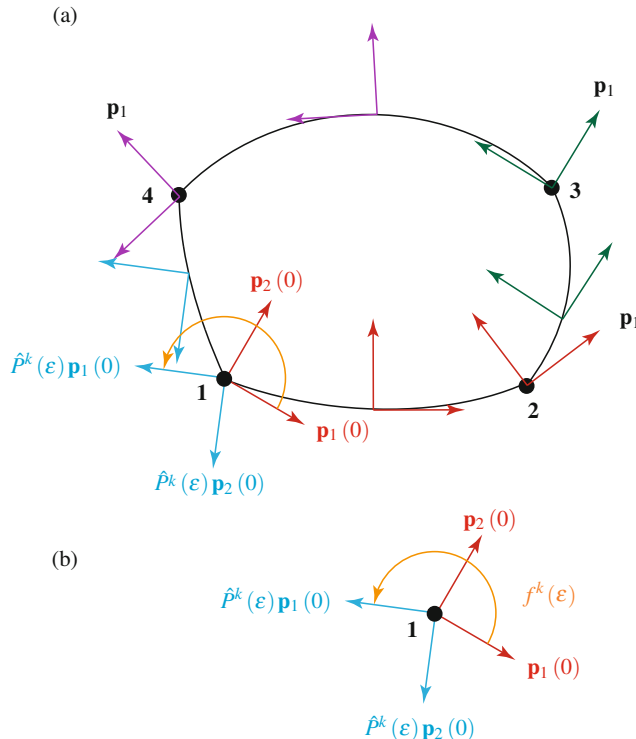


Fig. 7.6 (a) Schematic of the parallel propagation of a pair of vectors \mathbf{p}_1 and \mathbf{p}_2 around the sides of the quadrilateral. (b) The relative rotation of the pair $\mathbf{p}_1 - \mathbf{p}_2$ about \mathbf{t}^{k-1} induced by the transport is the angle $f^k(\epsilon)$

angle $f^k(\epsilon)$. Appealing to Eq. (7.3), the relative rotation of the rigid body in this case is given by the following decomposition:

$$f^k(\epsilon) = \int_{t_0}^{t_1} \underbrace{\boldsymbol{\omega} \cdot \mathbf{r}(\tau)}_{=0} d\tau + E, \quad (7.33)$$

where E is the solid angle enclosed by the quadrilateral. As curves connecting the ends of the vectors are great circles (i.e., geodesics on the unit sphere), the solid angle enclosed by the quadrilateral is simply given by the sum of the interior angles:

$$f^k(\epsilon) = E = \Theta_1 + \Theta_2 + \Theta_3 + \Theta_4. \quad (7.34)$$

Thus, f^k can be determined by measuring a solid angle on the sphere.

The second equivalent approach to compute the angle is to consider the parallel transport of a pair of orthonormal vectors \mathbf{p}_1 and \mathbf{p}_2 during the compound rotation.² For convenience, we choose $\mathbf{p}_1(0)$ to be tangent to the arc traced by $\mathbf{t}^{k-1}(0)$ as shown in Fig. 7.6. After parallel propagation of the vector \mathbf{p}_1 along the quadrilateral of great circles connecting the vertices $1, \dots, 4$ we find that this vector will have rotated by an amount E upon its return to 1 . Thus, we again conclude that $f^k(\epsilon) = E$.

7.4 The Angle $f^k(\epsilon)$ and the Reference Twist $m_{\text{ref}}^k(\epsilon) - m_{\text{ref}}^k(0)$

We now have the pieces in place to relate the spherical excess to an increment in the reference twist. This result is discussed in Bergou et al. [3] and Kaldor et al. [29] and we intend our forthcoming discussion to complement their expositions.

To proceed, we consider the propagation of the reference frame vector \mathbf{a}_1^{k-1} along the quadrilateral discussed in the previous section. We shall make frequent appeal to the identities [cf. Eqs. (4.20) and (4.23)]

$$\begin{aligned} \mathbf{a}_1^k(t + \Delta t) &= \bar{P}^k(t, \Delta t) \mathbf{a}_1^k(t), \\ \mathbf{a}_1^{k+1}(t) &= \cos(m_{\text{ref}}^{k+1}(t)) P_{\mathbf{t}^k}^{\mathbf{t}^{k+1}}(t) \mathbf{a}_1^k(t) + \sin(m_{\text{ref}}^{k+1}(t)) P_{\mathbf{t}^k}^{\mathbf{t}^{k+1}}(t) \mathbf{a}_2^k(t). \end{aligned} \quad (7.35)$$

²It might be helpful to recall that examples of parallel propagation of Bishop frame vectors were shown earlier in Figs. 2.6 and 2.7 on Page 22 for the cases where c_t was a great circle and a circle, respectively. Additional examples of parallel transport of vectors along a curve on a surface can be found in the textbooks on elementary differential geometry (see, e.g., [23, 53]).

Initially, $\mathbf{a}_1^{k-1} = \mathbf{a}_1^{k-1}(0)$. Thus, as the vector is transported from the vertex at **1** to the vertex at **2**:

$$P^k(0)\mathbf{a}_1^{k-1}(0) = \cos(m_{\text{ref}}^k(0))\mathbf{a}_1^k(0) - \sin(m_{\text{ref}}^k(0))\mathbf{a}_2^k(0). \quad (7.36)$$

The transport in this case is *not* a parallel transport in time of $\mathbf{a}_1^{k-1}(0)$. Along the vertex from **2** to **3**, the propagation of $P^k(0)\mathbf{a}_1^{k-1}(0)$ is parallel in time and so we readily conclude that

$$\tilde{P}^k(\epsilon)P^k(0)\mathbf{a}_1^{k-1}(0) = \cos(m_{\text{ref}}^k(0))\mathbf{a}_1^k(\epsilon) - \sin(m_{\text{ref}}^k(0))\mathbf{a}_2^k(\epsilon). \quad (7.37)$$

The operation on the vector $\tilde{P}^k(\epsilon)P^k(0)\mathbf{a}_1^{k-1}(0)$ from vertex **3** to **4** is parallel in space and so we need to invert Eq. (4.23) to get the appropriate transformation. After some manipulations we find that

$$\begin{aligned} \left(P^k(\epsilon)\right)^T \tilde{P}^k(\epsilon)P^k(0)\mathbf{a}_1^{k-1}(0) &= \cos(\Delta m_{\text{ref}}^k(\epsilon))\mathbf{a}_1^{k-1}(\epsilon) \\ &\quad + \sin(\Delta m_{\text{ref}}^k(\epsilon))\mathbf{a}_2^{k-1}(\epsilon), \end{aligned} \quad (7.38)$$

where

$$\Delta m_{\text{ref}}^k(\epsilon) = m_{\text{ref}}^k(\epsilon) - m_{\text{ref}}^k(0). \quad (7.39)$$

The final transformation features a parallel transport in time from **4** to **1**:

$$\begin{aligned} \left(\tilde{P}^{k-1}(\epsilon)\right)^T \left(P^k(\epsilon)\right)^T \tilde{P}^k(\epsilon)P^k(0)\mathbf{a}_1^{k-1}(0) &= \cos(\Delta m_{\text{ref}}^k(\epsilon))\mathbf{a}_1^{k-1}(0) \\ &\quad + \sin(\Delta m_{\text{ref}}^k(\epsilon))\mathbf{a}_2^{k-1}(0). \end{aligned} \quad (7.40)$$

This result leads us to the conclusion that \mathbf{a}_1^{k-1} has been rotated by an angle $\Delta m_{\text{ref}}^k(\epsilon)$. From our earlier results in Sect. 7.3.2, we can immediately conclude that

$$f^k(\epsilon) = \Delta m_{\text{ref}}^k(\epsilon) = m_{\text{ref}}^k(\epsilon) - m_{\text{ref}}^k(0). \quad (7.41)$$

This result is of great use in establishing an expression for the variation of $m_{\text{ref}}^k(t)$ when the vertices are varied.

7.4.1 A Related Result Featuring the Bishop Frame Vectors

In the earlier work Bergou et al. [4, Sect. 6], a result of the form we have just presented is to calculate angles of rotation they denote by $\psi_j(\epsilon)$ and Ψ^j . The expression found by these authors for the angles can be established by computing $\hat{P}^k(\epsilon)\mathbf{u}^{k-1}(0)$ instead of $\hat{P}^k(\epsilon)\mathbf{a}_1^{k-1}(0)$ where we use the abbreviated notation for the compound rotation:

$$\hat{P}^k(\epsilon) = \left(\tilde{P}^{k-1}(\epsilon)\right)^T \left(P^k(\epsilon)\right)^T \tilde{P}^k(\epsilon) P^k(0). \quad (7.42)$$

It is important to realize that, after completing the circuit formed by the arcs of the quadrilateral, both $\mathbf{u}^{k-1}(0)$ and $\mathbf{a}_1^{k-1}(0)$ will have been rotated by the same angle $f^k(\epsilon)$.

To elaborate further, on the arcs of the quadrilateral featuring a space-parallel transport (i.e., **1** → **2** and **3** → **4**), the transformations of the vector $\mathbf{u}^{k-1}(0)$ are parallel propagated. On the arcs of the quadrilateral featuring a time-parallel transport (i.e., **2** → **3** and **4** → **1**), the transformations of the vector $\mathbf{u}^{k-1}(0)$ rotate relative to a parallel propagated counterpart. The relevant angle of rotation is $\chi^i(\epsilon)$ and it is defined by $\tilde{P}^i(\epsilon)$ (cf. Eq. (4.24) and Fig. 4.5):

$$\tilde{P}^i(\epsilon)\mathbf{u}^i(0) = \cos(\chi^i(\epsilon))\mathbf{u}^i(\epsilon) - \sin(\chi^i(\epsilon))\mathbf{v}^i(\epsilon). \quad (7.43)$$

This angle is analogous to m_{ref}^k . It is straightforward calculate $\chi^{k-1}(\epsilon)$ and $\chi^k(\epsilon)$ using the developments in Sect. 4.2 and we are content to summarize the results in the commutative diagrams below:

$$\begin{array}{ccc} \mathbf{a}_1^{k-1}(\epsilon) & \xleftarrow[m_{\text{ref}}^k(\epsilon)]{} & \mathbf{a}_1^k(\epsilon) \\ \downarrow & \uparrow & \downarrow \chi^{k-1}(\epsilon) & \xleftarrow{-\chi^k(\epsilon)} & \uparrow \\ \mathbf{a}_1^{k-1}(0) & \xrightarrow[-m_{\text{ref}}^k(0)]{} & \mathbf{a}_1^k(0) & \mathbf{u}^{k-1}(0) & \xrightarrow{} & \mathbf{u}^k(0) \end{array}$$

Comparing these diagrams, it can be concluded that the change in the twist is related to the holonomy $f^k(\epsilon)$:

$$\begin{aligned} f^k(\epsilon) &= \Delta m_{\text{ref}}^k(\epsilon) = m_{\text{ref}}^k(\epsilon) - m_{\text{ref}}^k(0) \\ &= \chi^{k-1}(\epsilon) - \chi^k(\epsilon). \end{aligned} \quad (7.44)$$

That is, the angle $\psi_k(\epsilon)$ featured in Bergou et al. [4, Sect. 6] is equivalent to $f^k(\epsilon)$:

$$\psi_k(\epsilon) = f^k(\epsilon) = \chi^{k-1}(\epsilon) - \chi^k(\epsilon). \quad (7.45)$$

We invite the reader to compare these results to the original expositions in Bergou et al. [4, Sect. 6], Bergou et al. [3, Sect. 6], and Kaldor et al. [29, Appendix A].³

7.5 Variations of the Twist m_k and Reference Twist δm_{ref}^k

If the vertices $\mathbf{x}_{k-1}(\epsilon)$, $\mathbf{x}_k(\epsilon)$, and $\mathbf{x}_{k+1}(\epsilon)$ are perturbed, then $\mathbf{t}^{k-1}(\epsilon)$ and $\mathbf{t}^k(\epsilon)$ will be displaced as shown in Fig. 7.5b. The associated variation in the spherical excess E is

$$\delta E = \delta\Theta_1 + \delta\Theta_2 + \delta\Theta_3 + \delta\Theta_4. \quad (7.46)$$

To express this variation in terms of the variations to the tangent vectors, we use a result due to Etienne Vouga [65]. Applying Eq. (7.22) to the situation at hand:

$$\begin{aligned} \delta E &= \delta\Theta_1 + \delta\Theta_2 + \delta\Theta_3 + \delta\Theta_4 \\ &= - \left(\frac{\mathbf{t}^k(\epsilon) \times \mathbf{t}^{k-1}(\epsilon)}{1 + \mathbf{t}^k(\epsilon) \cdot \mathbf{t}^{k-1}(\epsilon)} \right) \cdot (\delta\mathbf{t}^k(\epsilon) + \delta\mathbf{t}^{k-1}(\epsilon)) \\ &\quad - \underbrace{\left(\frac{\mathbf{t}^k(0) \times \mathbf{t}^k(\epsilon)}{1 + \mathbf{t}^k(0) \cdot \mathbf{t}^k(\epsilon)} \right) \cdot \delta\mathbf{t}^k(\epsilon)}_{\text{underbrace}} - \underbrace{\left(\frac{\mathbf{t}^{k-1}(0) \times \mathbf{t}^{k-1}(0)}{1 + \mathbf{t}^{k-1}(0) \cdot \mathbf{t}^{k-1}(0)} \right) \cdot \delta\mathbf{t}^{k-1}(\epsilon)}. \end{aligned} \quad (7.47)$$

Taking the limit as $\epsilon \rightarrow 0$, the underbraced terms vanish and we can conclude that

$$\begin{aligned} \frac{dm_{\text{ref}}^k}{d\epsilon} &= \left(\frac{\mathbf{t}^{k-1}(0) \times \mathbf{t}^k(0)}{1 + \mathbf{t}^k(0) \cdot \mathbf{t}^{k-1}(0)} \right) \cdot \left(\frac{d\mathbf{t}^k}{d\epsilon}(0) + \frac{d\mathbf{t}^{k-1}}{d\epsilon}(0) \right) \\ &= (\kappa\mathbf{b})_k \cdot \frac{d\mathbf{t}^k}{d\epsilon}. \end{aligned} \quad (7.48)$$

In the final expression we have removed the explicit dependency on ϵ .

To compute the variation of the discrete integrated twist m_k , we recall from Eq. (5.19) that

$$m_k = \gamma^k - \gamma^{k-1} + m_{\text{ref}}^k. \quad (7.49)$$

³The referential discrete (integrated) twist m_{ref}^k in [3] and [29] is denoted by \underline{m}_k and $\hat{\psi}^k$, respectively.

However, a variation of the vertices is equivalent to rigidly rotating the material vectors, the reference vectors, and the Bishop frame vectors. Thus, the angles between these vectors are preserved:

$$\delta\gamma^k = 0, \quad \delta\gamma^{k-1} = 0. \quad (7.50)$$

Consequently,

$$\delta m_k = \delta m_{\text{ref}}^k. \quad (7.51)$$

Thus, the expression for the variation of m_k is identical to the expression for the variation of m_{ref}^k . The resulting expression is used in Bergou et al. [3] and differs by a sign from the expression used in Kaldor et al. [29].⁴

7.5.1 Variation of an Angle of Twist ψ_k

For completeness, we note a closely-related expression for the variation of an angle of twist ψ_k can be readily obtained:

$$\delta\psi_k = (\kappa\mathbf{b})_k \cdot \delta\mathbf{t}_{\gamma_k}. \quad (7.52)$$

Modulo a difference in sign (which we suspect to be a typographical error), this equation first appeared in Bergou et al. [4, Sect. 6].⁵ We also note that an alternative proof of the identity (7.48), which does not feature the exploitation of spherical trigonometry, can be found in Kirsch [32, Theorem 4.60].⁶ Kirsch's proof uses the identity (2.27) that was discussed in Chap. 2.

7.6 A Rod with Three Vertices

To explore the formulae for m_{ref}^k and δm_{ref}^k , we return to the example of a rod with three vertices that was discussed in Sect. 4.5. For the reader's convenience, the configurations of the rod are reproduced in Fig. 7.7. We recall, from Eq. (4.35), expressions for the tangent vectors:

$$\mathbf{t}^0(\epsilon) = \mathbf{E}_1, \quad \mathbf{t}^1(\epsilon) = \frac{1}{\sqrt{2+\epsilon^2}} (\mathbf{E}_1 + \mathbf{E}_2 + \epsilon\mathbf{E}_3). \quad (7.53)$$

⁴We have been unable to resolve this sign difference, but based on the example discussed in Sect. 7.6, we believe the sign difference is a typographical error.

⁵In the notation of [4], the solid angle f^j is denoted by ψ_j .

⁶Kirsch's thesis [32, Sect. A.2, Appendix A] also contains a helpful discussion which illuminate remarks in [4, Sect. 6] on the similarities between Eq. (7.48) and a formula for the writhing of a curve proposed by de Vries in [66, Eq. (4)].

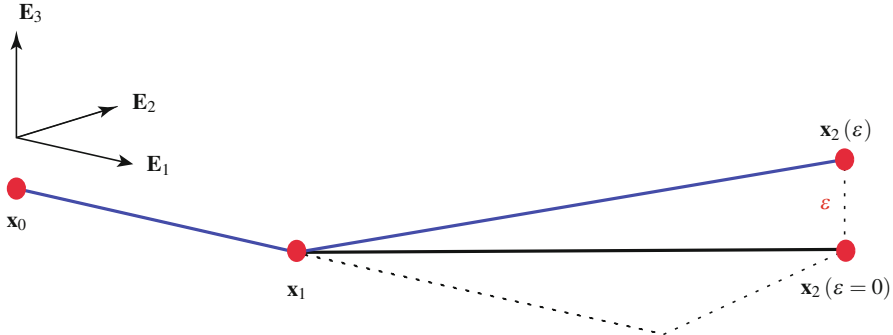


Fig. 7.7 The configurations of a rod which has three vertices. When $\epsilon = 0$, all of the vertices lie on a horizontal plane. As ϵ is increased from 0, the third vertex rises above this plane and a reference twist is induced in the second edge

Our goal is to establish an expression for the solid angle formed by the three vectors $\mathbf{t}^0, \mathbf{t}^1 (\epsilon = 0)$, and $\mathbf{t}^1 (\epsilon)$ as a function of ϵ . In addition, we wish to examine the rate of change of this angle with ϵ . These results will then be compared to our earlier derivations of the reference twist m_{ref}^1 for this simple rod in Sect. 4.5. In particular, we are able to demonstrate how Eqs. (7.41) and (7.48) relating spherical excess and its variation to m_{ref}^k and δm_{ref}^k yield results that are consistent with computations of these quantities involving the parallel transport operators in Sect. 4.5.

7.6.1 Spherical Excess and Reference Twist

The excess E for the spherical triangle formed by $\mathbf{t}^0 (0), \mathbf{t}^1 (0)$, and $\mathbf{t}^1 (\epsilon)$ is

$$E = \Theta_1 + \Theta_2 + \Theta_3 - \pi. \quad (7.54)$$

As can be seen from Fig. 7.8, the interior angles Θ_1 , Θ_2 , and Θ_3 in this equation can be defined using the tangent vectors:

$$\begin{aligned} \cos(\Theta_1) &= \frac{\mathbf{t}^0 (0) \times \mathbf{t}^1 (0)}{\|\mathbf{t}^0 (0) \times \mathbf{t}^1 (0)\|} \cdot \frac{\mathbf{t}^0 (0) \times \mathbf{t}^1 (\epsilon)}{\|\mathbf{t}^0 (0) \times \mathbf{t}^1 (\epsilon)\|}, \\ \cos(\Theta_2) &= \frac{\mathbf{t}^1 (0) \times \mathbf{t}^0 (0)}{\|\mathbf{t}^1 (0) \times \mathbf{t}^0 (0)\|} \cdot \frac{\mathbf{t}^1 (0) \times \mathbf{t}^1 (\epsilon)}{\|\mathbf{t}^1 (0) \times \mathbf{t}^1 (\epsilon)\|}, \\ \cos(\Theta_3) &= \frac{\mathbf{t}^1 (\epsilon) \times \mathbf{t}^0 (0)}{\|\mathbf{t}^1 (\epsilon) \times \mathbf{t}^0 (0)\|} \cdot \frac{\mathbf{t}^1 (\epsilon) \times \mathbf{t}^1 (0)}{\|\mathbf{t}^1 (\epsilon) \times \mathbf{t}^1 (0)\|}. \end{aligned} \quad (7.55)$$

The procedure used to compute these expressions is identical to that used earlier with the spherical quadrilateral (see Page 79).

Fig. 7.8 Spherical triangle formed by the three tangent vectors $\mathbf{t}^0(\epsilon) = \mathbf{E}_1$, $\mathbf{t}^1(0) = \frac{1}{\sqrt{2}}(\mathbf{E}_1 + \mathbf{E}_2)$, and $\mathbf{t}^1(\epsilon) = \frac{1}{\sqrt{2+\epsilon^2}}(\mathbf{E}_1 + \mathbf{E}_2 + \epsilon\mathbf{E}_3)$. As ϵ increases from 0 to 1, the spherical excess E increases from 0 to $\frac{\pi}{12}$

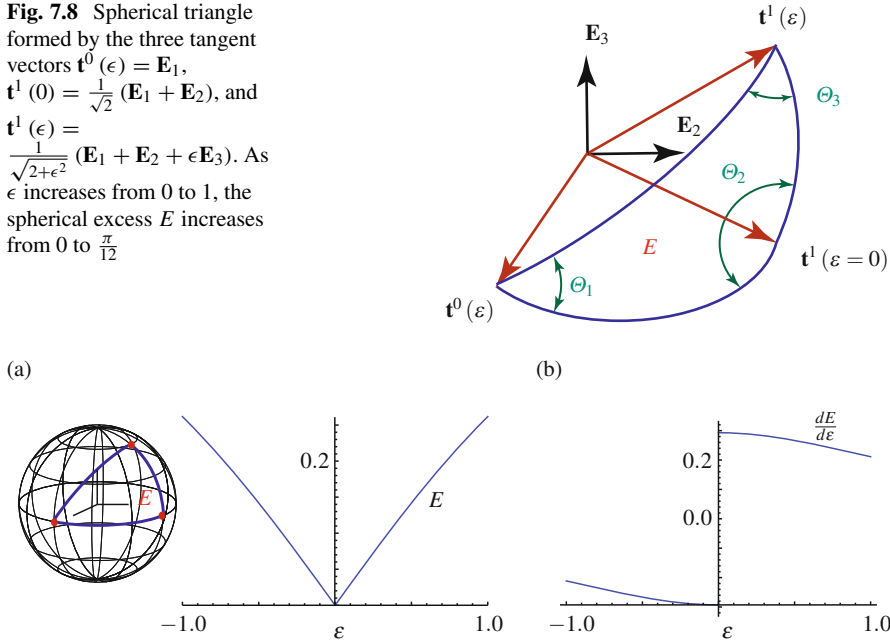


Fig. 7.9 (a) The spherical excess E as a function of ϵ computed using Eq. (7.57) for the spherical triangle shown in Fig. 7.7. (b) The corresponding value of $\frac{dE}{d\epsilon}$ computed using Eq. (7.61)

Substituting for the tangent vectors and computing the inner products, we find that

$$\cos(\Theta_1) = \frac{1}{\sqrt{1+\epsilon^2}}, \quad \Theta_2 = \frac{\pi}{2}, \quad \cos(\Theta_3) = \frac{|\epsilon|}{\sqrt{2}\sqrt{1+\epsilon^2}}. \quad (7.56)$$

Consequently,

$$E = \cos^{-1}\left(\frac{1}{\sqrt{1+\epsilon^2}}\right) + \cos^{-1}\left(\frac{|\epsilon|}{\sqrt{2}\sqrt{1+\epsilon^2}}\right) - \frac{\pi}{2}. \quad (7.57)$$

Comparing this result to the expression \tilde{m}_{ref} for m_{ref}^1 that we found in Sect. 4.5 on Page 46, we find that $E = m_{\text{ref}}^1$ when $\epsilon > 0$, as anticipated. For example, when $\epsilon = 1$, then $E = \frac{\pi}{12}$. The function (7.57) for $E(\epsilon)$ is shown in Fig. 7.9a. Clearly, when $\epsilon < 0$, then we can only state that $|m_{\text{ref}}^1| = E$.

7.6.2 Variation of the Spherical Excess

To establish an expression for the variation of the excess E , we repeat the constructions leading to (7.22). This time the construction is applied to the spherical triangle where only one of the vertices is varied: $\delta \mathbf{t}^0(0) = 0$ and $\delta \mathbf{t}^1(0) = 0$. With a modest amount of work, we find that

$$\delta E = \left(\frac{\mathbf{t}^1(\epsilon) \times \mathbf{t}^1(0)}{1 + \mathbf{t}^1(0) \cdot \mathbf{t}^1(\epsilon)} \right) \cdot \delta \mathbf{t}^1(\epsilon) + \left(\frac{\mathbf{t}^0(0) \times \mathbf{t}^1(\epsilon)}{1 + \mathbf{t}^0(0) \cdot \mathbf{t}^1(\epsilon)} \right) \cdot \delta \mathbf{t}^1(\epsilon). \quad (7.58)$$

Whence,

$$\frac{dE}{d\epsilon} = \left(\frac{\mathbf{t}^1(\epsilon) \times \mathbf{t}^1(0)}{1 + \mathbf{t}^1(0) \cdot \mathbf{t}^1(\epsilon)} \right) \cdot \frac{d\mathbf{t}^1}{d\epsilon} + \left(\frac{\mathbf{t}^0(0) \times \mathbf{t}^1(\epsilon)}{1 + \mathbf{t}^0(0) \cdot \mathbf{t}^1(\epsilon)} \right) \cdot \frac{d\mathbf{t}^1}{d\epsilon}. \quad (7.59)$$

For the application of interest:

$$\frac{d\mathbf{t}^1}{d\epsilon} = \frac{1}{\sqrt{2 + \epsilon^2}} \mathbf{E}_3 - \left(\frac{\epsilon}{2 + \epsilon^2} \right) \mathbf{t}^1(\epsilon). \quad (7.60)$$

Substituting the expressions for the tangent vectors and $\frac{d\mathbf{t}^1}{d\epsilon}$ into Eq. (7.59) enables us to conclude that

$$\frac{dE}{d\epsilon} = \frac{-\text{sgn}(\epsilon) |\epsilon| + \epsilon \sqrt{2 + \epsilon^2}}{(1 + \epsilon^2) \sqrt{\epsilon^2 (2 + \epsilon^2)}}. \quad (7.61)$$

As can be observed from Fig. 7.9b, when $\epsilon > 0$ this expression is precisely in agreement with $\frac{d\tilde{m}_{\text{ref}}}{d\epsilon}$ for the function \tilde{m}_{ref} that we found previously in Sect. 4.5.

Chapter 8

Equations of Motion and Energetic Considerations



8.1 Introduction

In the discrete elastic rod formulation, a state vector \mathbf{q} is formulated using the components of the position vectors of the n vertices and the rotations of the material frames relative to the reference frames on each of the $n - 1$ edges:

$$\mathbf{q} = \left[\mathbf{x}_0 \cdot \mathbf{E}_1, \mathbf{x}_0 \cdot \mathbf{E}_2, \mathbf{x}_0 \cdot \mathbf{E}_3, \gamma^0, \dots, \mathbf{x}_{(n-2)} \cdot \mathbf{E}_1, \mathbf{x}_{(n-2)} \cdot \mathbf{E}_2, \mathbf{x}_{(n-2)} \cdot \mathbf{E}_3, \gamma^{n-2}, \mathbf{x}_{(n-1)} \cdot \mathbf{E}_1, \mathbf{x}_{(n-1)} \cdot \mathbf{E}_2, \mathbf{x}_{(n-1)} \cdot \mathbf{E}_3 \right]^T. \quad (8.1)$$

Complementing this vector, a pair of generalized force vectors are also formulated:

$$\begin{aligned} \mathbf{F}_{\text{ext}} &= \mathbf{F}_{\text{ext}}(t_k, \mathbf{q}(t_k), \dot{\mathbf{q}}(t_k)) = \left[\mathbf{F}_{\text{ext}}^0, \dots, \mathbf{F}_{\text{ext}}^{(4n-1)} \right]^T, \\ \mathbf{F}_{\text{int}} &= \mathbf{F}_{\text{int}}(\mathbf{q}(t_k), \dot{\mathbf{q}}(t_k)) = \left[\mathbf{F}_{\text{int}}^0, \dots, \mathbf{F}_{\text{int}}^{(4n-1)} \right]^T. \end{aligned} \quad (8.2)$$

As discussed in Bergou et al. [3], the motion of the rod is determined by using Newton's method to solve the following equations for $\mathbf{q}(t_{k+1})$ and $\dot{\mathbf{q}}(t_{k+1})$:

$$\begin{aligned} (t_{k+1} - t_k) \dot{\mathbf{q}}(t_{k+1}) &= \mathbf{q}(t_{k+1}) - \mathbf{q}(t_k), \\ \mathbf{M}(\dot{\mathbf{q}}(t_{k+1}) - \dot{\mathbf{q}}(t_k)) &= (t_{k+1} - t_k) (\mathbf{F}_{\text{ext}}(t_k, \mathbf{q}(t_k), \dot{\mathbf{q}}(t_k)) \\ &\quad + \mathbf{F}_{\text{int}}(\mathbf{q}(t_{k+1}), \dot{\mathbf{q}}(t_{k+1}))). \end{aligned} \quad (8.3)$$

In these equations, \mathbf{M} is a mass matrix and we shall explore shortly how the components of this matrix are prescribed. An additional purpose of this chapter is to

explore prescriptions for the components of \mathbf{F}_{int} in terms of the gradients of elastic energies and viscous damping forces and the components \mathbf{F}_{ext} in terms of assigned forces and moments.

Newton's method requires the gradient of the internal forces (or Hessians of the elastic energies). Having banded Hessians reduces the computational expense. This is one of the reasons why the reference frame and time-parallel transport was employed in [3, 29] as opposed to space-parallel transport of the Bishop frame in the earlier formulation [4].

8.2 Kinetic Energies, Momenta, and Inertias

Prescriptions for kinetic energies and inertias for the discrete rod follow standard procedures that are adopted from classic rod theories. In particular, volume and surface integrals are used to determine weighted inertias and mass parameters. The most comprehensive work in the literature on these types of approximations is arguably Green et al. [19] and their work significantly influenced our exposition.¹

The velocity vector of the k th vertex is simply denoted by $\dot{\mathbf{x}}_k$. Expressions for $\dot{\mathbf{m}}_1^k$ and $\dot{\mathbf{m}}_2^k$ were established earlier [cf. Eq. (5.28)]:

$$\begin{aligned}\dot{\mathbf{m}}_1^k(t) &= \bar{\boldsymbol{\omega}}^k(t) \times \mathbf{m}_1^k(t) \\ &= \dot{\gamma}^k(t) \mathbf{m}_2^k(t) - (\mathbf{m}_1^k(t) \cdot \dot{\mathbf{t}}^k(t)) \mathbf{t}^k(t), \\ \dot{\mathbf{m}}_2^k(t) &= \bar{\boldsymbol{\omega}}^k(t) \times \mathbf{m}_2^k(t) \\ &= -\dot{\gamma}^k(t) \mathbf{m}_1^k(t) - (\mathbf{m}_2^k(t) \cdot \dot{\mathbf{t}}^k(t)) \mathbf{t}^k(t).\end{aligned}\quad (8.4)$$

As mentioned previously, the velocity of the material vectors have two components: one due to the twist $\dot{\gamma}^k$ and the other due to the motion of the edge vector \mathbf{e}^k (i.e., bending).

8.2.1 Masses and Inertias

In the sequel, we assume that the discrete curve approximates the centerline of the three-dimensional body that the rod is modeling. The body is divided into a series of segments with each segment modeled using an edge of the discrete elastic curve.

¹A discussion of the developments in Green et al. [19] along with illustrative examples, can be found in [51, Chap. 5]. We also refer the reader to the review article by Naghdi [45] and Rubin's textbook [56].

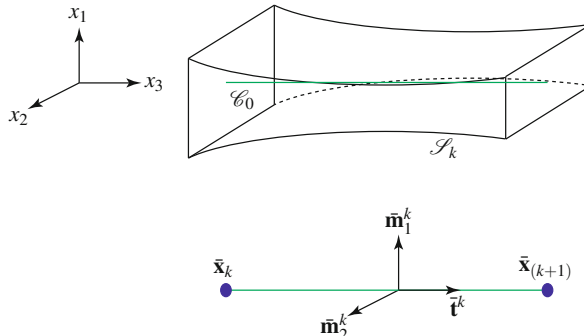


Fig. 8.1 Reference configuration for a segment \mathcal{S}_k of a three-dimensional body that the k th edge of a discrete elastic rod is modeling. The line \mathcal{C}_0 that will be approximated by the edge is shown. On this line, which is often chosen to be the centerline of the segment \mathcal{S}_k , the Cartesian coordinates x_1 and x_2 are both 0. The reference state of the k th edge is also shown and the reference values of the kinematic quantities associated with the discrete elastic rod are distinguished by an overbar

We assume that the fixed reference configuration of each segment of the body can be parameterized by a Cartesian coordinate system $x_1 - x_2 - x_3$ with x_3 parameterizing the centerline and x_1 and x_2 parameterizing the cross-section (cf. Fig. 8.1). For simplicity, we assume that x_1 and x_2 are principal axes of the cross-section and the material vectors \mathbf{m}_1^k and \mathbf{m}_2^k in the fixed reference configuration are parallel to these axes and are labelled with an overbar in Fig. 8.1.

The mass M_i associated with the i th vertex is the average mass of the edges meeting at this vertex:

$$M_i = \frac{1}{2} (M^i + M^{i-1}). \quad (8.5)$$

For a homogeneous rod with a uniform cross-section in its reference configuration (or reference state),

$$M^i = \rho_0 A^i \|\bar{\mathbf{e}}^i\|, \quad (8.6)$$

where ρ_0 is the mass density per unit volume in the reference configuration, A^i is the cross-sectional area in the reference configuration, and $\|\bar{\mathbf{e}}^i\|$ denotes the length of the i th edge in the reference configuration. If the rod is not homogeneous or of a uniform cross-section, then M^i must be computed using a more primitive prescription:

$$M^i = \int \int \int \rho_0 dx_1 dx_2 dx_3, \quad (8.7)$$

where the integration is performed over the segment of the three-dimensional body that the i th edge is modeling.

The mass moments of inertia associated with the i th edge are defined with the help of volume integrals:

$$\begin{aligned}\rho_0^i &= \int \int \int \rho_0 dx_1 dx_2 dx_3, \\ \rho_0^i I_1^i &= \int \int \int x_1^2 \rho_0 dx_1 dx_2 dx_3, \quad \rho_0^i I_2^i = \int \int \int x_2^2 \rho_0 dx_1 dx_2 dx_3, \\ \rho_0^i I^i &= \rho_0^i I_1^i + \rho_0^i I_2^i.\end{aligned}\tag{8.8}$$

Thus, for a segment of length ℓ of a homogeneous rod with a rectangular cross-section of height h (in the x_2 direction) and width w (in the x_1 direction):

$$\rho_0^i I_1^i = \rho_0 \ell \frac{wh^3}{12} = \frac{M^i h^2}{12}, \quad \rho_0^i I_2^i = \rho_0 \ell \frac{hw^3}{12} = \frac{M^i w^2}{12}.\tag{8.9}$$

Observe that we have used the definition of the mass M^i of the i th edge to simplify these expressions.

The mass matrix \mathbf{M} can now be prescribed:

$$\mathbf{M} = \left[\begin{array}{ccccccccc} M_0 & 0 & 0 & 0 & \dots & 0 & 0 & 0 & 0 \\ 0 & M_0 & 0 & 0 & \dots & 0 & 0 & 0 & 0 \\ 0 & 0 & M_0 & 0 & \dots & 0 & 0 & 0 & 0 \\ 0 & 0 & 0 & \rho_0^0 I^0 & \dots & 0 & 0 & 0 & 0 \\ \ddots & & \ddots & & & \ddots & & & \\ \ddots & & \ddots & & & \ddots & & & \\ \ddots & & \ddots & & & \ddots & & & \\ \ddots & & \ddots & & & \ddots & & & \\ 0 & 0 & 0 & 0 & \dots & \rho_0^{(n-2)} I^{(n-2)} & 0 & 0 & 0 \\ 0 & 0 & 0 & 0 & \dots & 0 & M_{(n-1)} & 0 & 0 \\ 0 & 0 & 0 & 0 & \dots & 0 & 0 & M_{(n-1)} & 0 \\ 0 & 0 & 0 & 0 & \dots & 0 & 0 & 0 & M_{(n-1)} \end{array} \right].\tag{8.10}$$

The reader is invited to relate the components of this matrix to the components of the vector \mathbf{q} [cf. Eq. (8.1)]. It is also important to note that the masses in this matrix are associated with a vertex while the inertias are associated with an edge.

8.2.2 Linear Momentum, Angular Momentum, and Kinetic Energy

The masses and inertias we have defined are central to the definitions of momenta and kinetic energy. The linear momentum \mathbf{G} of the discrete elastic rod is the sum of the linear momenta of the vertices:

$$\mathbf{G} = \sum_{k=0}^{n-1} M_k \dot{\mathbf{x}}_k. \quad (8.11)$$

The rod in this case has n vertices and $n - 1$ edges. This expression for the linear momentum can also be expressed in terms of the velocity vector of the center of mass of each edge:

$$\mathbf{G} = \sum_{k=0}^{n-2} \frac{M^k}{2} (\dot{\mathbf{x}}_k + \dot{\mathbf{x}}_{k+1}). \quad (8.12)$$

Similarly, the angular momentum of the rod relative to a fixed point O is

$$\mathbf{H}_O = \sum_{k=0}^{n-1} (\mathbf{x}_k \times M_k \dot{\mathbf{x}}_k) + \sum_{k=0}^{n-2} \left(\mathbf{m}_1^k \times \rho_0^k I_2^k \dot{\mathbf{m}}_1^k + \mathbf{m}_2^k \times \rho_0^k I_1^k \dot{\mathbf{m}}_2^k \right). \quad (8.13)$$

Finally, we note that the following expression denotes a kinetic energy T^* of the rod:

$$T^* = \frac{1}{2} \sum_{k=0}^{n-1} (\dot{\mathbf{x}}_k \cdot M_k \dot{\mathbf{x}}_k) + \frac{1}{2} \sum_{k=0}^{n-2} \left(\dot{\mathbf{m}}_1^k \cdot \rho_0^k I_2^k \dot{\mathbf{m}}_1^k + \dot{\mathbf{m}}_2^k \cdot \rho_0^k I_1^k \dot{\mathbf{m}}_2^k \right). \quad (8.14)$$

In this expression for T^* ,

$$\dot{\mathbf{m}}_1^k \cdot \rho_0^k I_2^k \dot{\mathbf{m}}_1^k = \rho_0^k I_2^k \left(\dot{y}^k \right)^2 + \rho_0^k I_2^k \left(\mathbf{m}_1^k \cdot \left(\frac{\dot{\mathbf{x}}_{k+1}(t) - \dot{\mathbf{x}}_k(t)}{\|\mathbf{x}_{k+1}(t) - \mathbf{x}_k(t)\|} \right) \right). \quad (8.15)$$

Here, we used the representation (4.16) for $\dot{\mathbf{t}}^k$. The kinetic energy T that plays a role in the sequel is defined by a portion of T^* :

$$T = \frac{1}{2} \dot{\mathbf{q}}^T \mathbf{M} \dot{\mathbf{q}} = \frac{1}{2} \sum_{k=0}^{n-1} (\dot{\mathbf{x}}_k \cdot M_k \dot{\mathbf{x}}_k) + \frac{1}{2} \sum_{k=0}^{n-2} \rho_0^k I_2^k \left(\dot{y}^k \right)^2. \quad (8.16)$$

For future reference, we note that $\dot{T} = \dot{\mathbf{q}} \cdot \mathbf{M} \ddot{\mathbf{q}}$.

8.3 Elastic Energies

Expressions for the gradients and Hessians of kinematical quantities were computed in Chap. 6. We now use these representations in order to compute the internal forces associated with the potential energy function for the discrete elastic rod. As the rod is allowed to twist, stretch and bend, the potential energy function will feature bending strains, twisting strains, and extensional strains. In its simplest form, the elastic potential energy E_e can be decomposed into the sum of three energies:

$$E_e = E_s + E_t + E_b. \quad (8.17)$$

Consistent with [3], we assume that each edge has an elliptical cross-section with major and minor radii a^i and b^j , respectively, so that the cross-sectional area $A^j = \pi a^j b^j$. At the vertices, we define $a_i = (a^{i-1} + a^i)/2$ and $b_i = (b^{i-1} + b^i)/2$, so that the cross-sectional area at the vertices are $A_i = \pi a_i b_i$.

The decomposition of E_e assumes that there is no inherent coupling between bending, twisting, and stretching of the rod. More complex energies E_e are possible. Indeed, if the discrete elastic rod formulation were to be used to model DNA strands or wire rope, then these more complex energies would be needed to model twist-stretch and twist-bending coupling that is observed in these systems.²

The respective extensional E_s , twisting E_t , and bending E_b elastic energy functions are assumed to be quadratic functions of the strains:

$$\begin{aligned} E_s &= \frac{1}{2} \sum_{j=0}^{n-2} EA^j \left(\frac{\|\mathbf{e}^j\|}{\|\bar{\mathbf{e}}^j\|} - 1 \right)^2 \|\bar{\mathbf{e}}^j\|, \\ E_t &= \frac{1}{2} \sum_{i=1}^{n-2} \frac{GA_i(a_i^2 + b_i^2)}{4} \frac{(m_i - \bar{m}_i)^2}{\bar{\ell}_i}, \\ E_b &= \frac{1}{2} \sum_{i=0}^{n-2} \frac{EA_i a_i^2}{4\bar{\ell}_i} (\kappa_{i_1} - \bar{\kappa}_{i_1})^2 + \frac{EA_i b_i^2}{4\bar{\ell}_i} (\kappa_{i_2} - \bar{\kappa}_{i_2})^2. \end{aligned} \quad (8.18)$$

In these expressions, the overbars ornamenting ℓ_k , \mathbf{e}^j , m_i , κ_{i_1} , and κ_{i_2} denote the values of these quantities in a fixed reference configuration, and E and G denote the Young's modulus and the shear modulus, respectively. Observe that the expression for E_t was simplified slightly because

$$m_0 = 0, \quad \bar{m}_0 = 0. \quad (8.19)$$

²For further details on constitutive relations, material symmetry, and coupled deformation in elastic rods, we refer the reader to [1, 22, 37, 49, 51] and references therein.

The discrete twist m_i has several representations [cf. Eq. (5.19)]:

$$\begin{aligned} m_i &= \vartheta^i - \vartheta^{i-1} \\ &= \gamma^i - \gamma^{i-1} + m_{\text{ref}}^i. \end{aligned} \quad (8.20)$$

We recall that the referential twist m_{ref}^i is needed in order to accommodate the parallel transport of the reference vectors \mathbf{a}_1^i and \mathbf{a}_2^i . When interpreting Eq. (8.18), it is important to note that the stretching is a quantity associated with the edges while the twisting and bending are associated with the vertices.

The expression for stretching energy E_s is similar to that found in other discrete elastic rod formulations such as Lang et al. [35], Loock et al. [39], and Lv et al. [41]. However, the bending and twisting energies found in Eq. (8.18) differ from these works in the manner in which the bending and torsional strains are defined. We take this opportunity to note that the perspectives of Lang et al. and Lv et al.'s of a discrete elastic rod as a collection of masses connected by springs may be useful for many readers.

8.4 Forces, Moments, and Gradients of Elastic Energies

In addition to the twisting moment $M_{t_{3k}} \mathbf{t}^k$ acting on the k th edge, a force \mathbf{F}_{e_i} acting on the i th vertex can be prescribed by solving an energy balance:

$$\dot{E}_e = - \sum_{k=0}^{n-2} M_{t_{3k}} \dot{\gamma}^k - \sum_{i=0}^{n-1} \mathbf{F}_{e_i} \cdot \dot{\mathbf{x}}_i. \quad (8.21)$$

This energy balance pertains to the mechanical power of the forces acting on the vertices and the moments acting on the edges. What is perhaps not obvious is that the term $M_{t_{3k}} \dot{\gamma}^k$ in this expression is a simplification of the expression for the mechanical power of the moment $M_{t_{3k}} \mathbf{t}^k$ acting on the discrete elastic rod:

$$M_{t_{3k}} \mathbf{t}^k \cdot \bar{\boldsymbol{\omega}}^k = M_{t_{3k}} \mathbf{t}^k \cdot (\dot{\gamma}^k \mathbf{t}^k + \mathbf{t}^k \times \dot{\mathbf{t}}^k), \quad (8.22)$$

where the angular velocity vector $\bar{\boldsymbol{\omega}}^k$ is defined by Eq. (5.25). For the choice of E_e we have selected, it is possible to decompose the force vector at the i th vertex:

$$\mathbf{F}_{e_i} = \mathbf{F}_{s_i} + \mathbf{F}_{t_i} + \mathbf{F}_{b_i}. \quad (8.23)$$

Here, the force \mathbf{F}_{s_i} is associated with stretching, the force \mathbf{F}_{t_i} is associated with twisting or torsion, and the force \mathbf{F}_{b_i} is associated with bending or flexure. These forces and the aforementioned moments can be prescribed by assuming that they satisfy the following energy balance for all motions of the rod:

$$\dot{E}_s + \dot{E}_t + \dot{E}_b = - \sum_{k=0}^{n-2} M_{t_{3k}} \dot{\gamma}^k - \sum_{i=0}^{n-1} (\mathbf{F}_{s_i} + \mathbf{F}_{t_i} + \mathbf{F}_{b_i}) \cdot \dot{\mathbf{x}}_i. \quad (8.24)$$

That is, the mechanical power of the forces \mathbf{F}_{e_i} balances the negative of the time-rate of change of the elastic energy. The energies E_s , E_t , and E_b are functions of \mathbf{e}^k and m_i . After the time derivatives of the energies have been taken, we substitute for $\dot{\mathbf{e}}^k$ and \dot{m}_k in terms of $\dot{\gamma}^i$ and $\dot{\mathbf{x}}_i$:

$$\begin{aligned} \dot{\mathbf{e}}^0 &= \dot{\mathbf{x}}_1 - \dot{\mathbf{x}}_0, \dots, \dot{\mathbf{e}}^k = \dot{\mathbf{x}}_{k+1} - \dot{\mathbf{x}}_k, \dots, \dot{\mathbf{e}}^{n-2} = \dot{\mathbf{x}}_{n-1} - \dot{\mathbf{x}}_{n-2}, \\ \dot{m}_0 &= \dot{\gamma}^0, \dots, \dot{m}_k = \dot{\gamma}^k - \dot{\gamma}^{k-1} + \dot{m}_{\text{ref}}^k, \dots, \dot{m}_{n-2} = \dot{\gamma}^{n-2} - \dot{\gamma}^{n-1} + \dot{m}_{\text{ref}}^{n-2}. \end{aligned} \quad (8.25)$$

The expression for \dot{m}_{ref}^k in terms of the velocity vectors of the vertices is given in Eq. (6.41).

After some rearranging, we find that Eq. (8.24) can be expressed as

$$\sum_{k=0}^{n-2} \Gamma^k \dot{\gamma}^k + \sum_{i=0}^{n-1} \mathbf{X}_i \cdot \dot{\mathbf{x}}_i = 0. \quad (8.26)$$

In this equation,

$$\begin{aligned} \mathbf{X}_0 &= -\frac{\partial E_e}{\partial \mathbf{e}^0} + \mathbf{F}_{s_0} + \mathbf{F}_{t_0} + \mathbf{F}_{b_0}, \\ \Gamma^0 &= \frac{\partial E_e}{\partial m_0} - \frac{\partial E_e}{\partial m_1} + M_{t_{30}}, \\ \mathbf{X}_k &= -\frac{\partial E_e}{\partial \mathbf{e}^k} + \frac{\partial E_e}{\partial \mathbf{e}^{k-1}} + \mathbf{F}_{s_k} + \mathbf{F}_{t_k} + \mathbf{F}_{b_k}, \\ \Gamma^k &= \frac{\partial E_e}{\partial m_k} - \frac{\partial E_e}{\partial m_{k+1}} + M_{t_{3k}}, \\ \mathbf{X}_{n-1} &= -\frac{\partial E_e}{\partial \mathbf{e}^{n-2}} + \mathbf{F}_{s_{n-1}} + \mathbf{F}_{t_{n-1}} + \mathbf{F}_{b_{n-1}}, \\ \Gamma^{n-2} &= \frac{\partial E_e}{\partial m_{n-2}} + M_{t_{3n-2}}, \end{aligned} \quad (8.27)$$

where $E_e = E_b + E_s + E_t$. As Γ^k and \mathbf{X}_i are independent of the rates $\dot{\mathbf{x}}_i$ and $\dot{\gamma}^k$, and Eq. (8.26) is assumed to hold for all motions of the rod, we conclude that $\Gamma^k = 0$

and $\mathbf{X}_i = \mathbf{0}$.³ In this manner, we find lengthy expressions for $M_{t_{3k}}$, \mathbf{F}_{t_i} , \mathbf{F}_{s_i} , and \mathbf{F}_{b_i} in terms of the derivatives of the energies that are energetically consistent. The expressions are recorded in Sect. 8.5.

8.5 Hessians of the Elastic Energies

The gradients and Hessians of the elastic energies are needed in order to solve the discrete time equations for the configuration of the rod. The discrete equations are found by imposing the Euler-Lagrange necessary condition for the extremization of a functional. Consistent with Eqs. (8.24) and (8.26), the negative of the gradient of a potential energy can be identified with an internal force (or moment) in the rod (cf. Fig. 8.2). As Newton's method is used to solve the set of implicit equations [cf. Eq. (8.3)] provided by the Euler-Lagrange necessary condition, expressions for the Hessians of the energies are also needed in order to compute Jacobians. We remind the reader that background on the notation for Hessians and gradients were presented in Sect. 6.2.

From Eq. (8.26), we find an expression for the internal force \mathbf{F}_{s_j} due to stretching acting on the vertex \mathbf{x}_j in terms of the stretching energy E_s :

$$\begin{aligned}\mathbf{F}_{s_0} &= \frac{\partial E_s}{\partial \mathbf{e}^0} = EA^0 \left(\frac{\|\mathbf{e}^0\|}{\|\bar{\mathbf{e}}^0\|} - 1 \right) \mathbf{t}^0, \\ \mathbf{F}_{s_j} &= -\frac{\partial E_s}{\partial \mathbf{e}^{j-1}} + \frac{\partial E_s}{\partial \mathbf{e}^j} = -EA^{j-1} \left(\frac{\|\mathbf{e}^{j-1}\|}{\|\bar{\mathbf{e}}^{j-1}\|} - 1 \right) \mathbf{t}^{j-1} + EA^j \left(\frac{\|\mathbf{e}^j\|}{\|\bar{\mathbf{e}}^j\|} - 1 \right) \mathbf{t}^j,\end{aligned}$$

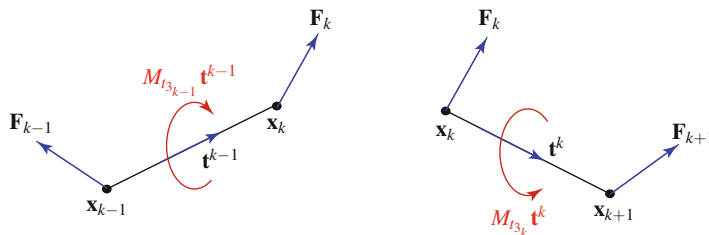


Fig. 8.2 Three vertices of a discrete elastic rod and the internal forces and the twisting moment associated with the vertices and edges. The forces are produced by elastic deformation and viscous damping, $\mathbf{F}_k = \mathbf{F}_{d_k} + \mathbf{F}_{e_k}$, are discussed in Sects. 8.5 and 8.6

³A procedure of this type is used in continuum mechanics to prescribe constitutive relations for the Cauchy stress tensor for a hyperelastic material. For further details on this matter, see the text books by Chadwick [8] or Gurtin [20].

$$\mathbf{F}_{s_{n-1}} = -\frac{\partial E_s}{\partial \mathbf{e}^{n-2}} = -EA^{n-2} \left(\frac{\|\mathbf{e}^{n-2}\|}{\|\bar{\mathbf{e}}^{n-2}\|} - 1 \right) \mathbf{t}^{n-2}. \quad (8.28)$$

As anticipated, the components of the forces \mathbf{F}_{s_k} are parallel to tangent vectors to the edges that meet at the k th vertex. The associated Hessian can be computed from the following expression:

$$\frac{\partial E_s}{\partial \mathbf{e}^k \partial \mathbf{e}^j} = \left(EA^j \left(\frac{1}{\|\bar{\mathbf{e}}^j\|} - \frac{1}{\|\mathbf{e}^j\|} \right) (\mathbf{I} - \mathbf{t}^j \otimes \mathbf{t}^j) + \frac{EA^j}{\|\bar{\mathbf{e}}^j\|} \mathbf{t}^j \otimes \mathbf{t}^j \right) \delta_k^j, \quad (8.29)$$

where δ_k^j is the Kronecker delta: $\delta_k^j = 1$ if $j = k$ and is otherwise 0. Further simplification of the Hessian leads to the following representation:

$$\begin{aligned} \frac{\partial^2 E_s}{\partial m_k \partial m_i} &= 0, \\ \frac{\partial E_s}{\partial \mathbf{e}^k \partial \mathbf{e}^j} &= \left(EA^j \left(\frac{1}{\|\bar{\mathbf{e}}^j\|} - \frac{1}{\|\mathbf{e}^j\|} \right) \mathbf{I} + \frac{EA^j}{\|\bar{\mathbf{e}}^j\|} \mathbf{t}^j \otimes \mathbf{t}^j \right) \delta_k^j. \end{aligned} \quad (8.30)$$

The Hessian formed by the components of $\frac{\partial E_s}{\partial \mathbf{e}^k \partial \mathbf{e}^j}$ will be sparse with elements banded along the diagonal. For the elastic energies specified here, there is no coupling between twisting and stretching, and hence $\frac{\partial^2 E_s}{\partial m_k \partial m_i} = 0$.

Again appealing to Eq. (8.26), the internal force \mathbf{F}_{t_i} due to twisting (or torsion) acting on the vertex \mathbf{x}_i and the twisting moment $M_{t_3 k} \mathbf{t}^k$ acting on the k th edge are computed using the twisting energy E_t :

$$\begin{aligned} \mathbf{F}_{t_0} &= \frac{\partial E_t}{\partial \mathbf{e}^0} \\ &= \frac{\partial E_t}{\partial m_1} \left(\frac{1}{2 \|\mathbf{e}^0\|} (\kappa \mathbf{b})_1 \right), \\ M_{t_3 0} &= -\frac{\partial E_t}{\partial m_0} + \frac{\partial E_t}{\partial m_1}, \\ \mathbf{F}_{t_i} &= -\frac{\partial E_t}{\partial \mathbf{e}^{i-1}} + \frac{\partial E_t}{\partial \mathbf{e}^i} \\ &= \frac{\partial E_t}{\partial m_i} \left(\frac{1}{2 \|\mathbf{e}^i\|} - \frac{1}{2 \|\mathbf{e}^{i-1}\|} \right) (\kappa \mathbf{b})_i \\ &\quad - \frac{\partial E_t}{\partial m_{i-1}} \left(\frac{1}{2 \|\mathbf{e}^{i-1}\|} \right) (\kappa \mathbf{b})_{i-1} + \frac{\partial E_t}{\partial m_{i+1}} \left(\frac{1}{2 \|\mathbf{e}^i\|} \right) (\kappa \mathbf{b})_{i+1}, \end{aligned}$$

$$\begin{aligned}
M_{t_{3k}} &= -\frac{\partial E_t}{\partial m_k} + \frac{\partial E_t}{\partial m_{k+1}}, \\
\mathbf{F}_{t_{n-1}} &= -\frac{\partial E_t}{\partial \mathbf{e}^{n-2}} \\
&= \frac{\partial E_t}{\partial m_{n-2}} \left(\frac{1}{2 \|\mathbf{e}^{n-2}\|} - \frac{1}{2 \|\mathbf{e}^{n-3}\|} \right) (\kappa \mathbf{b})_{n-2} \\
&\quad - \frac{\partial E_t}{\partial m_{n-3}} \left(\frac{1}{2 \|\mathbf{e}^{n-3}\|} \right) (\kappa \mathbf{b})_{n-3}, \\
M_{t_{3n-2}} &= -\frac{\partial E_t}{\partial m_{n-2}},
\end{aligned} \tag{8.31}$$

where

$$\frac{\partial E_t}{\partial m_k} = \frac{GA_k (a_k^2 + b_k^2)}{4\bar{\ell}_k} (m_k - \bar{m}_k), \tag{8.32}$$

and

$$\begin{aligned}
\frac{\partial E_t}{\partial \mathbf{e}^i} &= \frac{GA_i (a_i^2 + b_i^2)}{4\bar{\ell}_i} (m_i - \bar{m}_i) \frac{\partial m_i}{\partial \mathbf{e}^i} \\
&\quad + \frac{GA_{i+1} (a_{i+1}^2 + b_{i+1}^2)}{4\bar{\ell}_{i+1}} (m_{i+1} - \bar{m}_{i+1}) \frac{\partial m_{i+1}}{\partial \mathbf{e}^i}.
\end{aligned} \tag{8.33}$$

The force terms in Eq. (8.31) can be directly attributed to the fact that the referential twist m_{ref}^k is a function of the position vectors of the vertices. We have provided two representations for \mathbf{F}_{t_i} . The first is easiest to use when computing the Hessian of E_t and the second allows one to see that the twisting force is directly related to the discrete integrated curvature vectors and produce couples in the edges of the discretized rod.

In the interest of brevity, we refrain from writing the full expressions for the components of the Hessian associated with the torsion of the rod. However, we hope to provide sufficient detail so that the interested reader can establish the lengthy expressions for themselves. To begin computing the Hessian associated with \mathbf{F}_{t_i} and $M_{t_{3k}}$, we first appeal to the identities

$$\frac{\partial}{\partial \mathbf{e}^k} \left(\frac{1}{\|\mathbf{e}^j\|} \right) = -\frac{\delta_k^j}{\|\mathbf{e}^k\|^3} \mathbf{e}^k, \quad \frac{\partial (\kappa \mathbf{b})_k}{\partial m_j} = \mathbf{0}, \tag{8.34}$$

and the expressions for the derivatives $\frac{\partial(\kappa\mathbf{b})_k}{\partial\mathbf{e}^j}$ that can be found in Eq.(6.24) in Sect. 6.5. In addition, several components of the Hessian can be computed from⁴

$$\begin{aligned}\frac{\partial^2 E_t}{\partial m_i \partial m_k} &= \frac{GA_k(a_k^2 + b_k^2)}{4\bar{\ell}_k} \delta_k^i, \\ \frac{\partial^2 E_t}{\partial \mathbf{e}^k \partial \mathbf{e}^i} &= \frac{GA_i(a_i^2 + b_i^2)}{4\bar{\ell}_i} \left(\frac{\partial m_i}{\partial \mathbf{e}^i} \otimes \frac{\partial m_i}{\partial \mathbf{e}^k} + (m_i - \bar{m}_i) \frac{\partial^2 m_i}{\partial \mathbf{e}^k \partial \mathbf{e}^i} \right) \\ &\quad + \frac{GA_{i+1}(a_{i+1}^2 + b_{i+1}^2)}{4\bar{\ell}_{i+1}} \left(\frac{\partial m_{i+1}}{\partial \mathbf{e}^i} \otimes \frac{\partial m_{i+1}}{\partial \mathbf{e}^k} + (m_{i+1} - \bar{m}_{i+1}) \frac{\partial^2 m_{i+1}}{\partial \mathbf{e}^k \partial \mathbf{e}^i} \right).\end{aligned}\quad (8.35)$$

When computing the derivatives of m_k , it is important to note that the angles γ^k are unaltered by changes to the edge vectors $\mathbf{e}^0, \dots, \mathbf{e}^{n-2}$. Consequently,

$$\frac{\partial m_i}{\partial \mathbf{e}^k} = \frac{\partial m_{\text{ref}}^i}{\partial \mathbf{e}^k}, \quad \frac{\partial^2 m_i}{\partial \mathbf{e}^j \partial \mathbf{e}^k} = \frac{\partial^2 m_{\text{ref}}^i}{\partial \mathbf{e}^j \partial \mathbf{e}^k}. \quad (8.36)$$

Expressions for the derivatives of m_{ref}^i can be found in Sects. 6.8 and 6.10.

The following expression for the internal force due to bending \mathbf{F}_{b_i} acting at the vertex \mathbf{x}_i is computed using the bending energy E_b by appealing to Eq. (8.26):

$$\begin{aligned}\mathbf{F}_{b_0} &= \frac{\partial E_b}{\partial \mathbf{e}^0}, \\ \mathbf{F}_{b_i} &= -\frac{\partial E_b}{\partial \mathbf{e}^{i-1}} + \frac{\partial E_b}{\partial \mathbf{e}^i}, \\ \mathbf{F}_{b_{n-1}} &= -\frac{\partial E_b}{\partial \mathbf{e}^{n-2}},\end{aligned}\quad (8.37)$$

where

$$\begin{aligned}\frac{\partial E_b}{\partial \mathbf{e}^i} &= \frac{EA_i}{4\bar{\ell}_i} \left[a_i^2 (\kappa_{i1} - \bar{\kappa}_{i1}) \frac{\partial \kappa_{i1}}{\partial \mathbf{e}^i} + b_i^2 (\kappa_{i2} - \bar{\kappa}_{i2}) \frac{\partial \kappa_{i2}}{\partial \mathbf{e}^i} \right. \\ &\quad \left. + a_{i+1}^2 (\kappa_{(i+1)1} - \bar{\kappa}_{(i+1)1}) \frac{\partial \kappa_{(i+1)1}}{\partial \mathbf{e}^i} + b_{i+1}^2 (\kappa_{(i+1)2} - \bar{\kappa}_{(i+1)2}) \frac{\partial \kappa_{(i+1)2}}{\partial \mathbf{e}^i} \right].\end{aligned}\quad (8.38)$$

⁴Given a vector-valued function $\mathbf{a}(\mathbf{b})$ where \mathbf{b} is a vector, we recall from Sect. 6.2 that $\frac{\partial \mathbf{a}}{\partial \mathbf{b}} = \sum_{r=1}^3 \sum_{s=1}^3 \frac{\partial a_r}{\partial b_s} \mathbf{E}_r \otimes \mathbf{E}_s$ where $\mathbf{a} = \sum_{r=1}^3 a_r \mathbf{E}_r$ and $\mathbf{b} = \sum_{s=1}^3 b_s \mathbf{E}_s$.

The associated Hessian has the following representation:

$$\begin{aligned} \frac{\partial^2 E_b}{\partial m_k \partial m_i} &= 0, \\ \frac{\partial^2 E_b}{\partial \mathbf{e}^k \partial \mathbf{e}^i} &= \frac{EA_i}{4\bar{\ell}_i} \left[a_i^2 (\kappa_{i_1} - \bar{\kappa}_{i_1}) \frac{\partial^2 \kappa_{i_1}}{\partial \mathbf{e}^k \partial \mathbf{e}^i} + a_i^2 \frac{\partial \kappa_{i_1}}{\partial \mathbf{e}^i} \otimes \frac{\partial \kappa_{i_1}}{\partial \mathbf{e}^k} \right. \\ &\quad + b_i^2 (\kappa_{i_2} - \bar{\kappa}_{i_2}) \frac{\partial^2 \kappa_{i_2}}{\partial \mathbf{e}^k \partial \mathbf{e}^i} + b_i^2 \frac{\partial \kappa_{i_2}}{\partial \mathbf{e}^i} \otimes \frac{\partial \kappa_{i_2}}{\partial \mathbf{e}^k} \\ &\quad + a_{i+1}^2 (\kappa_{(i+1)_1} - \bar{\kappa}_{(i+1)_1}) \frac{\partial^2 \kappa_{(i+1)_1}}{\partial \mathbf{e}^k \partial \mathbf{e}^i} + a_{i+1}^2 \frac{\partial \kappa_{(i+1)_1}}{\partial \mathbf{e}^i} \otimes \frac{\partial \kappa_{(i+1)_1}}{\partial \mathbf{e}^k} \\ &\quad \left. + b_{i+1}^2 (\kappa_{(i+1)_2} - \bar{\kappa}_{(i+1)_2}) \frac{\partial^2 \kappa_{(i+1)_2}}{\partial \mathbf{e}^k \partial \mathbf{e}^i} + b_{i+1}^2 \frac{\partial \kappa_{(i+1)_2}}{\partial \mathbf{e}^i} \otimes \frac{\partial \kappa_{(i+1)_2}}{\partial \mathbf{e}^k} \right]. \end{aligned} \quad (8.39)$$

In the interests of brevity, we have refrained from substituting for the derivatives of κ_{k_1} , κ_{k_2} , and m_k . The relevant substitutions can be found in Sects. 6.10 and 6.11.

8.5.1 Validating the Expressions for the Hessians

For the purpose of discussion, we denote the Hessians of E_s , E_t , and E_b by \mathcal{H}_s , \mathcal{H}_t , and \mathcal{H}_b , respectively. A rod with n vertices and $n - 1$ edges has $n \times 3$ translational degrees-of-freedom due to the motion of the n vertices and $n - 1$ rotational degrees-of-freedom due to the twisting of the edges. Consequently, the symmetric matrices have the following dimensions:

$$\begin{aligned} \dim(\mathcal{H}_s) &= (4n - 1) \times (4n - 1), \\ \dim(\mathcal{H}_t) &= (4n - 1) \times (4n - 1), \\ \dim(\mathcal{H}_b) &= (4n - 1) \times (4n - 1). \end{aligned} \quad (8.40)$$

Thus, each of these matrices has $(4n - 1)^2$ components.

Notice that the Hessian components for $\frac{\partial^2 E_b}{\partial \mathbf{e}^k \partial \mathbf{e}^i}$ and $\frac{\partial^2 E_t}{\partial \mathbf{e}^k \partial \mathbf{e}^i}$ are zero unless $k = i - 1$, $k = i$, or $k = i + 1$. This is because the curvature at a point is only dependent on the edges directly preceding and following the vertex. Consequently, the matrices formed by the components of $\frac{\partial^2 E_t}{\partial \mathbf{e}^k \partial \mathbf{e}^i}$ and $\frac{\partial^2 E_b}{\partial \mathbf{e}^k \partial \mathbf{e}^i}$ produce sparse tridiagonal Hessian matrices.

To validate the complex expressions for the Hessians, a simple case of a rod with four vertices and three edges was considered. For a given configuration of the rod, the forces \mathbf{F}_{s_j} , \mathbf{F}_{t_k} , and \mathbf{F}_{b_k} , and moments $M_{t_{3k}}$ are computed using

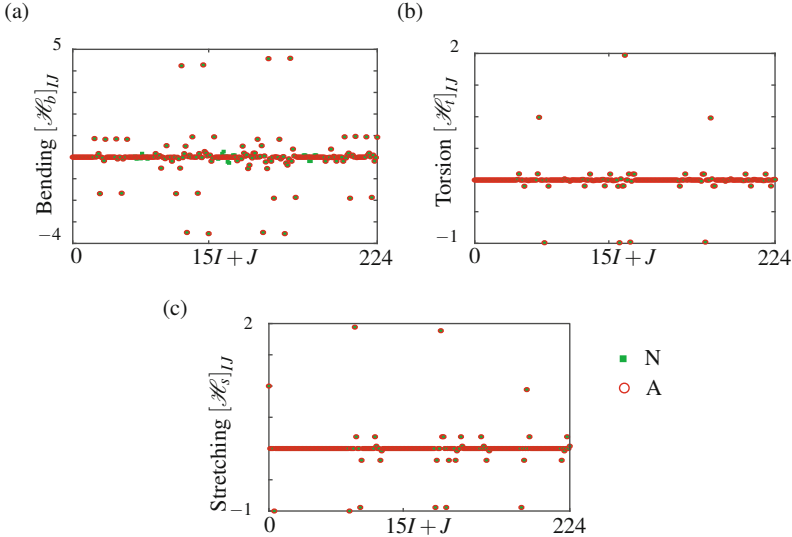


Fig. 8.3 Comparison of the components of the Hessians for (a) bending, (b) torsional (or twisting), and (c) stretching energies obtained by first using the representations (8.30), (8.35), and (8.39) and then comparing the values to the corresponding perturbations to forces and moments using Eqs. (8.28), (8.31), and (8.37). The former values are labelled *A* and the latter values are labelled *N*. The indices *I* and *J* range from 0 to 14

Eqs. (8.28), (8.31), and (8.37). Next, the edges of the rod are perturbed and the forces and moment components for this perturbed configuration are computed. This computation then provides estimates for the values of the components of the Hessians which are compared to the values computed using the representations (8.30), (8.35), and (8.39). Most of the components \mathcal{H}_{IJ} of the various Hessians shown in the figure are zero: $\mathcal{H}_{IJ} = 0$ when $|I - J| > 5$. Here, \mathcal{H} represents \mathcal{H}_s , \mathcal{H}_t , and \mathcal{H}_b . As can be seen from Fig. 8.3, agreement between the two sets of results is excellent.⁵

8.6 Viscous Dissipation

Viscous damping forces are accommodated in the discrete elastic rod formulation by prescribing damping forces at the vertices. The damping force at the *k*th node is

$$\mathbf{F}_{dk} = -\eta \ell_k \mathbf{v}_k, \quad (8.41)$$

⁵These computations were also invaluable to us while attempting to eliminate typographical errors from the lengthy expressions for the Hessians.

where η is a non-negative constant and ℓ_k is the length of the Voronoi region associated with the k th vertex. For the example discussed in Sect. 1.3, $\eta = 0.1 \text{ Pa}\cdot\text{s}$.

8.7 Composing the Generalized Force Vector \mathbf{F}_{int}

The discrete formulation has a generalized force vector \mathbf{F}_{int} of size $4n - 1$. If we consider the k th node and the $(k-1)$ th and k th edges bounding this vertex, then the components of the force vector are

$$\begin{bmatrix} \vdots \\ \mathbf{F}_{\text{int}}^{4k-1} \\ \mathbf{F}_{\text{int}}^{4k} \\ \mathbf{F}_{\text{int}}^{4k+1} \\ \mathbf{F}_{\text{int}}^{4k+2} \\ \mathbf{F}_{\text{int}}^{4k+3} \\ \vdots \end{bmatrix} = \begin{bmatrix} \vdots \\ M_{t_{3k-1}} \\ \mathbf{F}_k \cdot \mathbf{E}_1 \\ \mathbf{F}_k \cdot \mathbf{E}_2 \\ \mathbf{F}_k \cdot \mathbf{E}_3 \\ M_{t_{3k}} \\ \vdots \end{bmatrix}. \quad (8.42)$$

where the resultant elastic and dissipative force acting on the k th node has the decomposition

$$\mathbf{F}_k = \mathbf{F}_{d_k} + \mathbf{F}_{s_k} + \mathbf{F}_{t_k} + \mathbf{F}_{b_k}. \quad (8.43)$$

The moment $M_{t_{3k}} \mathbf{t}^k$ on the k th edge is associated with the twisting of the rod. Referring to Eq. (8.37), we observe that, in contrast to classic rod theories, the moment induced by bending the rod must be implemented by a force couple. That is, the force $\frac{\partial E_b}{\partial \mathbf{e}^k}$ acts on the k th vertex, while the force $-\frac{\partial E_b}{\partial \mathbf{e}^k}$ acts on the $(k+1)$ th vertex and thereby produces a force couple.

8.8 Composing the Generalized Force Vector \mathbf{F}_{ext} from Applied Forces and Applied Moments

As discussed in the example of a straight rod that is bent into a helical form in Sect. 1.3, the discrete formulation has a generalized force vector \mathbf{F}_{ext} of size $4n - 1$. This array accommodates applied forces acting on the vertices and applied moments acting on an edge that are parallel to that edge. Applied moments acting on an edge that have components in the plane normal to the tangent vector to the edge must be accommodated using a force couple.

Given a force \mathbf{P} acting on the vertex \mathbf{x}_k , a moment $M_a \mathbf{t}^{k-1}$ acting on the $(k-1)$ th edge, and a moment $M_b \mathbf{t}^k$ acting on the k th edge, then

$$\begin{bmatrix} \vdots \\ \mathbf{F}_{\text{ext}}^{4k-1} \\ \mathbf{F}_{\text{ext}}^{4k} \\ \mathbf{F}_{\text{ext}}^{4k+1} \\ \mathbf{F}_{\text{ext}}^{4k+2} \\ \mathbf{F}_{\text{ext}}^{4k+3} \\ \vdots \end{bmatrix} = \begin{bmatrix} \vdots \\ M_a \\ \mathbf{P} \cdot \mathbf{E}_1 \\ \mathbf{P} \cdot \mathbf{E}_2 \\ \mathbf{P} \cdot \mathbf{E}_3 \\ M_b \\ \vdots \end{bmatrix}. \quad (8.44)$$

The force couple requires a more detailed discussion which we now present by way of an example.

8.8.1 Prescribing Terminal Moments: An Example

We return to the example of the terminally loaded rod discussed in Sect. 1.3. In this example, a rod of length ℓ was loaded by equal and opposite terminal moments. To implement these moments in the discrete elastic rod formulation, an equivalent force couple is used.

As mentioned earlier, for the solution shown in Fig. 1.3 the rod is discretized using 99 edges and has $n = 100$ vertices (or nodes) $\mathbf{x}_0, \dots, \mathbf{x}_{n-1}$. The edges of the rod are $\mathbf{e}^0, \dots, \mathbf{e}^{n-2}$. Each of the terminal moments are accommodated using a pair of force couples and an applied moment parallel to the edge.

To elaborate, consider the following representation for the moment \mathbf{M}_ℓ acting on the $n-2$ edge:

$$\mathbf{M}_\ell = M_{\ell_1} \mathbf{m}_1^{n-2} + M_{\ell_2} \mathbf{m}_2^{n-2} + M_{\ell_3} \mathbf{t}^{n-2}. \quad (8.45)$$

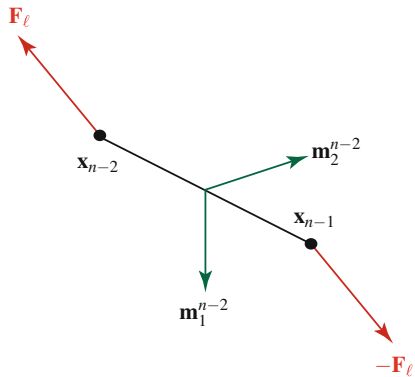
The discrete formulation has a generalized force vector $\mathbf{F}_{\text{ext}}^K$, ($K = 0, \dots, 4n - 2$) of size $4n - 1$. The torque M_{ℓ_3} is the easiest to apply since we can simply set the $(4n - 5)$ th component of the external force vector to M_{ℓ_3} such that

$$\mathbf{F}_{\text{ext}}^{4n-5} = M_{\ell_3}. \quad (8.46)$$

Referring to Fig. 8.4, for the moments M_{ℓ_1} and M_{ℓ_2} , we apply an external force \mathbf{F}_ℓ (and $-\mathbf{F}_\ell$) on the nodes \mathbf{x}_{n-2} (and \mathbf{x}_{n-1}) such that

$$-\mathbf{e}^{n-2} \times \mathbf{F}_\ell = M_{\ell_1} \mathbf{m}_1^{n-2} + M_{\ell_2} \mathbf{m}_2^{n-2}. \quad (8.47)$$

Fig. 8.4 The force couple applied to the nodes \mathbf{x}_{n-2} and \mathbf{x}_{n-1} to generate a moment vector in the plane of the material vectors \mathbf{m}_1^{n-2} and \mathbf{m}_2^{n-2} along the $(n - 2)$ th edge of the discretized curve



Whence,

$$\mathbf{F}_\ell = \frac{M_{\ell_1}}{\|\mathbf{e}^{n-2}\|} \mathbf{m}_2^{n-2} - \frac{M_{\ell_2}}{\|\mathbf{e}^{n-2}\|} \mathbf{m}_1^{n-2}. \quad (8.48)$$

The indices of the Cartesian components of the last two nodes, \mathbf{x}_{n-2} and \mathbf{x}_{n-1} , are $(4n - 8, 4n - 7, 4n - 6)$ and $(4n - 4, 4n - 3, 4n - 2)$, respectively. Thus, we set the corresponding components of the external force vector \mathbf{F}_{ext} equal to the values obtained from Eq. (8.48):

$$\begin{aligned} \mathbf{F}_{\text{ext}}^{4n-8} &= \mathbf{F}_\ell \cdot \mathbf{E}_1, & \mathbf{F}_{\text{ext}}^{4n-7} &= \mathbf{F}_\ell \cdot \mathbf{E}_2, & \mathbf{F}_{\text{ext}}^{4n-6} &= \mathbf{F}_\ell \cdot \mathbf{E}_3, \\ \mathbf{F}_{\text{ext}}^{4n-4} &= -\mathbf{F}_\ell \cdot \mathbf{E}_1, & \mathbf{F}_{\text{ext}}^{4n-3} &= -\mathbf{F}_\ell \cdot \mathbf{E}_2, & \mathbf{F}_{\text{ext}}^{4n-2} &= -\mathbf{F}_\ell \cdot \mathbf{E}_3. \end{aligned} \quad (8.49)$$

Observe that it may be necessary to update the components M_{ℓ_1} , M_{ℓ_2} , and M_{ℓ_3} at each time step if the vectors \mathbf{m}_1^{n-2} , \mathbf{m}_2^{n-2} , and \mathbf{t}^{n-2} are changing.

8.9 Work-Energy Theorem

A work-energy theorem for the discrete elastic rod can be formulated with the help of the earlier expressions for E_e and T and the equations of motion. First, we need to recognize that Eq. (8.3) are the discretized version of

$$\mathbf{M}\ddot{\mathbf{q}} = \mathbf{F}_{\text{ext}} + \mathbf{F}_{\text{int}}. \quad (8.50)$$

Next, we use Eq. (8.24) and the identity $\dot{T} = \dot{\mathbf{q}} \cdot \mathbf{M}\ddot{\mathbf{q}}$, to establish the desired theorem:

$$\frac{d}{dt} (T + E_e) = \sum_{k=0}^{n-1} \mathbf{F}_{d_k} \cdot \dot{\mathbf{x}}_k + \mathbf{F}_{\text{ext}} \cdot \dot{\mathbf{q}}. \quad (8.51)$$

If some of the external generalized forces \mathbf{F}_{ext} in this expression are conservative then a potential energy function U composed of E_e and the potential energy of the applied forces can be composed. A work-energy theorem for the total energy $E_T = T + U$ can then be established from Eq. (8.51). An example of this situation is discussed in Sect. 8.11.

8.10 Displacement Boundary Conditions

Common boundary conditions in classic rod theories include clamped and pinned ends. The counterparts to these conditions for the discrete elastic rod formulation are defined using the nodal position vectors \mathbf{x}_k and the twist angles γ^i associated with the edges. Thus, if a rod is pinned at one end, then the nodal displacement \mathbf{x}_0 is set to zero. If a rod is clamped at one end, then \mathbf{x}_0 , \mathbf{x}_1 and γ^0 are fixed.

8.11 A Vibrating Sagged Cable

We now consider a long slender body which is initially straight. Then, after moving one of its end supports, the rod sags under its own weight and is placed into a state of forced vibration by vertically oscillating the same support. This problem is classic and typically the body is modeled as a heavy inextensible string (or cable) (cf. the review articles by Rega [54, 55] and references therein). Here, we model the body as a discrete elastic rod that is allowed to extend, bend, and twist.

In the discrete elastic rod formulation of this problem, the rod is discretized with 100 vertices (i.e., $n = 99$). In its undeformed state, the rod is assumed to have a circular cross-section of radius r_0 and a length ℓ . For the example shown in Fig. 8.5, the geometric and material properties of the rod have the following values:

$$\ell = 0.1 \text{ m}, \quad r_0 = 0.001 \text{ m}, \quad E = 1 \times 10^6 \text{ Nm}^2, \quad G = 0.333E. \quad (8.52)$$

The mass density per unit volume of the body is $\rho_0 = 1000 \text{ kg/m}^3$. The leftmost end of the rod is assumed to be clamped. Thus, the first two nodes are fixed and the twist of the first edge is constrained to be zero:

$$\mathbf{x}_0(t) = \mathbf{0}, \quad \mathbf{x}_1(t) = \frac{\ell}{99} \mathbf{E}_1, \quad \gamma^0 = 0. \quad (8.53)$$

The motion of the other support is prescribed as follows:

$$\mathbf{x}_{99}(t) = \begin{cases} \left(\ell - \frac{\ell}{10}t\right) \mathbf{E}_1, & t \in [0, 1]; \\ \left(\ell - \frac{\ell}{10}t\right) \mathbf{E}_1 + \frac{\ell}{100} \sin(20\pi t) \mathbf{E}_2, & t > 1.0. \end{cases} \quad (8.54)$$

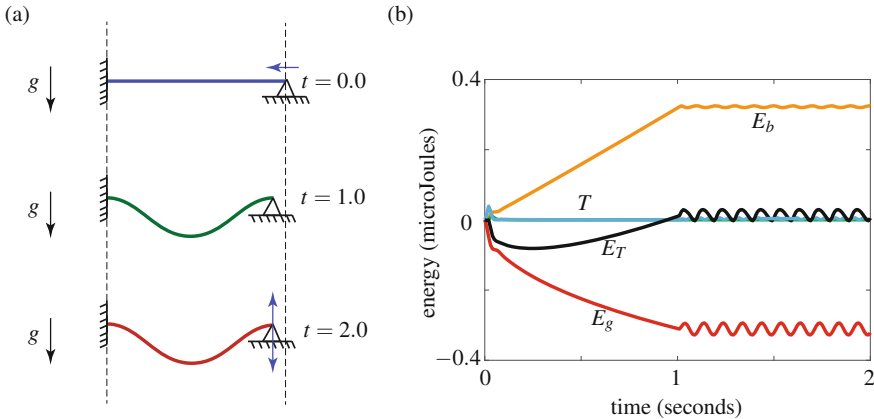


Fig. 8.5 Vibration of a rod for which one end is fixed and the other is being harmonically excited at 10 Hz. (a) The configurations of the rod at times $t = 0$, $t = 1$, and $t = 2$ s. (b) Time traces of the energies in the rod. Here, E_T denotes the total energy, T is the kinetic energy, E_b is the elastic flexural energy, E_g is the gravitational potential energy. The elastic energy stored due to the stretching of the rod is negligible for this example and the energy stored by twisting the rod is zero: $E_s \approx 0$ and $E_t = 0$

and

$$\mathbf{x}_{98}(t) = \mathbf{x}_{99}(t) - \frac{\ell}{99} \mathbf{E}_1. \quad (8.55)$$

The twist in the last edge of the rod, $\gamma^{98}(t)$, is not constrained.

As shown in Fig. 8.5a and described in Eq. (8.54), one end of the rod is fixed and the other end is slowly displaced horizontally so the rod sags under gravity. At $t = 1$ s, the horizontal displacement ceases and then the same end of the rod is given a vertical oscillation at 10 Hz. As can be seen from Fig. 8.5b, the plots of various components of the potential energy and the total energy capture the dynamics of this problem. Observe that eventually, the energy oscillates at approximately 10 Hz and the rod vibrates about a sagged configuration. This example illustrates the capabilities of the discrete elastic rod formulation to simulate dynamic problems.

8.12 Closing Remarks

This concludes our discussion of the kinematics of discrete elastic rods. The equations of motion (8.3) can be viewed as a $(4n - 1)$ -degree-of-freedom mechanical system composed of mass particles connected by discrete deformable elements. While the stretching of these elements is easy to accommodate and the bending can be modeled using the vector $\kappa_i \mathbf{b}_i$ at each vertex, the twisting of the rod is challenging to model in a computationally efficient manner.

Initially, the twist of the rod was measured using the Bishop frame in Bergou et al.'s formulation in [4]. However, it was subsequently realized that a more efficient formulation would use a reference frame attached to an edge that was updated using a parallel transport operator at each instant in time. This lead to the alternative formulations in Bergou et al.'s [3] and Kaldor et al. [29]. A second novelty in the formulations is the use of spherical geometry to arrive at a representation for the variation of the twisting of the rod. This variation is required to numerically integrate the equations of motion (8.3). We hope we have presented sufficient background in Chaps. 5 and 7 for the reader to be able to appreciate the novel use of spherical geometry in Bergou et al.'s work.

Much more could be included in this Brief on the discrete elastic rod formulation of Bergou et al. Additional topics might include applications to contact problems and connected rods and detailed analysis of the C++ source code. Unfortunately, these topics are beyond the limited number of published pages available to us. Hopefully, the background we have supplied will enable others to pursue expository works on these topics as well as using this Brief to aid them in employing the discrete elastic rod formulation for their research.

References

1. Antman, S.S.: Nonlinear Problems of Elasticity, *Applied Mathematical Sciences*, vol. 107, second edn. Springer-Verlag, New York (2005). URL <http://dx.doi.org/10.1007/0-387-27649-1>
2. Audoly, B., Clauvelin, N., Brun, P.T., Bergou, M., Grinspun, E., Wardetzky, M.: A discrete geometric approach for simulating the dynamics of thin viscous threads. *Journal of Computational Physics* **253**, 18–49 (2013). URL <http://dx.doi.org/10.1016/j.jcp.2013.06.034>
3. Bergou, M., Audoly, B., Vouga, E., Wardetzky, M., Grinspun, E.: Discrete viscous threads. *ACM Transactions on Graphics (SIGGRAPH)* **29**(4), 116:1–116:10 (2010). URL <http://dx.doi.org/10.1145/1778765.1778853>
4. Bergou, M., Wardetzky, M., Robinson, S., Audoly, B., Grinspun, E.: Discrete elastic rods. *ACM Transactions on Graphics (SIGGRAPH)* **27**(3), 63:1–63:12 (2008). URL <http://dx.doi.org/10.1145/1360612.1360662>
5. Bishop, R.L.: There is more than one way to frame a curve. *The American Mathematical Monthly* **82**(3), 246–251 (1975). URL <http://dx.doi.org/10.2307/2319846>
6. Bobenko, A.I.: Geometry II: Discrete Differential Geometry (2015). URL http://page.math.tu-berlin.de/~bobenko/Lehre/Skripte/DDG_Lectures.pdf
7. Casey, J., Lam, V.C.: On the relative angular velocity tensor. *ASME Journal of Mechanisms, Transmissions, and Automation in Design* **108**, 399–400 (1986). URL <http://dx.doi.org/10.1115/1.3258746>
8. Chadwick, P.: Continuum Mechanics, second corrected and enlarged edn. Dover Publications, New York (1999)
9. Cosserat, E., Cosserat, F.: Sur la statique de la ligne déformable. *Compte Rendus de l'Académie des Sciences, Paris* **145**, 1409–1412 (1907)
10. Daily-Diamond, C.A., Gregg, C.E., O'Reilly, O.M.: The roles of impact and inertia in the failure of a shoelace knot. *Proceedings of the Royal Society of London A: Mathematical, Physical and Engineering Sciences* **473**(2200) (2017). URL <http://dx.doi.org/10.1098/rspa.2016.0770>
11. Euler, L.: *Methodus Inveniendi Lineas Curvas Maximi Minimive Proprietate Gaudentes, sive Solutio Problematis Isoperimetrici Lattissimo Sensu Accepti: Additamentum 1 De Curvis Elasticis.* Leonhardi Euleri Opera Omnia, Series prima (*Opera mathematica*), Vol. XXIV, Auctoritate et impensis Societatis Scientiarum Naturalium Helveticae. Orell Füssli, Zürich (1952). An English translation of this work can be found in [47]

12. Evangelista, D., Hotton, S., Dumais, J.: The mechanics of explosive dispersal and self-burial in the seeds of the filaree, *Erodium cicutarium* (Geraniaceae). *Journal of Experimental Biology* **214**(4), 521–529 (2011). URL <http://dx.doi.org/10.1242/jeb.050567>
13. Frenet, F.: Sur quelques propriétés des courbes à double courbure. *Journal de Mathématiques Pures et Appliquées* **17**, 437–447 (1852) URL http://sites.mathdoc.fr/JMPA/PDF/JMPA_1852_1_17_A22_0.pdf
14. Fuller, F.B.: Decomposition of the linking number of a closed ribbon: A problem from molecular biology. *Proceedings of the National Academy of Sciences of the United States of America* **75**(8), 3557–3561 (1978). URL <http://www.jstor.org/stable/68719>
15. Goodman, L.E., Robinson, A.R.: Effect of finite rotations on gyroscopic sensing devices. *ASME Journal of Applied Mechanics* **25**, 210–213 (1952)
16. Goriely, A.: The Mathematics and Mechanics of Biological Growth. Springer-Verlag, New York (2017). URL <http://dx.doi.org/10.1007/978-0-387-87710-5>
17. Green, A.E., Laws, N.: Remarks on the theory of rods. *Journal of Elasticity* **3**(3), 179–184 (1973). URL <http://dx.doi.org/10.1007/BF00052892>
18. Green, A.E., Naghdi, P.M.: A unified procedure for construction of theories of deformable media. II. Generalized continua. *Proceedings of the Royal Society. London. Series A. Mathematical, Physical and Engineering Sciences* **448**(1934), 357–377 (1995). URL <http://dx.doi.org/10.1098/rspa.1995.0021>
19. Green, A.E., Naghdi, P.M., Wenner, M.L.: On the theory of rods. I Derivations from three-dimensional equations. *Proceedings of the Royal Society. London. Series A. Mathematical, Physical and Engineering Sciences* **337**(1611), 451–483 (1974). URL <http://dx.doi.org/10.1098/rspa.1974.0061>
20. Gurtin, M.E.: An Introduction to Continuum Mechanics. Academic Press, New York (1981)
21. Hanson, A.J., Ma, H.: Parallel transport approach to curve framing. *Indiana University, Techreports-TR425* **11**, 3–7 (1995). URL <ftp://ftp.cs.indiana.edu/pub/hanson/iucs-tr425.ps>
22. Healey, T.J.: Material symmetry and chirality in nonlinearly elastic rods. *Mathematics and Mechanics of Solids* **7**(4), 405–420 (2002). URL <http://dx.doi.org/10.1177/108128028482>
23. Henderson, D.W.: Differential Geometry: A Geometric Introduction. Prentice Hall, Upper Saddle River, New Jersey (1998)
24. Hoffmann, T.: Discrete Differential Geometry of Curves and Surfaces. Math-for-Industry (MI) Lecture Notes Series, Faculty of Mathematics, Kyushu University, Japan (2009)
25. Jawed, M.K.: Geometrically nonlinear configurations in rod-like structures. Ph.D. thesis, Massachusetts Institute of Technology, Cambridge, MA (2016). URL <http://hdl.handle.net/1721.1/106703>
26. Jawed, M.K., Da, F., Joo, J., Grinspun, E., Reis, P.M.: Coiling of elastic rods on rigid substrates. *Proceedings of the National Academy of Sciences of the United States of America* **111**(41), 14,663–14,668 (2014). URL <http://dx.doi.org/10.1073/pnas.1409118111>
27. Jawed, M.K., Khouri, N.K., Da, F., Grinspun, E., Reis, P.M.: Propulsion and instability of a flexible helical rod rotating in a viscous fluid. *Physical Review Letters* **115**(16), 168,101 (2015). URL <http://dx.doi.org/10.1103/PhysRevLett.115.168101>
28. Jung, P., Leyendecker, S., Linn, J., Ortiz, M.: A discrete mechanics approach to the Cosserat rod theory - Part 1: static equilibria. *International Journal for Numerical Methods in Engineering* **85**(1), 31–60 (2011). URL <http://dx.doi.org/10.1002/nme.2950>
29. Kaldor, J.M., James, D.L., Marschner, S.: Efficient yarn-based cloth with adaptive contact linearization. In: ACM SIGGRAPH 2010 Papers, SIGGRAPH '10, pp. 105:1–105:10. ACM, New York, NY, USA (2010). URL <http://doi.acm.org/10.1145/1833349.1778842>
30. Kelvin, L., Tait, P.G.: A Treatise on Natural Philosophy, Reprinted edn. Cambridge University Press, Cambridge (1912)
31. Kirchhoff, G.: Über des gleichgewicht und die Bewegung eines unendlich dünnen elastischen Stabes. *Crelles Journal für die reine und angewandte Mathematik* **56**, 285–313 (1859). URL <http://dx.doi.org/10.1515/crll.1859.56.285>
32. Kirsch, A.: Discrete elastic rods (2012). Bachelor's Thesis in Mathematics

33. Klenin, K., Langowski, J.: Computation of writhe in modeling of supercoiled DNA. *Biopolymers* **54**(5), 307–317 (2000). URL [http://dx.doi.org/10.1002/1097-0282\(20001015\)54:5<307::AID-BIP20>3.0.CO;2-Y](http://dx.doi.org/10.1002/1097-0282(20001015)54:5<307::AID-BIP20>3.0.CO;2-Y)
34. Kreyszig, E.: Differential Geometry, Revised and reprinted edn. Toronto University Press, Toronto (1964)
35. Lang, H., Linn, J., Arnold, M.: Multi-body dynamics simulation of geometrically exact Cosserat rods. *Multibody System Dynamics* **25**(3), 285–312 (2011). URL <https://doi.org/10.1007/s11044-010-9223-x>
36. Langer, J., Singer, D.: Lagrangian aspects of the Kirchhoff elastic rod. *SIAM Review* **38**(4), 605–618 (1996). URL <http://www.jstor.org/stable/2132934>
37. Lauderdale, T.A., O'Reilly, O.M.: On transverse and rotational symmetries in elastic rods. *Journal of Elasticity* **82**(1), 31–47 (2006). URL <http://dx.doi.org/10.1007/s10659-005-9022-4>
38. Linn, J., Dreßler, K.: Discrete Cosserat rod models based on the difference geometry of framed curves for interactive simulation of flexible cables. In: L. Ghezzi, D. Hömberg, C. Landry (eds.) *Math for the Digital Factory, Mathematics in Industry*, vol. 27, pp. 289–319. Springer International Publishing AG, Cham, Switzerland (2017). URL https://doi.org/10.1007/978-3-319-63957-4_14
39. Loock, A., Schömer, E., Stadtwald, I.: A virtual environment for interactive assembly simulation: From rigid bodies to deformable cables. In: 5th World Multiconference on Systemics, Cybernetics and Informatics, pp. 325–332 (2001)
40. Love, A.E.H.: *A Treatise on the Mathematical Theory of Elasticity*, fourth edn. Cambridge University Press, Cambridge (1927)
41. Lv, N., Liu, J., Ding, X., Liu, J., Lin, H., Ma, J.: Physically based real-time interactive assembly simulation of cable harness. *Journal of Manufacturing Systems* **43**(Part 3), 385–399 (2017). URL <https://doi.org/10.1016/j.jmsy.2017.02.001>. Special Issue on the 12th International Conference on Frontiers of Design and Manufacturing
42. Marsden, J.E., Ratiu, T.S.: Introduction to Mechanics and Symmetry: A Basic Exposition of Classical Mechanical Systems, *Texts in Applied Mathematics*, vol. 17, second edn. Springer-Verlag, New York (1999). URL <http://dx.doi.org/10.1007/978-0-387-21792-5>
43. Meier, C., Popp, A., Wall, W.A.: Geometrically exact finite element formulations for slender beams: Kirchhoff-Love theory versus Simo-Reissner theory. *Archives of Computational Methods in Engineering: State of the Art Reviews* pp. 1–81 (2017). URL <https://doi.org/10.1007/s11831-017-9232-5>
44. Montgomery, R.: How much does the rigid body rotate? A Berry's phase from the 18th century. *American Journal of Physics* **59**(5), 394–398 (1991). URL <https://doi.org/10.1119/1.16514>
45. Naghdi, P.M.: Finite deformation of elastic rods and shells. In: D.E. Carlson, R.T. Shield (eds.) *Proceedings of the IUTAM Symposium on Finite Elasticity: Held at Lehigh University, Bethlehem, PA, USA August 10–15, 1980*, pp. 47–104. Springer Netherlands, Dordrecht (1982). URL https://doi.org/10.1007/978-94-009-7538-5_4
46. Novelja, A., O'Reilly, O.M.: On geodesics of the rotation group SO(3). *Regular and Chaotic Dynamics* **20**(6), 729–738 (2015). URL <http://dx.doi.org/10.1134/S1560354715060088>
47. Oldfather, W.A., Ellis, C.A., Brown, D.M.: Leonhard Euler's elastic curves. *Isis* **20**(1), 72–160 (1933). URL <http://www.jstor.org/stable/224885>
48. O'Reilly, O.M.: On the computation of relative rotations and geometric phases in the motions of rigid bodies. *ASME Journal of Applied Mechanics* **64**(4), 969–974 (1997). URL <http://dx.doi.org/10.1115/1.2789008>
49. O'Reilly, O.M.: On constitutive relations for elastic rods. *International Journal of Solids and Structures* **35**(11), 1009–1024 (1998). URL [http://dx.doi.org/10.1016/S0020-7683\(97\)00100-5](http://dx.doi.org/10.1016/S0020-7683(97)00100-5)
50. O'Reilly, O.M.: *Intermediate Engineering Dynamics: A Unified Treatment of Newton-Euler and Lagrangian Mechanics*. Cambridge University Press, Cambridge (2008). URL <https://doi.org/10.1017/CBO9780511791352>

51. O'Reilly, O.M.: Modeling Nonlinear Problems in the Mechanics of Strings and Rods: The Role of the Balance Laws. Interaction of Mechanics and Mathematics. Springer International Publishing, New York (2017). URL <http://dx.doi.org/10.1007/978-3-319-50598-5>
52. Pai, D.K.: STRANDS: Interactive simulation of thin solids using Cosserat models. Computer Graphics Forum **21**(3), 347–352 (2002). URL <http://dx.doi.org/10.1111/1467-8659.00594>
53. Pressley, A.: Elementary Differential Geometry, second edn. Springer Undergraduate Mathematics Series. Springer-Verlag London, Ltd., London (2010). URL <http://dx.doi.org/10.1007/978-1-84882-891-9>
54. Rega, G.: Nonlinear vibrations of suspended cables - Part I: Modeling and analysis. ASME Applied Mechanics Reviews **57**(6), 443–478 (2005). URL <http://dx.doi.org/10.1115/1.1777224>
55. Rega, G.: Nonlinear vibrations of suspended cables - Part II: Deterministic phenomena. ASME Applied Mechanics Reviews **57**(6), 479–514 (2005). URL <http://dx.doi.org/10.1115/1.1777225>
56. Rubin, M.B.: Cosserat Theories: Shells, Rods, and Points. Kluwer Academic Press, Dordrecht (2000). URL <http://dx.doi.org/10.1007/978-94-015-9379-3>
57. Schweickart, E., James, D.L., Marschner, S.: Animating elastic rods with sound. ACM Transactions on Graphics **36**(4), 115:1–115:10 (2017). URL <http://doi.acm.org/10.1145/3072959.3073680>
58. Serret, J.A.: Sur quelques formules relatives à la théorie des courbes à double courbure. Journal de Mathématiques Pures et Appliquées **16**, 193–207 (1851). URL http://sites.mathdoc.fr/JMPA/PDF/JMPA_1851_1_16_A12_0.pdf
59. Shuster, M.D.: A survey of attitude representations. American Astronautical Society. Journal of the Astronautical Sciences **41**(4), 439–517 (1993)
60. Simo, J.C., Vu-Quoc, L.: On the dynamics in space of rods undergoing large motions - a geometrically exact approach. Computer Methods in Applied Mechanics and Engineering **66**(2), 125–161 (1988). URL [http://dx.doi.org/10.1016/0045-7825\(88\)90073-4](http://dx.doi.org/10.1016/0045-7825(88)90073-4)
61. Spillmann, J., Teschner, M.: CORDE: Cosserat rod elements for the dynamic simulation of one-dimensional elastic objects. In: D. Metaxas, J. Popovic (eds.) Eurographics/SIGGRAPH Symposium on Computer Animation. The Eurographics Association (2007). URL <http://dx.doi.org/10.2312/SCA/SCA07/063-072>
62. Synge, J.L., Schild, A.: Tensor Calculus. University of Toronto Press, Toronto (1949)
63. Thomson, W., Tait, P.G.: Treatise on Natural Philosophy. Oxford University Press, Oxford (1867)
64. Todhunter, I.: Spherical Trigonometry: For the Use of Colleges and Schools. Macmillan & Co., London, U. K. (1886)
65. Vouga, E.: Personal communication by email (2016)
66. de Vries, R.: Evaluating changes of writhe in computer simulations of supercoiled DNA. The Journal of Chemical Physics **122**, 064,905 (2005). URL <http://dx.doi.org/10.1063/1.1846052>
67. Wang, Z.: Development of techniques for modeling the static buckling of Euler beam and dynamic response of Kirchhoff rods. Ph.D. Dissertation, Texas A&M University (2016). URL <http://oaktrust.library.tamu.edu/handle/1969.1/157054>
68. Zhuravlev, V.F.: The solid angle theorem in rigid body dynamics. Journal of Applied Mathematics and Mechanics (PMM) **60**(2), 319–322 (1996). URL [http://dx.doi.org/10.1016/0021-8928\(96\)00040-8](http://dx.doi.org/10.1016/0021-8928(96)00040-8)

Index

A

adapted frames, 12

angle

- α^k , 36
- β^k , 53
- χ^k , 40
- $\hat{\vartheta}^k$, 52, 88
- ψ_k , 89
- \underline{m}_k , 52, 68, 88
- φ_k , 37
- ϑ^k , 49
- m_{ref}^0 , 40, 45
- m_{ref}^{k+1} , 39, 45
- γ^k , 52

angle of twist ϕ , 14

angular velocity vector

- $\bar{\omega}^k(t)$, 55, 94
- ω_B , 16
- ω_D , 16
- ω_{SF} , 16
- $p\bar{\omega}^k(t)$, 36, 55

applied force, 107

applied moment, 107

B

Bishop frame, 12, 38

circle, 21

helix, 21

C

Călugăreanu's theorem, 76

curvature

κ , 16

κ_1 , 16

κ_2 , 16

κ_{k_1} , 50, 65

κ_{k_2} , 50, 65

D

Darboux vector

- v_B , 16
- v_D , 16
- v_{SF} , 16
- $\kappa_k b_k$, 34

director triad, 12

E

elastic energy, 98

Euler's elastica, 2

F

force

- F_{bi} , 104
- F_{si} , 101
- F_{ti} , 102
- F_{ext} , 94, 107
- F_{int} , 94, 107

force couple, 107

Frenet triad, 12

G

Gauss-Bonnet theorem, 76

geodesic curvature κ_g , 21

geometric torsion τ , 16

gradient
 elastic energy, 101
 notation, 59

H

helix, 21
 Hessian
 κ_{k_1} , 71
 κ_{k_2} , 71
 m_{ref}^k , 70
 elastic energy, 101
 notation, 59
 holonomy, 40, 76, 88
 holonomy of a connection, 84

K

kinetic energy
 T , 97
 T^* , 97
 Kirchhoff's rod theory, 5, 11

M

mass density ρ_0 , 2, 95
 mass matrix \mathbf{M} , 94, 96
 material curve \mathcal{L} , 12
 material triad, 48
 moment
 $M_{t_{3k}}$, 102
 momentum
 angular, 96
 linear, 96

N

Newton's method, 94

O

operator
 $M_{t_{k-1}}^k$, 48
 $P_{t_{k-1}}^k$, 34
 $\dot{M}^k(t, \Delta t)$, 48
 $\dot{\bar{P}}^k(t, \Delta t)$, 35

P

parallel propagation, 12, 21
 space, 33
 time, 33

parallel transport, 81
 potential energy, 98

R

reference frame, 38
 referential discrete (integrated) twist m_{ref}^i , 40, 42, 52, 56
 relative angular velocity vector, 14, 18, 55

S

solid angle, 75
 spherical excess, 75, 77
 spherical quadrilateral, 77
 spherical triangle, 91

T

tangent indicatrix c_t , 11, 21, 76
 terminal moment, 6, 108
 torsional strain v_3 , 16
 twist-free frame, 12, 38

V

variation
 δE , 79
 $\delta \psi_k$, 88
 δm_{ref}^k , 67, 88
 δm_k , 88
 $\delta \Delta \mathbf{t}^k$, 61
 $\delta \kappa_{k_1}$, 65
 $\delta \kappa_{k_2}$, 65
 $\delta (\kappa \mathbf{b})_k$, 62
 $\delta \mathbf{m}_1^k$, 64
 $\delta \mathbf{m}_2^k$, 64
 $\delta \mathbf{t}^k$, 61
 $\delta \mathbf{t}_{\gamma_k}$, 61
 $\delta \varphi_k$, 61
 velocity vector
 $\dot{\mathbf{m}}_1^k$, 56, 94
 $\dot{\mathbf{m}}_2^k$, 56, 94
 $\dot{\mathbf{x}}_k$, 94
 $\rho \bar{\mathbf{o}}^k(t)$, 38

W

work-energy theorem, 109
 writhe, 76, 89